STUDIES ON MECHANICAL PERFORMANCE AND ELECTROMAGNETIC SHIELDING EFFECTIVENESS OF ELECTROSPUN FIBER/ EPOXY COMPOSITES

A Thesis submitted

in partial fulfillment for the Degree of

Doctor of Philosophy

By

BATTULA DURGA SIVA DEERAJ

Department of Chemistry

Indian Institute of Space Science and Technology

(A Deemed to be University u/s 3 of the UGC Act 1956)

Department of Space, Government of India

Valiamala, Thiruvananthapuram- 695547

Kerala, India

November 2022

Dedicated to my beloved parents

Mr. Battula Siva Mallikarjuna Rao &

Mrs. Battula Gowri Kalyani

CERTIFICATE

This is to certify that the thesis entitled **Studies on Mechanical Performance and Electromagnetic Shielding Effectiveness of Electrospun Fiber/Epoxy Composites** submitted by **Battula Durga Siva Deeraj** to the Indian Institute of Space Science and Technology, Thiruvananthapuram, in partial fulfillment for the award of the degree of **Doctor of Philosophy** is a *bona fide* record of research work carried out by him under my supervision. The contents of this thesis, in full or in parts, have not been submitted to any other Institution or University for the award of any degree or diploma.

Prof. Kuruvilla Joseph
Supervisor
Outstanding Professor
Dean (SA,SW and OR)
Department of Chemistry

Counter signature of the HOD with seal

Thiruvananthapuram
November, 2022

DECLARATION

I declare that this thesis entitled **Studies on Mechanical Performance and Electromagnetic Shielding Effectiveness of Electrospun Fiber/Epoxy Composites** submitted in partial fulfillment of the degree of **Doctor of Philosophy** is a record of original work carried out by me under the supervision of Prof. Kuruvilla Joseph, and has not formed the basis for the award of any other degree or diploma, in this or any other Institution or University. In keeping with the ethical practice in reporting scientific information, due acknowledgements have been made wherever the finding of others have been cited.

Battula Durga Siva Deeraj
SC16D035

Thiruvananthapuram-695 547
November, 2022

ACKNOWLEDGEMENTS

Firstly, I would like to take this opportunity to express my gratitude to my beloved mentor and guide, Dr. Kuruvilla Joseph, Outstanding Professor and Dean (Student Activities), Department of Chemistry, IIST, for his excellent guidance, inspiration, encouragement in directing and designing the work. His positive motivation and never-give-up attitude helped me to complete this work. It is an honor to be associated with him. I learned a lot professionally and personally with him.

I owe my sincere thanks to Dr. D Sam Dayala Dev, Director, IIST and former Directors Shri S.Somnath and V.K. Dhadwal for the research facilities provided to me during the tenure of my research work. I am pleased to extend my deep gratitude to Dr. K. Y. Sandhya, Head of the Department of Chemistry, former heads Dr. K. Prabhakaran and Dr. Nirmala R. James for their continuous support and encouragement during my stay.

The discussions with my doctoral committee members Dr. Ramesh, Dr. Anup, and Dr. Gomathi sharpened my views and supported my work. I extend my heartfelt thanks to Dr. S.S. Bose, Associate Professor, IISc Bangalore and Dr. S. Sampath, Professor, IISc Bangalore for their valuable academic help. I also thank all the faculty members of the Department of chemistry, IIST for their helpful guidance, which enabled the successful completion of the research work.

I extend my sincere thanks to STIC, CUSAT Cochin, CSIR-National Institute for Interdisciplinary Science & Technology (NIIST), Thiruvananthapuram and PSG Coimbatore for kindly providing access to characterize my samples. I am thankful to Vikram Sarabhai Space Center, Thiruvananthapuram for proving me the required polymers.

This work would not have been possible without the support extended to me by my lab mates and project students. My gratitude to all of them, especially, Dr. Raneesh, Dr. Kiran, Mr. Harikrishnan, and Ms. Akhila. I wish to express my sincere appreciation to all the non-teaching staff in Department of Chemistry IIST, especially to Mr. Loveson Albert and Mrs. Jayasree for helping me in every possible way. I would like to sincerely thank Dr. Saritha A, Dr. Jitha S. Jayan and Dr. Gejo George for their help in correcting my documents.

Finally, I thank my beloved parents, sister & family for their patience, affection and constant support that paved way towards the successful completion of this research work.

Battula Durga Siva Deeraj

ABSTRACT

Electrospinning technique is a proven and matured nanofabrication process due to its special characteristics. These fibers have unique features that make them useful in a wide range of applications. These fibers act as excellent reinforcements, due to their high surface area and aspect ratio. The main objective of this research work is to explore the role of electrospun fibers in epoxy matrix and investigate their performance. For this purpose, electrospun fibers were made from poly(styrene-co-butadiene) (SBC) and polyimide and their epoxy composites were prepared and characterized. These composites were observed to have enhanced mechanical and fracture properties, without compromising the comprehensive properties. Electrospun carbon fibers with zirconia and titanium carbide (TiC) @ titania (TiO_2) core-shell structures were prepared from carbonizing the polyacrylonitrile (PAN) fibers. These fibers were used as reinforcements in epoxy matrix and composites were made. These carbon fiber loaded epoxy composites with fillers were observed to have good EMI properties along with enhanced mechanical properties. The results demonstrate that the prepared filler loaded carbon fibers have tremendous potential to be used as effective EMI shielding materials and further carbon fiber loaded epoxy composites can be employed as potential structural EMI shields

TABLE OF CONTENTS

LIST OF TABLES

LIST OF FIGURES

ABBREVATIONS

CA	Cellulose acetate
CNT	Carbon Nanotube
CNF	Carbon Nanofiber
DMA	Dynamic Mechanical Analyzer
DMF	Dimethylformamide
EM	Electromagnetic
EMI	Electromagnetic interference
FTIR	Fourier Transform Infrared Spectroscopy
FRC	Fiber reinforced composites
GO	Graphene Oxide
HRTEM	High Resolution Transmission Electron Microscopy
HTPB	Hydroxyl-terminated polybutadiene
MWCNT	Multi-Walled Carbon Nanotube
PA	Polyamide
PMMA	Poly(methyl methacrylate)
PAN	Polyacrylonitrile
PBI	Polybenzimidazole
PCL	Polycaprolactone
PVA	Poly vinyl alcohal
PET	Polyethylene terephthalate
PLA	Poly lactic acid
PNC	Polymer Nanocomposite
PAA	Poly (amic acid)
PES	Polyether Sulfone
PEO	Polyethylene Oxide
PS	Polystyrene
PI	Polyimide
PC	Polycarbonate

PU	Polyurethane
PVC	Poly(vinylene chloride
PVDF	Polyvinylidene fluoride
SBC	Styrene Butadiene copolymer
SBS	Poly (styrene-block-butadiene-block-styrene)
SWCNT	Single-Walled Carbon Nanotube
SE	Shielding effectiveness
SSE	Specific shielding effectiveness
TGA	Thermogravimetric Analyzer
TiO_2	Titanium Dioxide
TiC	Titanium carbide
THF	Tetrahydrofuran
UTM	Universal Testing Machine
XRD	X-Ray Diffractometer
XPS	X-Ray Photoelectron Spectroscopy

NOTATIONS

a	Crack length
G_{IC}	Fracture energy
B	Fracture test specimen thickness
W	Fracture test specimen width
T_g	Glass transition temperature
E”	Loss modulus
γ	Shear rate
τ	Shear stress
E’	Storage modulus
K_{IC}	Stress intensity factor
T	Temperature
t	time
η	Viscosity
υ_f	Volume fraction of the filler
E_c	Modulus of the composite
E_m	Modulus of the epoxy matrix
E_f	Modulus of the filler
L	Load at crack initiation
dB	decibel

CHAPTER 1

INTRODUCTION

The aim of this chapter is to provide an introduction on electrospinning, epoxy composites and provide literature on electrospun reinforced epoxy composites and their promising applications. This chapter gives an introduction to electrospun carbon fibers, EMI shielding and the potential of electrospun fibers for EMI shielding applications. This chapter presents the objective and motivation of the research work. The organization of this thesis and short introduction to each chapter is also presented towards the end of this chapter.

Part of this chapter has been communicated as book chapter in book Handbook of Epoxy/Fiber Composites (2022). (ISBN: 978-981-15-8141-0)

DOI: 10.1007/978-981-15-8141-0_3-1

1.1. Electrospinning

Electrospinning technique is one of the most widely used nanofabrication techniques for preparing continuous fibers in the nano and sub-micron scale (Agarwal et al., 2011; Y. He et al., 2014; Jian et al., 2018; J. Wu et al., 2013; Zucchelli et al., 2011). When compared to other nanofabrication techniques, an easily scale-up facility, diverse material choice and low cost makes this technique unique(Garg et al., 2011; Valizadeh et al., 2014). These electrospun fibers have interesting characteristics like a high surface area and surface to volume ratio which makes them potential candidates in various fields of material science. Based on the application, these fibers can be prepared in different geometries like mats, aligned fibers, yarns etc (Zhan et al., 2012). This technique offers an effective way to mix polymers, developed nanocomposite continuous fibers, hollow fibers, core-shell type fibers, and electrospun carbon fibers. These nanofibers find applications in energy storage and conversion, a protective coating , composite reinforcement, sensing, EMI shielding and bio-medical fields (Aussawasathien et al., 2005; C. Chen et al., 2018; W. Chen et al., 2016; Duan et al., 2017; Duan et al., 2015; Z.-M. Huang et al., 2003; Inagaki et al., 2012; Jiang et al., 2017; X. Liao et al., 2017; Reich et al., 2018; Safikhani et al., 2017; Shen et al., 2015; Si et al., 2015; Wei et al., 2019; W. Xu, Ding, Jiang, Chen, et al., 2014; W. Xu, Ding, Jiang, Zhu, et al., 2014; Zeng et al., 2015; S. Zhou et al., 2017). In Figure 1.1, the experimental setup of electrospinning equipment and the process parameters are presented.

1.1.1. History and Mechanism of Electrospinning

In 1897, Rayleigh observed the electrospinning process for the first time. Later in 1914, this process was studied in detail by Zeleny on electrospraying (Rayleigh, 1882; Zeleny, 1917) . A series of patents were secured by Anton and Formahls on the preparation of polymer filaments with application of electrostatic potential in 1934

(Anton, 1934). Later, Simons secured a patent on the apparatus or the preparation of ultrathin and lightweight fabrics in 1966 (Simons, 1966).

In 1969, Taylor revealed the mechanism of electrospinning and the formation of jet during electrospinning process. He demonstrated how the polymer droplets are subject to deformation when the surface tension of the droplets is countered by the electrostatic potential. After his explanation of this phenomenon, the conical shaped droplet is named as Taylor cone (Taylor, 1969). In the present scenario, electrospinning is one of the widely used techniques, owing to its vast range of applications due to its nanofiber morphology.

Darrell H. Renakar and his co-workers made significant contributions in understanding and further exploring the electrospinning technique. They explored the various parameters influencing electrospinning technique and highlighted potential applications of the prepared electrospun fibers(Reneker, 1993). They contributed in controlling electrospinning process to obtain specified diameters, beaded nanofibers and nanometric diameter fibers (Liu et al., 2019; Lukáš et al., 2009; Ramakrishna et al., 1996; Reneker & Yarin, 2008). There investigations on electrospun jets, bending instabilities in electrospinning process have revitalized the electrospun fibers (Liu et al., 2017; Reneker et al., 2000).

Electrospinning is a technique which produces nanofibers from a polymer solution or jet through an electrically charged jet. This process is suitable for most of the polymer solutions or polymer melts that have the ability to spin. It is possible to obtain fibers in a variety of sizes and shapes, with a widespread property range that are applicable for industrial applications. Though electrospinning needs a very simple and economical setup, it is a complex process that depends on several technical factors (Garg et al., 2011).

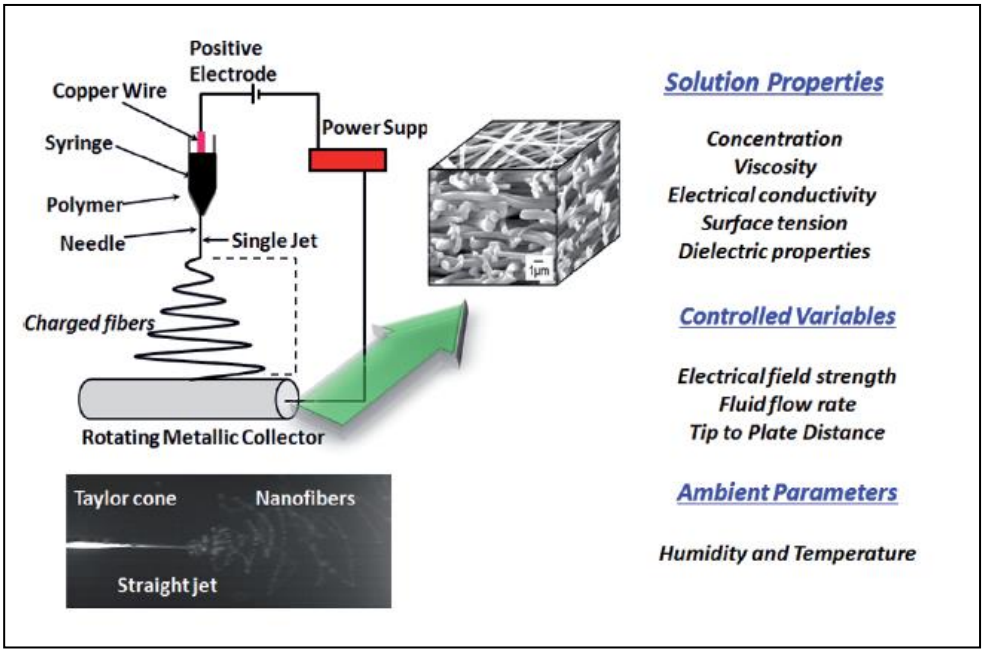

Figure 1.1: Schematic representation of electrospinning setup and parameters (Gopiraman et al., 2019).

The electrospinning setup basically consists of three main components; (a) a high voltage supply unit, (b) a feed pump unit and, (c) a collector unit (either stationary or moving). The basic setups of electrospinning are presented in Figure 1.1 and 1.2. In a conventional single jet electrospinning mechanism, a voltage supply of around 5-50 kV is applied between the needle tip and collector depending on the spinnablility of the precursor solution. From the voltage unit, one electrode is linked to needle of syringe and the other electrode is linked to a collector, which is generally grounded. The electrode connected to the needle will charge the polymer fluid and the other electrode is grounded (Abdel-Hady et al., 2011). During the application of voltage, an electrical field is created in-between the collector and the needle. The syringe pump injects the polymer solution at a pre-controlled rate (X. Lu et al., 2009). In the initial stage, the polymer solution at the tip of needle will form a droplet because of surface tension. When, a high voltage is applied, this droplet surface will be charged. This charged surface experiences a mutual electrostatic repulsion in-between the droplet surface

charges and also a columbic force due to the external field (X. Zhang, 2014). This interaction makes the charged droplet to elongate and form a conical surface, which is termed as Taylor cone. When a critical voltage is reached, a charged jet is ejected from the Taylor cone tip (J.-H. He et al., 2005). Then, this ejected jet is stretched thousands of times, and solvent evaporation happens and travels towards the collector. During traveling, initially the jet will take a linear path, but after some time it will take random movements due to the instabilities of the jet. The jet follows helical path from this point and higher order whipping and bending instabilities happen as the jet spirals towards the collector. This results in deposition of continuous fibers on the surface of collector. Usually, these fibers are randomly oriented and nonwoven type of fibers. It was observed that the collector geometry and architecture has a significant effect on the morphology and alignment of nanofibers. For preparation of uniformed aligned fibers of good mechanical performance, the use of rotating collector is recommended. Aligned electrospun fibers are reported to have better mechanical characteristics than randomly oriented fibers.

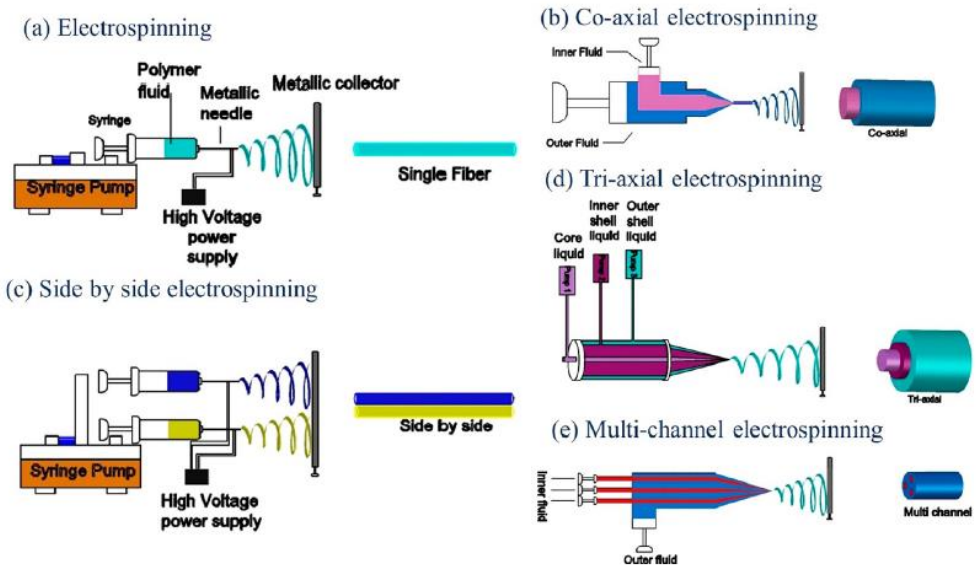

Figure 1.2. Different configurations for electrospinning setup: (a) electrospinning, (b) coaxial electrospinning, (c) side by side electrospinning, (d) triaxial electrospinning, and (e) multichannel electrospinning (G. K. Sharma et al., 2021)

The electrospinning process is not confined to single component polymer fibers. These fibers can be made of two different components as well. We can prepare fibers from polymer blends, polymers with metal additives, polymer with ceramic additives, polymers with carbon additives etc., (Jiang et al., 2018). Electrospun fibers can be a prepared with a single component system, two component systems, or multi-component system based on the required application. From literature , it can be noted that two component or multi-component electrospun fibers exhibit various compositions and functionalities (Jiang et al., 2018). Compared to bulk reinforcements, electrospun fibers possess unique properties which make them ideal candidates for reinforcing function. The properties like high axial molecular orientation, a high aspect ratio, high surface to volume ratio, pore size, inherent mechanical properties and fibrillar morphology. In table 1.1, few electrospun polymer fibers available in literature are tabulated.

Table 1.1: Electrospun fibers from different polymer sources(Rangappa et al., 2022).

S.No	Polymer	Solvent	Reference
1.	Polyacrylonitrile (PAN)	DMF	(Shakil et al., 2020)
2.	PA66	Formic acid	(Ahmadloo et al., 2017)
3.	Cellulose acetate (CA)	Acetone/DMA	(H. Liao et al., 2011)
4.	Lignin/PVA	water	(E. Lee et al., 2014)
5.	PLA	chloroform	(Sobczyk et al., 2018)
6.	PVA	Distilled water	(C. Zhang et al.,

			2005)
7.	PVDF	N,N-Dimethylacetamide	(Choi et al., 2004)
8.	PMMA	THF/DMF	(Ying Liu et al., 2009)
9.	SBS	Butyl acetate, LiBr, and crosslinker	(van der Heijden et al., 2017)
10.	SIS	THF/DMF	(Feng et al., 2009)
11.	Nylon 6	Formic acid	(Ryu et al., 2003)
12.	PET	Trifluoroacetic acid	(Z. Ma et al., 2005)
13.	Polystyrene	THF/DMF	(K. Lee et al., 2003)
14.	Polycarbonate	Chloroform, THF/DMF	(Krishnappa et al., 2003)
15.	PVP	ethanol	(J. Zhou et al., 2009)

1.1.2. Parameters Influencing Electrospinning Process

The factors that govern the electrospinning process can be typically categorized as (a) solution parameters; (b) controlled variables; and (c) ambient parameters. The solution properties include polymer solution concentration, solution viscosity, electrical conductivity, surface tension, and dielectric properties. The controlled parameters include employed flow rate, applied acceleration voltage, and gap between collector and syringe tip. The ambient properties include chamber humidity and temperature, which are noticed to effect the fiber geometry. For a polymer, there is no universal electrospinning parameters as such, these parameters are to be altered based on the

polymer type (Jiang et al., 2018). In table 1.2, an overview of electrospun parameters is presented.

Table 1.2: Overview of the influence of parameters on electrospinning (Shirazi et al., 2020).

Process parameter	**Effect(s) on morphology**	**Highlights**	**Importance**
Applied high voltage .	Fiber diameter	• Using high applied voltage can increase the fiber diameter. • Firstly, the solution jet carries more charges for fast elongation. • More jet can be ejected using high applied voltage	***
Tip-to collector distance	Bead formation	• Longer tip-to-collector distance can increase the number of bead on the surface. • Longer distance increases the jet elongation time. • It can form unstable nanofibers	*
Needle gauge	Fiber diameter	• Using needle with higher gauge (smaller inner diameter) can decrease the pore size. • Smaller needle can also decrease the fiber diameter	***
Dope injection rate	Fiber diameter and bead formation	• Higher dope injection rate ejects more solution in a jet.	*

		• So, it can increase the pore size. • It can also lead to bead formation due electrospraying.	

(* - important, ** - very important, *** - very very important)

1.1.3. Applications

Electrospun fibers have attracted researchers across the material science domain. These nonwoven fibers and their composites have unique characteristics that makes them an ideal choice for advanced functional applications. These fibers finds application in sensing, energy storage, catalysis, bio-medical, tissue engineering, filtration, EMI shielding, composite reinforcement, micro reactors, substrates, protective coatings etc., Depending on the application, the fibers can be designed accordingly, this makes the electrospinning process superior to other techniques. In Figure 1.3, different forms of electrospun fibers and their potential applications is presented.

These electrospun fibers are observed to enhance the electrochemical properties in Li-ion batteries (Lan et al., 2021). In case of biomedical applications, electrospun fibers are considered as an ideal material because of the ease of dissolution of water soluble drugs. A combination of electrospinning and subsequent e-jet printing are being followed for the preparation of electrospun polymers for drug delivery applications (Bai et al., 2021). Electrospun fibers are observed to display better ion-exchange performance over simple polymer membranes. So, these electrospun mats are being considered as a potential candidate for water purification application(Cseri et al., 2021). The use of electrospun nanofibers as reinforcements in nanocomposites, has attracted many researchers because of their advanced performance as a nanofiber reinforced polymer composites. The use of electrospun polymer fibers is noticed to alter the mechanical as well as other functional properties of resultant composites owing to their inherent properties (Uslu et al., 2021).

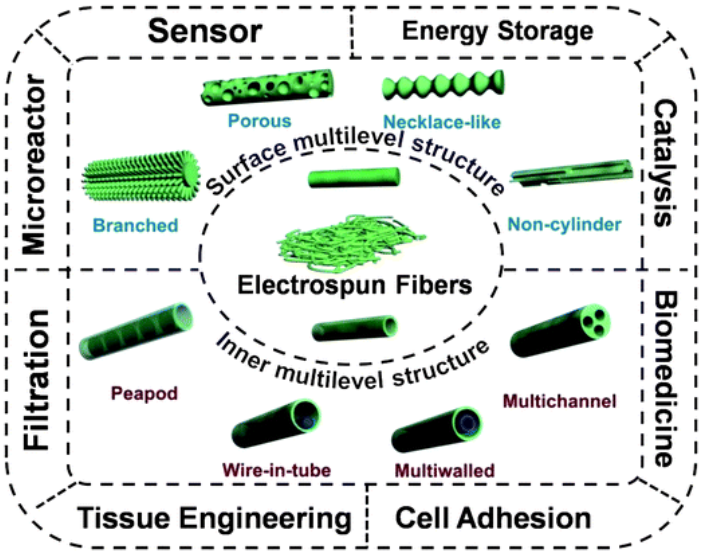

Figure 1.3: Applications of electrospun fibers (J. Wu et al., 2013).

1.2. Electrospun Fibers for Composite Reinforcement

1.2.1. Electrospun Fibers in Polymer Matrices

We can classify fiber-reinforced composites (FRCs) as a special advanced class of polymer composites. In the present scenario, they are the most popular and versatile engineered materials with interesting properties. These resultant properties of FRCs generally depend on the choice of fiber, choice of matrix, type of fibers, fiber functionalization and fiber concentration. These materials are widely being used in areas of civil, military, aerospace, defense, transport and mechanical fields (Al-Saleh et al., 2011; Brøndsted et al., 2005; Chand, 2000; Jiang et al., 2018; X. Li et al., 2007; Puglia et al., 2005; Thostenson et al., 2001). Traditionally, these fiber incorporated polymer composites have a continuous polymer matrix phase and a dispersed reinforcing fiber phase. The fibers are arranged inside the polymer matrix and the organization of the fiber phase and matrix determine the properties of the composite. This arrangement can be tailored to design composites that are suitable for a particular application.

Researchers are mainly interested to develop polymer-based FRCs with remarkable mechanical properties for commercial structural applications (Zucchelli et al., 2011). Generally, FRCs are developed and their applications in structural, functional, electronic applications are explored. The performance of these FRCs can be enhanced by imparting modifications to the reinforcing fibers. The properties like thermal, mechanical, electrical can be enhanced by fiber modification and the performance of composites can be tailored. Mostly, traditional FRCs consists of micrometer range fibers as the reinforcement component (Correa et al., 1998; Deshpande et al., 2000; S. M. Lee, 1992; Summerscales et al., 2011). In order to prepare and develop commercial superior grade composites, the concept of introducing nanosized fibers inside polymer matrix is highly endorsed. The utilization of nanosized fibers and combinations of nano and micro sized fibers is a excellent way to induce better mechanical properties than micro-sized fibers alone (Zucchelli et al., 2011). In Figure 1.4 and 1.5, the volume of publications and their classification is depicted, respectively.

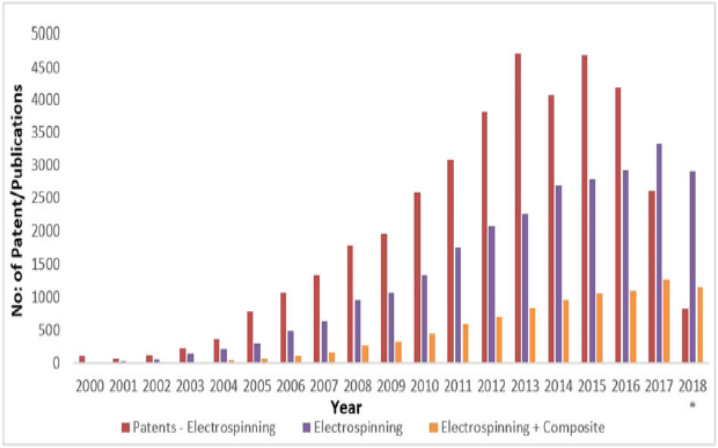

Figure 1.4: No. of publications based on electrospinning related topics (Vijay Kumar et al., 2019).

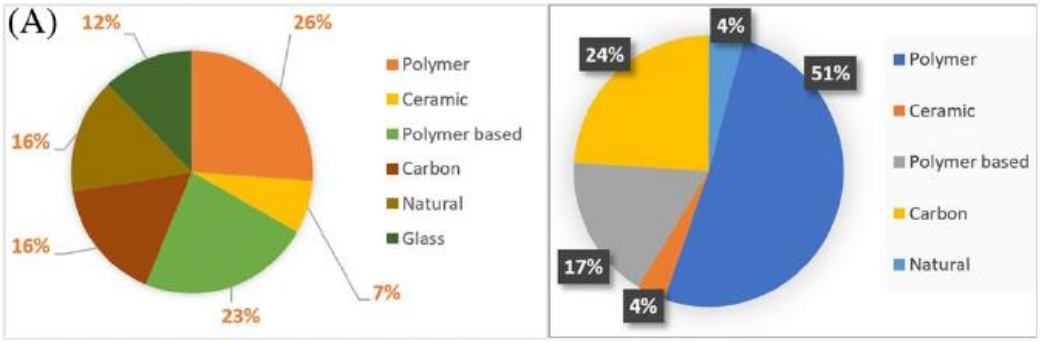

Figure 1.5: Distribution of publications based on electrospinning related topics Since 2018. (Vijay Kumar et al., 2019).

From literature, we can observe several polymers from which the electrospun fibers can be prepared. But, all the polymer fibers cannot be used as worthy reinforcements in polymer matrices. Only, few polymer electrospun fibers with good inherent mechanical strength can serve as potential reinforcements. In Figure 1.6, few electrospun fibers with their mechanical property is presented. From the Figure, we can see that Polyimides and polyamides can act as excellent reinforcements, other fiber forming polymers like PAN and PVDF also have potential to act as reinforcements.

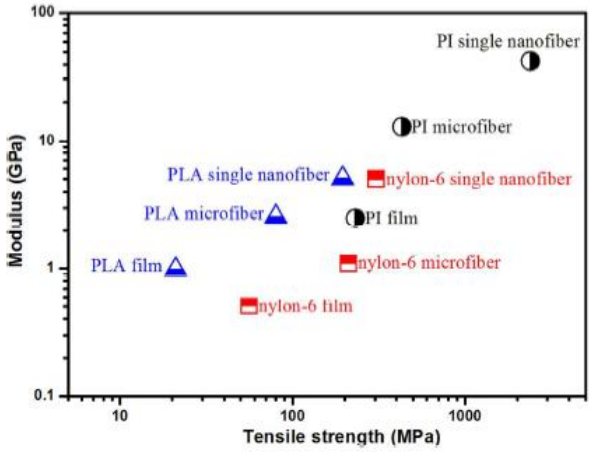

Figure 1.6: Mechanical properties of electrospun single PLA, nylon-6, and polyimide (PI) nanofibers compared with other formations (Jiang et al., 2018).

In the case of polymer nanocomposites, advanced nanofillers are used as reinforcement in weak polymer matrices to obtain resultant high-strength composites. For this purpose, nanofillers like carbon nanomaterials, inorganic nano materials, and nanoclay are employed and the performance is evaluated. Alongside, the use of electrospun polymer fibers as promising reinforcements in polymer matrices is an interesting area. In table 1.3, a list of polymer fibers and their matrices are presented. In this thesis, the focus is to provide a brief and systematic study of electrospun fiber reinforced polymer composites, especially epoxy based composites.

In a work, cellulose fibers were successfully prepared by electrospinning process and used as a reinforcement in poly(butylene succinate) matrix (Han et al., 2008). By using N-methyl morpholine-N-oxide hydrate as the spinning solvent, cellulose fibers of average diameter 560 nm were prepared. The dynamic mechanical properties of these PBS nanocomposites were tested and a 67% improvement was observed in the cellulose fiber reinforced biocomposites when compared with virgin PBS composites. These results confirm the reinforcing ability of cellulose fibers. Li et al., (B. Li et al., 2013) in their work prepared electrospun nylon 6 nanofibers by incorporating graphene in it. Later they used these composite fibers as reinforcements in PMMA matrix. They chopped these electrospun mats and stacked these mats layer-by-layer and hot pressed them to prepare the nanocomposite films. The graphene/nylon fiber incorporated nanocomposite films exhibited excellent improvement in the mechanical properties even at a very low graphene loading of 0.01 w%. They reported a significant improvement of 56% in tensile strength, 113% in modulus, and 250% in fracture toughness, respectively. The reinforcing capability of nanoclay loaded Polyhydroxy butyrate (PHB) was reported (Marega et al., 2015). For this the authors used two different nanoclays, i.e., cationic Cloisite (CL) and anionic Perkalite (PK). From the results it was observed that Polyhydroxy butyrate nanofibers with CL loading reinforced composites displayed superior tensile strength and modulus than that of Polyhydroxy butyrate nanofibers loaded with PK/PCL composites.

In another work, electrospun PLA nanofibers with graphene (1.3 w% loading) was prepared by electrospinning technique and was used as reinforcement in poly(butylene succinate) (PBS) matrix(Sisti et al., 2016). They observed that when a nanofiber loading of 0.8 w% was used, the increase in the tensile strength was 27% and the improvement in elongation of break was 47%. For the nanofiber reinforced composites without graphene, the improvement in tensile strength and elongation at break was only 16% and 26%. From the fractured images, they noticed that the nanofibers improved the toughening property by crack obstruction and deviation. In another work, short PMMA fibers were used as reinforcement in polycarbonate (PC) core-shell structure in the critical length limits. From the results, it can be noticed that an improvement of about 260% and 630% in both the stress and modulus, are observed respectively (Ura et al., 2021). In another work, the researchers found that electrospun fiber loaded polymer composites displayed better antifouling and photocatalytic properties (Bode-Aluko et al., 2021). In another work, electrospun monolithic composites which possess a complex core-sheath structure were presented. This work paves way for the use of these electrospun multi component nanofibers in multifunctional applications (S. Chang et al., 2020).

Table 1.3: List of electrospun fibers reinforced polymer composites (Rangappa et al., 2022)

S.No	Polymer fiber	Matrix	Reference
1.	Nylon-6	PMMA	(L. S. Chen et al., 2009)
2.	PBI	SBR rubber	(J. s. Kim et al., 1999)
3.	Nylon-6	PVA	(Stachewicz et al., 2012)
4.	Nylon-6	PANI	(Romo-Uribe et al., 2009)
5.	Nylon-6	PCL	(Neppalli et al., 2010)

6.	cellulose	PVA	(C. Tang et al., 2008)
7.	Nylon-6	PLA	(Neppalli et al., 2012)
8.	cellulose	Protein	(G. Chen et al., 2008)
9.	Nylon-6	TPU	(Jiang, Duan, et al., 2012)
10.	Nylon 6,6	Polyethylene	(Neppalli et al., 2012)
11.	Polyimide	Polyimide	(Jiang et al., 2013)
12.	Nylon 6	Melamine formaldehyde	(Jiang, Hou, et al., 2012)
13.	Polybenzimidazole	Rubber	(J. s. Kim et al., 1999)
14.	Polyurethane	Silicon film	(Tijing et al., 2013)
15.	Aligned PI	PI	(D. Chen et al., 2011)
16.	cellulose	Cellulose diacetate	(C. Chen et al., 2013)
17.	PI	PA6	(Y. Chen et al., 2012)
18.	poly (azo-naphthyl-imide)/carbon nanotube nanofiber	PI	(Kausar, 2016)
19.	PU	PU	(Z. J. Chang, 2011)
20.	PMMA	PMMA	(Matabola et al., 2011)
21.	PMMA	PCL	(Lamastra et al., 2012)
22.	PAN-PMMA core shell	BIS-GMA/TEGDMA dental resin	(Lin et al., 2008)

23.	Nylon 6/silicate crystals	BIS-GMA/TEGDMA dental resin	(Tian et al., 2007)
24.	Nylon 6	BIS-GMA/TEGDMA dental resin	(Fong, 2004)
25.	PAN	PMMA	(M. Wu et al., 2012)
26.	cellulose	Soybean protein isolate	(G. Chen et al., 2008)
27.	PCL	Gelatin	(Beachley et al., 2009)
28.	PCL	PU	(F. Guo et al., 2015)
29.	Nylon 6,6	HDPE	(B. Lu et al., 2015)
30.	PS/TiO_2	poly(butylene succinate-co-adipate)	(Neppalli et al., 2014)
31.	Electrospun carbon nanofibers	PI	(W. Xu et al., 2015)

1.2.2. Epoxy Resin and Toughening Agents

Epoxy is one the pre-dominantly used thermosetting matrices for high end applications because of its inherent properties (Jayan et al., 2021; Jayan et al., 2020b; Konnola et al., 2019). Because of its inbuilt properties like high mechanical strength, corrosion and wear resistance and thermal properties, it finds very important role in areas of aerospace, automobile, defense and other commercial grade applications. Usually, these epoxy polymers are categorized with two or more epoxy groups (oxirane rings) in their backbone structure. Based on the number and location of these oxirane

rings in the epoxy polymer, these resins are classified in different types. Out of all, diglycidyl ether of bisphenol A (DGEBA) type of epoxy resin was mostly studied and used. The structure of diglycidyl ether of bisphenol A is depicted in Figure 1.7. These polymers have a linear nature and will form a complex crosslinked structure when they are cured with a suitable hardener. But after curing, the crosslinked structure results in inherent brittleness, which is a deteriorating factor, as this leads to poor fracture toughness. Generally, secondary additives (toughening agents) are incorporated inside the epoxy matrix to address these issues and thereby enhance the toughness. All toughening agents are observed to improve the toughness, however a decrease in the mechanical property of few toughned epoxies is noticed. This confirms that, even though the toughness is being improved the mechanical property is getting reduced. So, the requirement is to develop toughened epoxy systems without comprising their mechanical properties. Researchers are focusing more on such works where simultaneous property enhancement is the key criteria. From earlier reports, secondary agents like particulate fillers, thermoplastic material, core-shell type particles, engineered block copolymers, etc., are being used to improve the fracture toughness of epoxy composites. But, the main drawback of these fillers is that the enhancement in toughness comes at the compromise of other properties like tensile strength and glass transition temperature. In this context, nanomaterials are highlighted to be a good alternative to improve the toughness without the compensation of other properties. Researchers have come up with nanofiller grafted polymer combinations for efficiently improving comprehensive performance of epoxy (Jayan et al., 2021; Jayan et al., 2020a, 2020b). The incorporation of conducting filler is also a promising idea to develop superior composite materials.

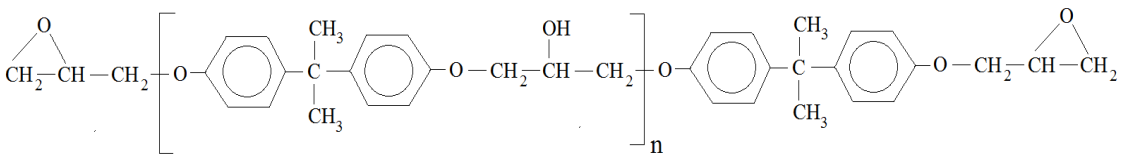

Figure 1.7: Chemical structure of DGEBA (Parameswaranpillai et al., 2018).

Titanium oxide in the form of both nanoparticle and nanowires was incorporated in epoxy and the effect of filler geometry on the performance of epoxy was investigated by Konnala et al. (Konnola et al., 2019). They prepared nanosized titania wires by employing hydrothermal method. They incorporated these nanofillers in epoxy and composites at 0.2 w% to 0.8 w% were prepared. From their results, an improvement of 136% in toughness is observed at 0.6 w% of filler loading. The tensile strength improved by 26% and modulus by 16%. The storage modulus of the composites was investigated and an improvement of 11% was observed at 30 ˚C. This work substantiates that high surface area nanomaterials serve as good reinforcements in epoxy even at very low loadings. Jayan et al. (Jayan et al., 2020a) tried to improve the epoxy performance by using nano titania aggregated graphene oxide hybrids as the toughening material. This aggregated material had typical core-shell type geometry, where titania form the inner core and the graphene oxide forms the outer shell. This work reports an overall toughness improvement in fracture toughness of 200%. The work signifies how the hybrid combination of nanofillers can act as promising toughening material in epoxy matrix. This hybrid system is observed to improve the toughness by 200%. Jayan et al.(Jayan et al., 2020c) developed graphene oxide grafted PEG/ epoxy composites and investigated their overall mechanical performance. They reported a significant enhancement in toughness of about 334%, at a filler loading of 0.1w%. The same group in 2021, prepared PVP grafted graphene oxide combinations from employing the 'grafting from' technique and used it as a reinforcement in epoxy(Jayan et al., 2021). From, the results an improvement in fracture toughness of more than 190% is noted. In table 1.4, a list of epoxy tougheners and percentage improvement are presented. The role of micro sized fibers in reinforcing epoxy was explored. However, the role of nanosized fibers in epoxy provides an improved chance of enhancing the fracture toughness without the reduction in tensile strength because of the high surface area. Nanofiber preparation is a challenging process; here electrospinning serves as a better and effective technique to fabricate fibers in the nano and submicron regime.

Table 1.4: List of epoxy tougheners and toughness improvement.(Rangappa et al., 2022)

S.No	Toughener	Toughness improvement (%)	Reference
1.	alumina	100	(McGrath et al., 2008)
2.	Carbon black	20	(B. C. Kim et al., 2008)
3.	nano-alumina	19	(Q. L. Ji et al., 2004)
4.	epoxidized soybean oil (ESO) grafted with carboxyl-terminated poly(acrylonitrile-co-butadiene)	68	(Bach et al., 2020)
5.	Amine-functionalized poly (styrene) microspheres	33	(Chaudhary et al., 2015)
6.	9,10-dihydro-9-oxa-10-phosphaphenanthrene10-oxide (DOPO) grafted epoxidized soybean oil	73	(Vu et al., 2020)
7.	Epoxidized natural rubber	48	(Chuayjuljit et al., 2006)
8.	silane-coupling-agent-treated GNPs (KH- GNPs) and hydroxyl multi-walled carbon nanotubes	34	(Yao et al., 2020)

9.	PES	60	(Mimura et al., 2000)
10.	Graphene oxide and Polyethylene Glycol-b-Polypropylene Glycol-b-Polyethylene Glycol	400	(Jayan et al., 2020b)
11.	HTPB	156	(Thomas et al., 2008)
12.	poly (allyl amine) grafted graphene oxide	87	(Sahu et al., 2019)
13.	PSF	20	(P. Huang et al., 1997)
14.	Polysiloxane	29	(S. Ma et al., 2011)
15.	POSS-Rubber core–shell nanoparticles	30	(Thitsartarn et al., 2015)
16.	GO-g-CTBN	128	(Konnola et al., 2015)
17.	Reactive hyper branched polyurethane	128	(B. Tang et al., 2014)
18.	polysiloxane-based core-shell particles	109	(J. Chen et al., 2013)
19.	poly (ether ether ketone) grafted graphene oxide	31	(Katti et al., 2017)

20.	PEP-PEO block copolymer	144	(J. Liu et al., 2010)
21.	core-shell rubber nano-particles	125	(Quan et al., 2015)
22.	silica	73	(Blackman et al., 2007)
23.	nanoclay	98	(M. Wang et al., 2015)
24.	Aligned carbon nanotubes	51	(C. Ma et al., 2015)
25.	graphene	57	(Chandrasekaran et al., 2014)
26.	Reduced graphene oxide/PCL-PPC-PCL	60	(Y. Liu et al., 2016)
27.	poly(ether sulfone) grafted multi-walled carbon nanotube	125	(Konnola et al., 2016)

1.2.3. Electrospun Fibers in Epoxy Matrices

Epoxy composites are the mostly used polymeric materials for structural applications. Fiber reinforced epoxy composites are advanced class of composite materials as they possess high mechanical properties. Natural fiber reinforced composites, synthetic fiber reinforced composites and hybrid composites are prepared using epoxy as the matrix and used in various applications (Safri et al., 2018; Zucchelli et al., 2011). The use of electrospun polymer fibers as a reinforcement in epoxy matrix is a promising area of research. These electrospun fibers can be introduced inside the epoxy thermosets in different forms, as chopped mats or laminates or as interleaved mats. Depending on the type of inclusion and loading, the properties can be altered. In Figure 1.8, a cartoonic representation of the different ways in which electrospun fibers can be incorporated in epoxy is presented.

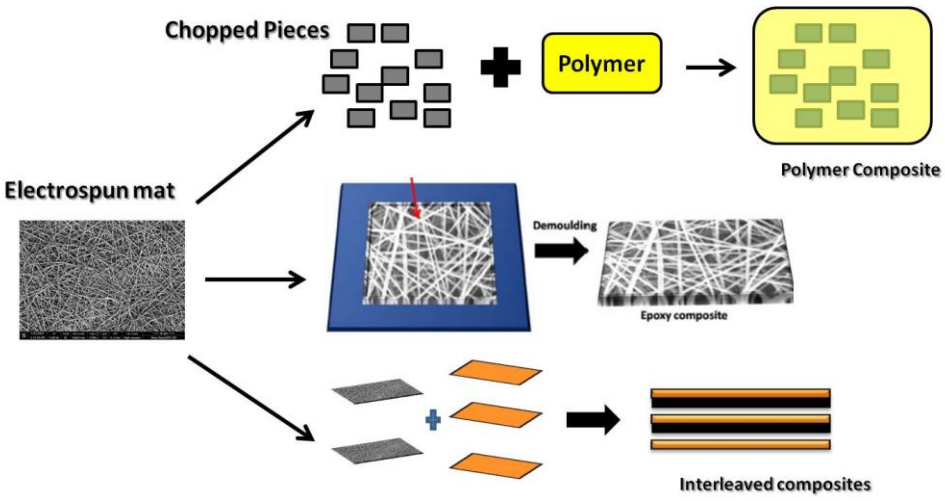

Figure 1.8: Schematics to prepare electrospun epoxy composites(Rangappa et al., 2022).

Each of the alternative ways presented have their unique advantage and usage. Especially the third alternative to include these electrospun fibers as interleaves in fiber reinforced composites is best for commercial applications. In 1999, Kim et al. (J. s. Kim et al., 1999) reported the initial work on using electrospun fibers for reinforcing polymer matrices. The authors used ultrafine polymer fibers of Polybenzimidazole (PBI) for this purpose. They incorporated these fibers both in epoxy and SBR matrix and evaluated their performance. From the results, the nonwoven fibers of Polybenzimidazole are observed to efficiently reinforce the epoxy system. With the increase in the fiber loading, there was an increase in the fracture toughness, the fracture energy and Young's modulus of the PBI fiber reinforced nanocomposites. The enhancement in the fracture toughness is contributed to the resistance exerted by the PBI fibers to the crack. So, for crack propagation, more amount of energy is needed as fibers obstruct the crack path. So, ultimately the fracture toughness of the composites increased. In another work, the researchers incorporated electrospun nanofibers into the epoxy composites to investigate the reinforcing capability (Dzenis et al., 2001).

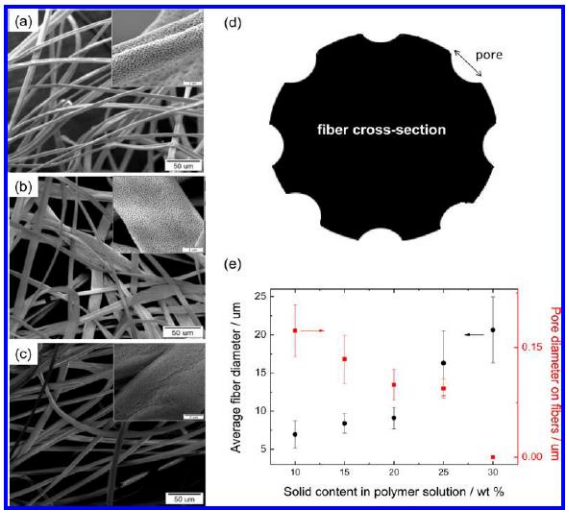

Figure 1.9: SEM images of polystyrene fibers at different weight percentages (a) 0.10, (b) 0.15, (c) 0.20 (d) cartoon of c/s view of electrospun polystyrene fibers (e) Average fiber and pore diameter as a function of polymer concentration(Demir et al., 2014).

From the results, they reported that these fibers have good potential to serve as reinforcements in epoxy. A comparison of electrospun nanofiber mat epoxy composites and short electrospun fiber epoxy composites was done and they concluded that the composites are having better mechanical performance due to better homogeneity (Sancaktar et al., 2009).

The mechanical interlocking phenomenon between the electrospun polystyrene porous fibers and epoxy was investigated (Demir et al., 2014). Electrospun polystyrene fibers were prepared using THF as the spinning solvent. By varying the polymer weight percentages (from 10 to 30%), electrospun fibers are prepared. The SEM micrographs of the fibers are presented in Figure 1.9 (a, b & c).

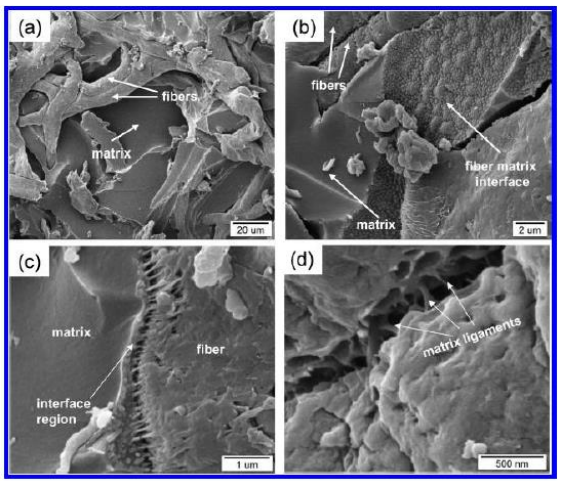

Figure 1.10: SEM images of compression tested PS fiber reinforced epoxy showing (a) the fiber network on the fracture surface, (b) the ligaments of the fiber debonding, (c) the fiber−matrix interface, and (d) matrix ligaments at the fiber matrix interface(Demir et al., 2014).

We can see that the prepared fibers are porous and the schematic representation of fibers is depicted in Figure 1.9(d). In Figure 1.9(e), the pore size and the average fiber diameter is presented. These porous fibers at a weight percentage of 0.2 are incorporated in the epoxy matrix and composites are prepared. These composites are compression tested at high strain rates and quasi-static conditions. The results show that the strength and compressive elastic modulus of these composites are more than the virgin epoxy samples. The fractured samples are observed in SEM and the micrographs are presented in Figure 1.10. From the SEM images, it can be observed that the porous surface resulted in improved mechanical interlocking and increased the energy required to deform the electrospun fiber loaded epoxy systems.

In a another study, functionalized core-sheath PAN/SBS electrospun fibers were prepared and their toughening effect was evaluated (T. Guo et al., 2014). They made these co-axial fibers with SBS as the core and PAN as the sheath by employing coaxial electrospinning. These fibers are subsequently functionalized using diethylenetriamine (amination). These functionalized fibers are incorporated in epoxy and toughening effect

is investigated. The results show that the SBS/PAN aminated fibers acted as better reinforcements when compared to PAN aminated fibers. In Figure 1.11, the impact energy results are presented. The impact energy (Charpy) of the composite samples increase with electrospun fiber loadings. An improvement of 150% is observed at 4 w% loading of core-sheath electrospun fibers. The results show that the rubbery core can absorb and dissipate more impact energy which is attributed to high impact resistance. The chemical bonding between the fibers and epoxy also contributed to better impact strength.

.

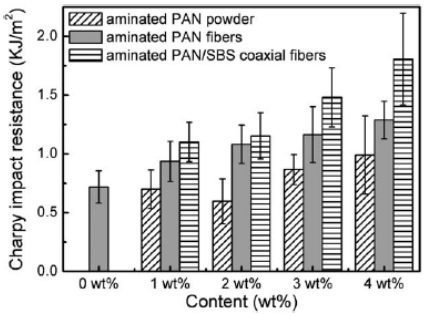

Figure 1.11: Effect of aminated PAN/SBS fiber, aminated PAN fiber, and aminated PAN powder on the Charpy impact strength of epoxy resin(T. Guo et al., 2014).

The effect of polymethyl methacrylate (PMMA) short nanofibers inside the epoxy thermosets was tested by Al-Assafi & Co-workers (Al-Assafi et al., 2016). PMMA nanofibers having an average diameters in the range 150-200 nm were procured. These mats were chopped into square pieces at cut size of 10mm. These chopped mats were added to Bisphenol A based epoxy resin and composites were made maintaining the fiber loading 0 to 5 w%. The composites were tested for their tensile and flexural properties to investigate the effect of fiber concentration. From the results, there is no noteworthy change in flexural properties but there is reduction in the tensile strength. They noted that no proper fiber/matrix interaction and porosity lead to this decrease. These results are in synchronisation with the other results, as the fiber decreased the mechanical performance. They concluded that a detailed study needs to be performed

and modifications made in the composite system to improve the adhesion between the fiber and matrix. The fractured surface of the PMMA loaded epoxy composites at 5 w% is presented in Figure 1.12.

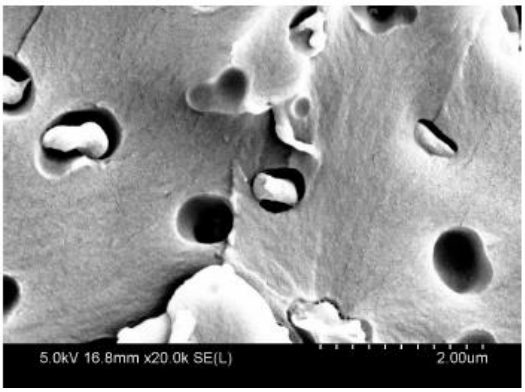

Figure 1.12: SEM Image of fractured samples at 5 w% loading(Al-Assafi et al., 2016).

Ahmadloo et al. (Ahmadloo et al., 2017) explored the use of nanofiber yarns in reinforcing epoxy composites. For this they used PA66 as the polymer precursor, they used formic acid as the solvent. For obtaining the yarn architecture, they used an adversely charged setup. The SEM images of PA66 nanofiber yarns at different magnifications are presented in Figure 1.13. After confirming the yarn structure, they introduced these yarns inside the epoxy resin and developed epoxy composites at a fiber loading from 0 to 3 w%, and investigated the overall mechanical properties from the results, in case of neat epoxy without any fiber complete failure was observed. But in the case of nanofiber yarn loaded epoxy samples, a plastic failure nature is observed. They confirmed that because of the presence of fiber yarns, a plastic work increased, which is not present in neat epoxy systems. Further, an improvement of 253% in the plastic work is noticed as the loading increased from 0.5 w% to 3 w%. The fracture toughness of these samples is tested and from the results a clear increase in the toughness of the fiber loaded samples are observed. As the yarn content increased until 3%, the plastic deformation in the samples increased, contributing to toughness enhancement. They

stated that increasing the fiber yarn loading leads to the overall improvement in plastic, elastic and total works. The load needed for crack to propagate also improved the fiber loading.

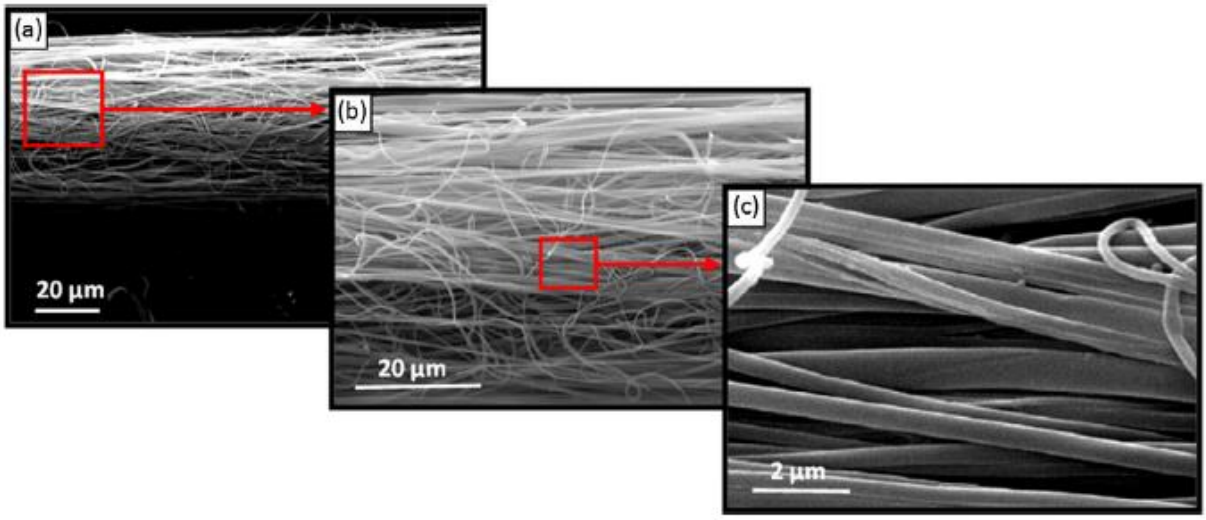

Figure 1.13: SEM micrographs of nanofiber yarns at magnification of (a) 625X,(b)1250X and (c)10000X(Ahmadloo et al., 2017).

In another work, cellulose nanofiber mat and their epoxy composites were prepared and the performance was investigated (Jahanbaani et al., 2016). Here, the authors used a new way of chemical treatment, subsequent electrospinning to prepare cellulose fibers. At first, the cellulose source wheat straw is subjected to chemical treatment like NaOH treatment (pretreatment), acid hydrolysis, alkali hydrolysis, followed by bleaching. After the complete removal of lignin and hemicelluloses, the cellulose nanofibers were prepared by using electrospinning process. Different solvent combinations like trifluoroacetic acid (TFA), TFA/methylene chloride, and sodium hydroxide/urea/thiourea was used to prepare spun fibers. Electrospun fibers with a mean diameter of 120 nm, without beads are produced with TFA solvent. Next, methylene chloride (5 w %) is added to the spinning solution (cellulose/TFA), and this resulted in

electrospun fibers of 150 nm average diameter. The microscopic observation of these fibers is presented in Figure 1.14.

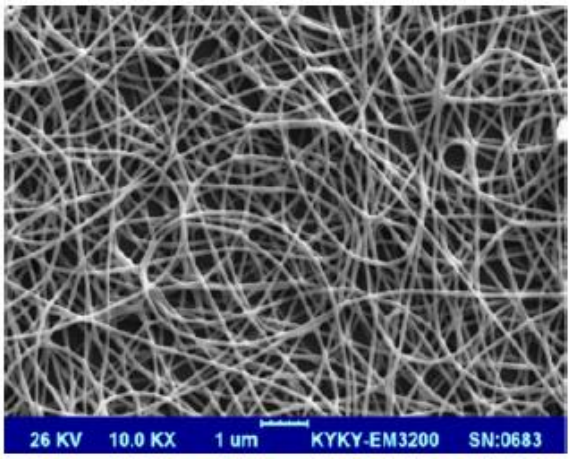

Figure 1.14: SEM image of electrospun cellulose nanofibers in cellulose/TFA solution (7.5 wt.%) with 5 wt.% methylene chloride(Jahanbaani et al., 2016).

These prepared cellulose fibers were kept in epoxy and laminated epoxy composites were prepared. Composites were prepared by using hand layup technique using epoxy as the matrix and cellulose microfiber as the reinforcement. These samples were tested for tensile performance, impact resistance and compared with neat epoxy samples. The overall properties of these laminated composites are presented in table 1.5. From the table, we can clearly see that fiber loaded samples have better mechanical performance than unloaded samples. The SEM images of the fractured samples were observed and we can notice that nanofiber layers handled the brittle epoxy because of good fiber-matrix adhesion, thereby contributing to reinforcement. Upon comparing cellulose microfiber mat laminates to electrospun nanofiber mats, the latter proved to be better because of high surface area.

Table 1.5: The tensile strength, elongation, and modulus of samples(Jahanbaani et al., 2016).

	Tensile (MPa)		Elongation (%)		Modulus(MPa)	
	Average	Standard deviation	Average	Standard deviation	Average	Standard deviation
Epoxy resin	88.6	1.29	0.82	0.02	10800.1	19.12
Microfiber laminated composite	94.2	1.48	0.86	0.04	11010.5	20.23
Nanofiber laminated Composite	117.3	2.90	0.96	0.01	12537.6	23.87

Aziz et al. (Aziz et al., 2021) prepared epoxy composites with electrospun carbon fibers as reinforcement and compared it with amine functionalized electrospun carbon fiber/epoxy composites. PAN polymer is used as the precursor polymer for carbon fibers. Electrospinning of PAN was done in DMF medium at 9 w%. After successfully electrospinning the PAN nonwoven mats, they were subjected to stabilization at 250 ˚C. These stabilized mats were then carbonized at a temperature of 1100 ˚C in the presence of nitrogen to obtain electrospun carbon fibers. In addition, these carbon fiber mats were acid functionalized using HNO_3 and amine functionalized (by employing Dicyclohexyl carbodiimide, N-hydroxysuccinimide, and ethylenediamine). Using these amine functionalized mats, epoxy composites from 0.5 to 10 w% is prepared, alongside neat carbon fiber/epoxy composites for comparison purpose. The composites were then investigated for their mechanical, thermal, and electrical performance. For 1 w% amine functionalized carbon fiber/epoxy samples, a 20% improvement in the glass transition temperature and 82% improvement in the storage modulus was observed. The improvement in the property is contributed to the better load transfer and interaction between the epoxy matrix and amine functionalized carbon fiber. This work signifies the

potential use of electrospun carbon fibers as composite reinforcements for multi-functional applications.

Ozden et al. (Özden-Yenigün et al., 2012), prepared a composite electrospun nanofiber from MWCNTs/P(St-co-GMA) combination. He used this fiber to reinforce epoxy and studied the properties of the resultant composites. The surface of the fibers were functionalized and MWCNTs were used as fiber reinforcements. These composite fibers were introduced into epoxy, expecting a better interaction of fibers with epoxy matrix as the fiber surface was functionalized with epoxy moieties. From the results, an overall 20% improvement in the flexural modulus was observed, which was from a combined contribution of inherent CNTs and better interfacial interactions. The dynamic mechanical storage modulus of fiber reinforced samples is presented in Figure 1.15 (a and b). When compared with the unloaded samples, fiber reinforced samples proved to have better storage modulus (in Figure 1.15 a). From Figure 1.15 b, the influence of CNT loading on the modulus is observed. The authors prepared high performance electrospun composite fiber/epoxy composites, and showed an excellent strategy to develop advanced epoxy composites. Few reports on electrospun fiber reinforced epoxy composites are presented in table 1.6.

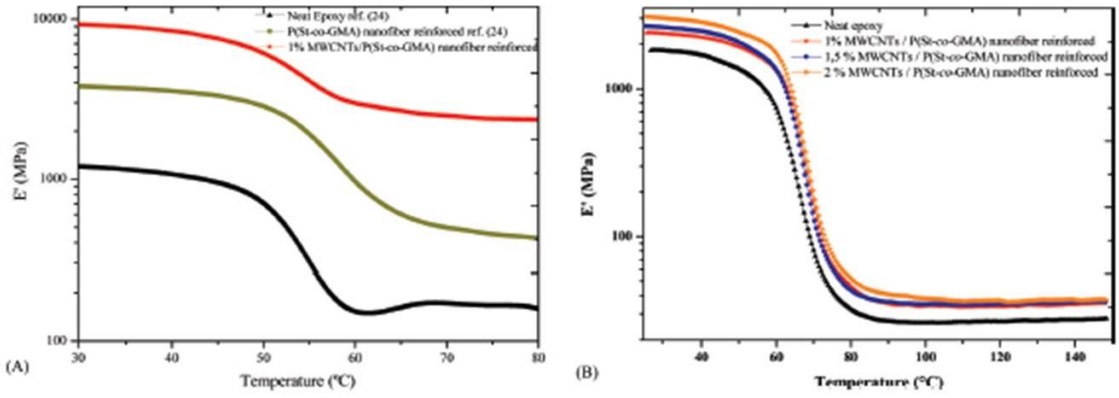

Figure 1.15: (A) Storage modulus vs. temperature measurements on nanofiber-reinforced materials (B) Storage modulus vs. temperature measurements on nanofiber reinforced hybrid materials(Özden-Yenigün et al., 2012).

.Table 1.6: List of electrospun fibers used to reinforce epoxy composites.(Rangappa et al., 2022)

S.No	Polymer fiber	matrix	Reference
1.	PEO	epoxy	(J.-R. Lee et al., 2004)
2.	PBI	epoxy	(J. s. Kim et al., 1999)
3.	Nylon 4,6	epoxy	(Bergshoef et al., 1999)
4.	P(S-co-GMA)	Araldite epoxy	(Ozden et al., 2010)
5.	Nylon 6,6	epoxy	(Borges et al., 2015)
6.	Nylon 4,6	Two component Phenolic epoxy	(Bergshoef et al., 1999)
7.	Nylon 6,6	Gr-epoxy	(Palazzetti et al., 2012)
8.	PC	Graphite/epoxy prepreg	(Sihn et al., 2008)
9.	Nylon 6,6	Epoxy /carbon	(Akangah et al., 2010)
10.	Nylon 6,6	Glass /epoxy	(Saghafi et al.,

			2014)
11.	Nylon 6,6	Aramid/epoxy	(Goodarz et al., 2017)
12.	PMMA	epoxy	(Iyengar et al., 2013)
13.	Nylon 6	Glass fiber/epoxy	(De Schoenmaker et al., 2013)
14.	Nylon 6,6	Carbon /epoxy	(Beckermann et al., 2015)
15.	PCL	Carbon epoxy	(J. Zhang et al., 2012)
16.	PAPBI/CNT-PA	epoxy	(Kausar, 2014)
17.	Electrospun carbon nanofibers	epoxy	(Q. Chen et al., 2014)
18.	PAN	Carbon/epoxy laminate	(Herwan et al., 2016)

For structural applications, till date, fiber reinforced composites are the best candidates to be used. As these composites are having less weight and high stiffness, these materials are mostly preferred. Even though fiber reinforced composites possess several comparative advantages, delamination is a major disadvantage (Daelemans et al., 2020). To solve this issue, electrospun fibers can be used as intermediate toughening materials. Daelemans and co-workers (Daelemans et al., 2016) proposed a multiscale toughening mechanism by employing electrospun fibers as intermediates in fiber

reinforced composites. They did multi-scale analysis at different levels, they are laminate level, matrix level, and interlaminar region level.

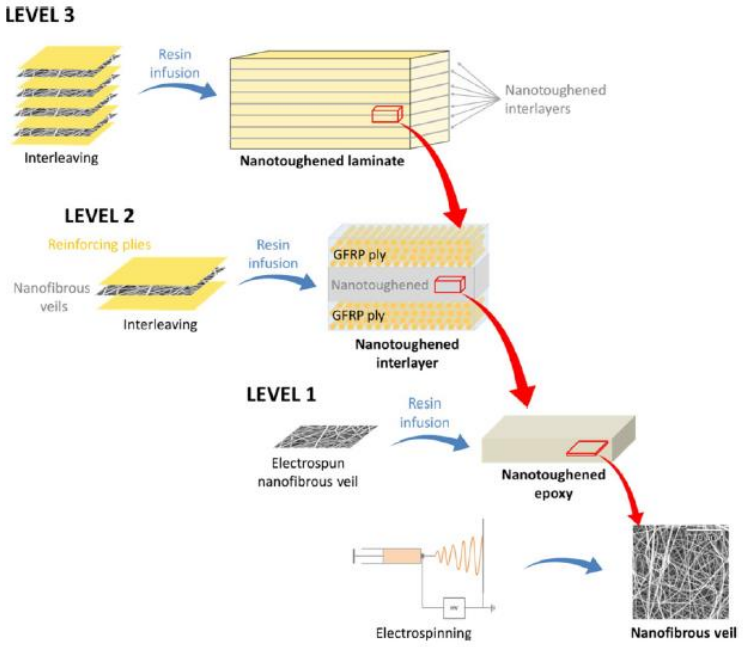

Figure 1.16: Multi-scale approach to study the performance of electrospun nanofiber interleaved composites(Daelemans et al., 2016).

The evaluation was done by using both PA6 fibers and PCL fibers. The schematic representation of the multiscale approach is presented in Figure 1.16. The mode I fracture toughness of the composites is presented in Figure 1.17. In the first stage (level 1), fracture toughness was significantly enhanced by nanofiber bridging and nanofiber yielding. This signifies the role of mechanical properties of electrospun fibers and their adhesion with matrix determines the fracture toughness. In the next stage (level 2), the delamination path was systematically analyzed. The interlaminar toughness is enhanced by the crossings in the interlaminar region. For a fully interleaved composites, the fracture mechanism in stage 3(level 3), is similar to stage 2 (level 2). The delamination growth was hindered by the formation of the interlaminar crossing. Along with this, the interlaminar crack in the nanotoughened interlayer provides local toughness, contributing to toughening effect. Thus a clear evaluation of multi-scale

approach is vital for investigating nanofiber interleaved composites and also helps us to design, damage resistant, novel and toughened structural composites.

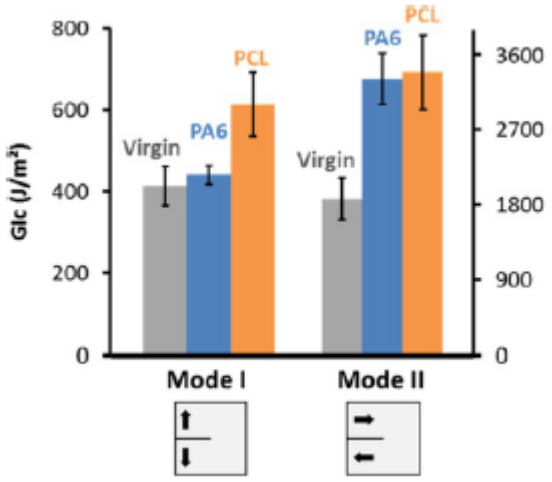

Figure 1.17: Mode I interlaminar fracture toughness of interleaved composites (Daelemans et al., 2016).

Electrospun styrene acrylonitrile (SAN) nanofibers were prepared by electrospinning technique and used for toughening fiber reinforced composites (Neisiany et al., 2018). Initially, using the electrospinning process, SAN fibers were directly spun on the carbon fabrics. The SEM investigations reveal that SAN fibers are smooth and bead free, with a average diameter of about 480 ± 102 nm. SAN fiber reinforced carbon/epoxy composites were prepared by vacuum assisted resin transfer molding (VARTM). From the results, the SAN nanofiber carbon/epoxy composites exhibited an improvement of 26% in flexural strength. The short beam shear strength was gained by 27% and impact energy absorption was gained by 8% for SAN loaded samples.

Goodarz et al. (Goodarz et al., 2017), investigated the role of graphene incorporated electrospun layers on the performance of fiber-reinforced epoxy systems. For this, they prepared electrospun graphene nanoplatelets (GNP)/nylon 66 mats and interleaved then in aramid fiber/epoxy composites. The nanofibers with 1 w% of GNP

loading is found to have good mechanical properties. The increase is attributed to both the thickness of nanofibrous webs and GNPs. They concluded that 35 and 17.5 µm are the optimum thickness for pristine and reinforced interleaves, respectively. They showed that compared to plain FRPs, the FRPs interleaved with composite electrospun fibers displayed better performance. Researchers developed multiscale composites by using electrospun carbon fibers as interlayers. Chen et al. (Q. Chen et al., 2011)., reported a work in which electrospun mats were used as interlayers and reported an interlaminar shear strength improvement of 86%. In other work, these electrospun fibers are attached to carbon fabrics on the surfaces and composites are developed (Q. Chen et al., 2013). They investigated the out-of-plane mechanical performance of prepared composites, and reported that these composites are found to have comparative behavior to traditional composites.

1.3. Electromagnetic Interference Shielding

At present, we are all living in a technological era, where our surroundings are full of electromagnetic radiations (EM). As the use of electronic devices and gadgets has increased, the EM waves associated with them too increased rapidly. This explosive growth resulted in an alarming situation, which is electromagnetic pollution, termed as electromagnetic interference (EMI). EMI is a condition in which, unwanted electromagnetic waves from a primary source interacts with a secondary electronic device and cause interference. This interference is not only deteriorating the function of the secondary device, but also reportedly cause damage to living beings as well. This situation is a matter of concern and across the globe many researchers are actively working to developing advanced materials that can be effectively used to shield these waves and diminish its harsh effects. (Deeraj et al., 2020; Kondawar et al., 2020; L. Zhang, 2014).

The phenomenon in which, appropriate shielding material is used to prevent the incoming electromagnetic waves to penetrate through them, is called electromagnetic interference (EMI) shielding. This shielding can happen via absorption of waves or reflection of the waves. In other words, these shielding materials obstruct the electromagnetic waves by acting as barrier, by either reflecting or absorbing, due to their intrinsic electrical and magnetic characteristics. The type of material, conductivity, geometry dictates the intensity of reflection and absorption, of that specific material. EMI waves are classified based on their frequency modes. EMI shielding materials must be suitably prepared based on their frequency range, as EMI can be created by EM waves of any frequency (Joshi et al., 2015). However, the main focus is on the radio wave and microwave frequency ranges. The electromagnetic frequency spectrum is depicted in Figure 1.18.

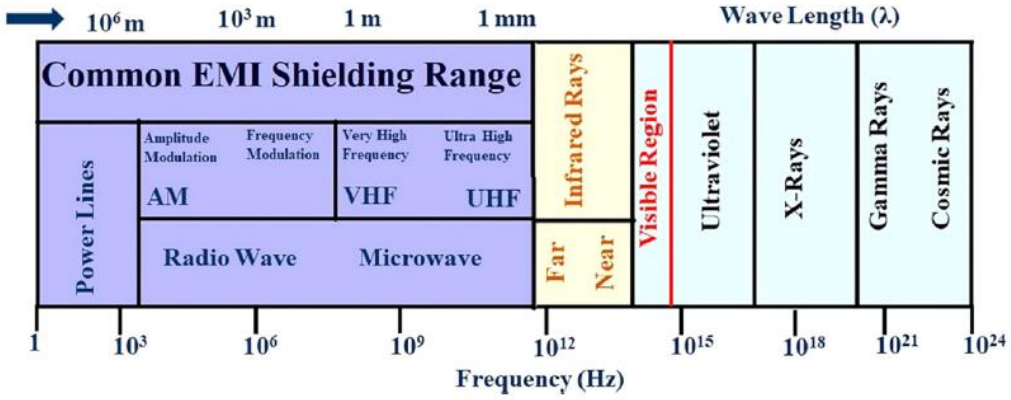

Figure 1.18: EM spectrum (Tong, 2016, G. K. Sharma et al., 2021).

The ability of the material to attenuate electromagnetic waves is defined by the term, shielding effectiveness (SE). it is expression in the terms of decibels (dB), as it is a logarithmic ratio of powers. Higher the value of SE, the more efficient is the shield for EMI shielding. For commercial applications, a shield material should have an effectiveness of minimum 20 dB (which corresponds to 99% shielding efficiency).

For a given material, its total shielding effectiveness (SE_T) is the aggregate sum of its shielding effectiveness by absorption (SE_A), shielding effectiveness by reflection

(SE_R), and shielding effectiveness by multiple reflections (SE_{MR}) (equation 1.1). Generally, in cases where SE_A is greater than 10 dB, the contribution of SE_{MR} is neglected (Gelves et al., 2011; Ohlan et al., 2008; W.-L. Song et al., 2014; Z. P. Wu et al., 2011).

$$SE_T = SE_A + SE_R + SE_{MR} \quad (1.1)$$

Shielding effectiveness by reflection (SE_R) is related to the impedance mismatch that is present in between the electromagnetic wave and the shield. This mechanism occurs in the materials that have free charge carriers and high electrical conductivity. The relation of SE_R in terms of electrical conductivity is given in equation 1.2(Saini et al., 2011).

$$SE_R = -10 \log_{10} (\sigma_T / 16\omega\varepsilon_0\mu) \quad (1.2)$$

Here, σ_T denotes the total conductivity and μ relates to permeability. From the above relation, we can clearly observe the relation between the conductivity-permeability ratio to the EM wave reflection. So, we can say that the non-magnetic materials manifest better reflection than magnetic materials. However, in the case of nanocomposites, this phenomenon is different. In the case of polymeric composites, effective permittivity is important; the SE_R^2 can be calculated by using permittivity in place of conductivity in equation 1.2. The absorption of the material is mainly due to the losses generated in the material, when EM wave passes through it. Electromagnetic waves consist of magnetic and electrical fields, when these waves are passed through a material with dipoles, these result in magnetic losses and dielectric losses. So, a shield material should contain magnetic and electrical dipoles in order for the shield to absorb the EM waves. The intensity of EM waves decay exponentially, while they are propagating through the material, so thickness of the material is a very important consideration. The shielding effectiveness by absorption is given by equation 1.3.

$$SE_A = -8.68\ t\ (\sigma_T\ \omega\mu/2)^{0.5} \quad (1.3)$$

Here, t denotes the shield thickness. From the relation, we can see that SE_A is governed by both the permeability and permittivity of the material, as absorption effectiveness depends on the product of both.

The term skin depth (δ) is expressed as the thickness of the shield, where the intensity of absorbed wave drops to 37% or 1/e (1/e= 0.37). The expression for the calculation of skin depth is represented in equation (1.4).

$$\delta = 1/\ (\boldsymbol{\pi}\ f\sigma\mu)^{0.5} \quad (1.4)$$

where f is the Electromagnetic wave frequency, when the shielding material is having a thickness of less than skin depth, the waves will reflect from multiple boundaries inside the shield material. The relation for estimating the shielding effectiveness by multiple reflections is presented in equation (1.5)

$$SE_{MR} = 20\ \log_{10}\ (1-e^{-2t/\delta}) \quad (1.5)$$

The multiple reflections are significant of materials with dispersed fillers and structures with multiple boundaries, and is dependent on the absorbing ability of the material. The shielding ability via multiple reflections can be neglected when the shielding is having very high SE_A and shield thickness. The EMI shielding effectiveness of the material is expressed as the logarithmic ratio of incoming power to the outgoing power. This shielding effectiveness can be defined using equation (1.6), (1.7) and (1.8);

$$SE(dB) = 10\log_{10}\ (P_T/P_I) \quad (1.6)$$

$$= 20\log_{10}\ (H_T/H_I) \quad (1.7)$$

$$= 20\log_{10}\ (E_T/E_I) \quad (1.8)$$

Where P_T and P_I denotes the transmitted power and incident power; H_T and H_I represents transmitted magnetic field strength and incident magnetic fields strength, and; E_T and E_I relates to transmitted electric field strength and incident electric fields strength. Both the medium and impedance governs the intensity of the reflected waves and absorbed waves of the shield.

The ratio of the intensity of electric field to magnetic field is expressed by wave impedance and is denoted by '**Z**'. Based on the distance between the material shield and the EM wave source, the electromagnetic shielding region is classified as far field shielding region and near field shielding region. When it comes to far field region, the distance between the EM source and the shielding material is more than $\lambda/2\boldsymbol{\pi}$, and the wave impedance is equal to the intrinsic impedance, which is equal to 377 Ω. In this case, the plane wave exists and plane wave theory is applied in this case. When it comes to near field region, the distance between the EM source and shielding material is less than $\lambda/2\boldsymbol{\pi}$. In this region, the wave impedance is not equal to the intrinsic impedance, which is not equal to 377 Ω. In this region, the wave front is not parallel to the material shield and is curved. In the near field region, the electric field and magnetic fields dominates the electromagnetic waves, and the electromagnetic shielding theory depends on the contribution of electrical and magnetic fields (Geetha et al., 2009; Kumari et al., 2020).

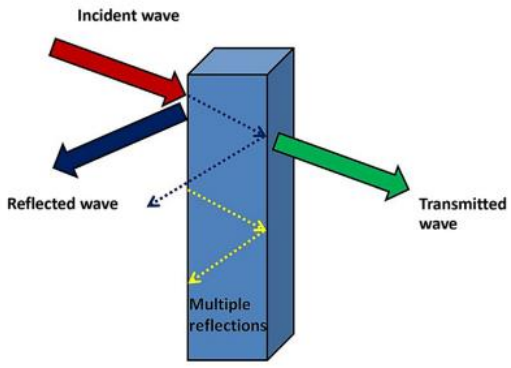

Figure 1.19: Schematic representation of the EMI shielding mechanism (Deeraj et al., 2020).

The scheme of EMI shielding mechanism by the shielding material is presented in Figure 1.19. An instrument called network analyzer is user to measure the shielding effectiveness of any material. This instrument will give the absorption loss and reflection loss of the test material. The performance of the shielding material is measured by four methods. They are

- Open field or space method
- Shielded room method
- Shielded box method and
- Co-axial transmission line method.

In case of scalar network analyzer, the amplitude of only signals can be obtained, but, vector network analyzer (VNA) gives both amplitude and signal phases. Thus, the instrument VNA can give information about the complex properties like permittivity and permeability of the test material. Usually, S parameters are used to get details of absorption, transmission and reflection coefficients of the test materials. The complex scattering parameters are

- S_{21}(forward transmission coefficient)
- S_{11} (forward reflection coefficient)
- S_{12}(reverse transmission coefficient)
- S_{22} (reverse reflection coefficient)

The equations corresponding to absorption, transmission and reflection coefficients are represented in equations (1.9), (1.10) and (1.11)

$$\text{Reflection coefficient}(R) = |S_{11}|^2 = |S_{22}|^2 \quad (1.9)$$

$$\text{Transmission coefficient } (T) = |S_{21}|^2 = |S_{12}|^2 \quad (1.10)$$

$$\text{Absorption coefficient } (A) = 1-T-R \quad (1.11)$$

1.3.1. Materials for EMI Shielding

At present, vigorous research is going on to develop novel and efficient EMI shielding materials by many researchers. Electromagnetic interference shields are the materials that reflect or absorb the electromagnetic waves, but nowadays, most of the research is on electromagnetic wave absorbers. As for wave reflectors, the dominant shielding occurs because of reflection and these reflected waves can cause 'Secondary EMI' elsewhere, that is not recommended. So, to completely solve the issue of EMI, wave absorbers mostly recommended their dominant shielding mechanism as via absorption. In Figure 1.20, a model representing the wave transmission is presented, to show the dependence of wave transmission on material properties.

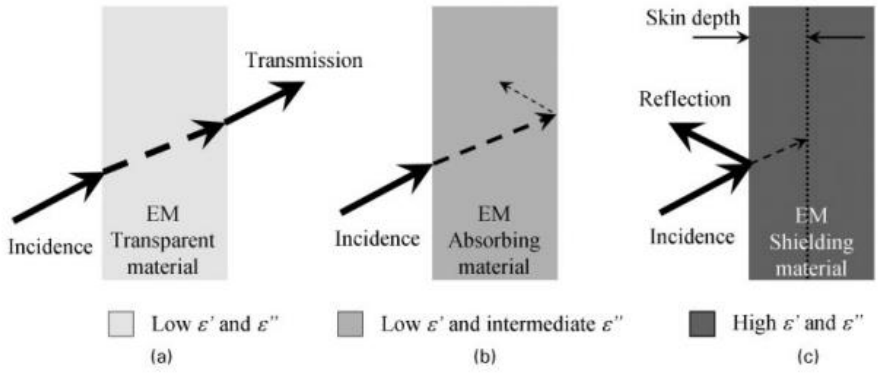

Figure 1.20: Transmission model for materials with different complex permittivities.(Yin et al., 2014).

Generally, materials that offer high electrical conductivity, complex microwave properties, and high saturation magnetization are required to attenuate electromagnetic waves and provide shielding. Based on the requirement and the application, EMI shielding materials are designed and engineered (D. Chung, 2001; D. D. L. Chung, 2000; Shacklette et al., 1992). Absorption and reflection are the main shielding mechanisms, whereas in case of thinner shields, multiple scattering plays a dominant role (Al-Saleh et al., 2013; Saini et al., 2009). Reflection of waves happen due to the impedance mismatch between the shield and the air (X. Guo et al., 2009; Meena et al.,

2010; K.-Y. Park et al., 2006; Saini et al., 2012). Due to the earlier mentioned reasons, the reflection mechanism for shielding is not preferred. So, the requirement is to penetrate the electromagnetic waves by matching the impedance between the air and the shield, for which the material characteristics like permittivity and permeability plays a major role (Cao et al., 2010; Z. Liu, Bai, Huang, Li, et al., 2007; Z. Liu, Bai, Huang, Ma, et al., 2007; Shi et al., 2008). The major selection is based on materials that can attenuate electromagnetic waves by magnetic and dielectric losses. Keeping this in mind, many materials were processed with different functional and design criteria's. Electrically conducting materials are used as EMI shields (Bigg, 1984; Colaneri et al., 1992; Simon, 1981). Due to their complex and dielectric behaviors, conducting carbon materials, ceramics, ferrites, metals are often used for shielding. The materials used for EMI shielding can be grouped as;

- Thermoplastics with additives
- Thermosetting with additives
- Elastomers with additives
- Bio-derived carbon materials and biocomposites with additives
- Polymer blends with suitable additives
- Conducting polymer composites
- Hybrid polymer composites
- Conducting carbon materials
- Ceramic materials
- Metals and alloys
- Textile based materials and
- Cement based materials.

1.3.2. Electrospun Fibers for EMI Shielding

Electrospinning can be regarded as the most versatile process for the fabrication of novel materials with unique morphologies that finds vast applications; especially in EMI shielding. Electrospun fibers possess one-dimensional slim structure and interconnectivity that helps to reflect and absorb electromagnetic waves, contributing to electromagnetic interference shielding. The incorporation of suitable fillers into electrospun fibers pave path for developed conducting three dimensional pathways improving the overall conductivity and thereby enhancing the EMI shielding characteristics. The increment in EMI shielding can be contributed to interfacial polarization between the electrospun fibers and the incorporated fillers. In Figure 1.21, a schematic of nanofiller incorporation in electrospun fibers for EMI shielding is presented.

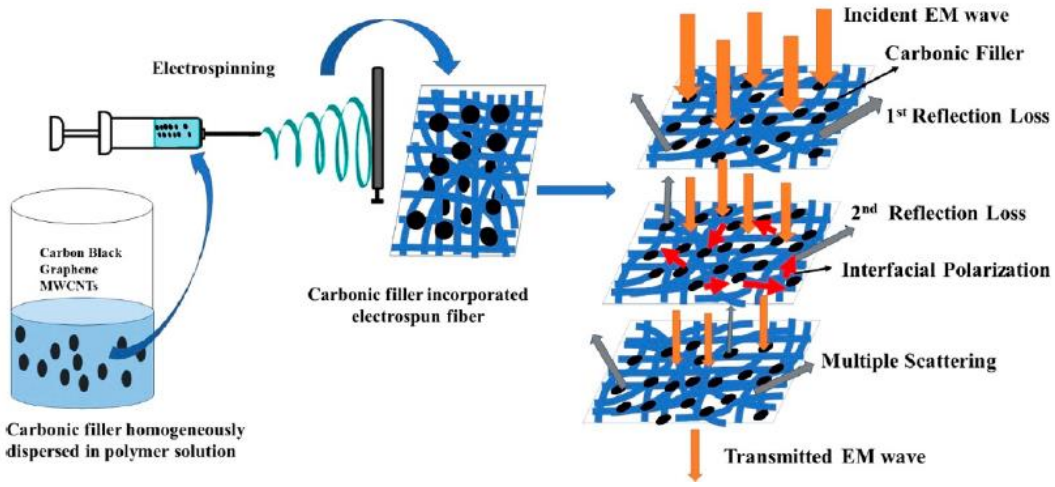

Figure 1.21: Carbonic filler incorporated electrospun fiber for EMI shielding(G. K. Sharma et al., 2021)

Electrospun fibers are incorporated with carbonaceous fillers like carbon nanotubes (Salimbeygi et al., 2013), graphene (Y. Guo et al., 2019), carbon black (Im et al., 2009); metal additives (H. Ji et al., 2018), metal-oxide materials (Nakhaei et al., 2016), and metal carbides (H. Guo, Wang, et al., 2021) for using them in EMI shielding application. Conducting polymers were electrospun into nonwoven mats and used as

shields (Im et al., 2010b). Recently, MXenes loaded electrospun mats are also used for EMI shielding purpose (Cui et al., 2019). In Figure 1.22, a cartoon of different fillers which are incorporated in electrospun fibers for EMI shielding application is depicted.

Most of the polymers are non-conducting or non magnetic when used alone. So we are introducing EM wave active particles in them for employing them in shielding. Another way of using electrospun polymer fibers for EMI shielding is by carbonizing them to carbon nanofibers by thermal treatment. These electrospun carbon fibers are attractive materials benefitted by their electrical conductivity. These carbon fibers can be used as such or coated with suitable fillers or incorporated with fillers to make them more beneficial for EMI shielding applications.

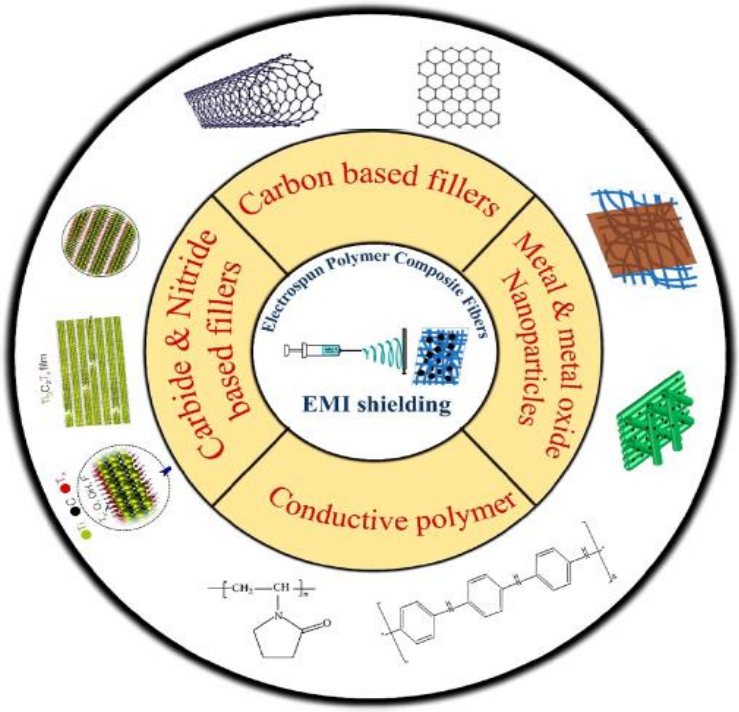

Figure 1.22: Fillers used in electrospun polymer composite fibers for EMI shielding.(G. K. Sharma et al., 2021)

1.3.3. Electrospun Carbon Fibers (Derived from Precursor Polymer fibers) and Applications

Carbon fibers prepared from melt spinning played an important role in the overall development of carbon fibers since 1960. These fibrous carbon materials are formed by using polyacrylonitrile, phenolic resins and pitch as the main precursor materials. Later, vapor grown carbon fibers with unique characteristics were produced from chemical vapor deposition (CVD) process. At present, carbon nanofibers (CNFs) produced via electrospinning followed by carbonization is considered best, as it can give multifunctional carbon materials. Even though carbon nanotubes are considered as best carbon materials owing to its properties, carbon nanofibers have noteworthy advantages than carbon nanotubes.

Firstly, carbon nanofibers are economic and easy to fabricate and secondly there is a chance to carefully design and control the morphology and microstructure. The inner surface of the carbon fibers can be made hollow or porous by altering the spinneret setup (Chan Kim et al., 2007; Eyal Zussman et al., 2006). The microstructure of the fiber can be controlled by catalytic graphitization additives or changing the carbonization temperatures (Hong et al., 2007; B.-S. Lee et al., 2020; Shin et al., 2016). Compared to traditional carbon fibers, carbon nanofibers from electrospinning exhibit different material characteristics because of the size effect and high surface to volume ratio (K. J. Lee et al., 2010). By controlling the solution and electrospinning parameters, the diameter of CNFs can be obtained from nanometer to sub-micron range (Yang Liu et al., 2009). In Figure 1.23, generally used carbon precursors are presented.

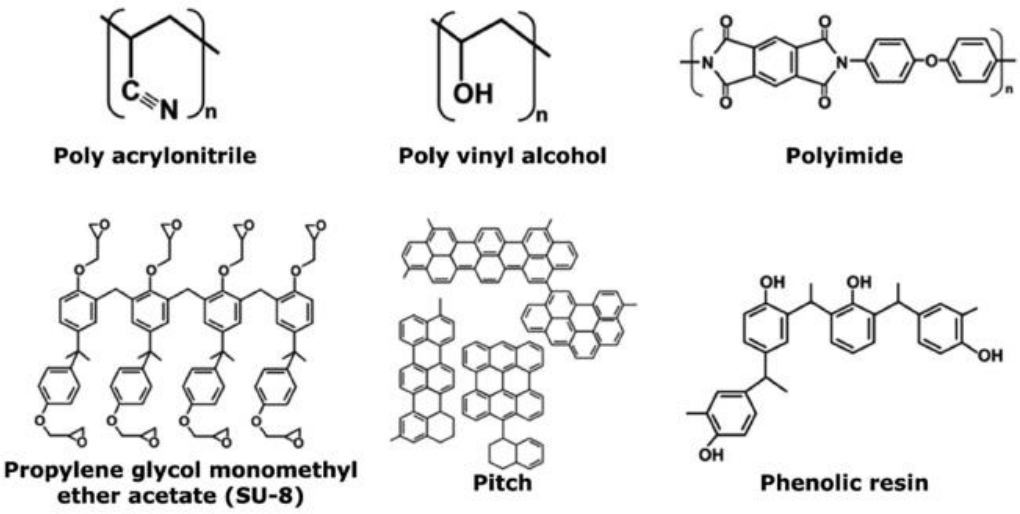

Figure 1.23: Frequently used carbon nanofiber precursors (B.-S. Lee et al., 2020).

In 1999, Chun et al. (Chun et al.) first reported thermally treated electrospun carbon nanofibers. In 2003, Kim et al.(C Kim et al., 2003) used these carbon nanofibers for supercapacitor electrode applications. Since its first report, the research and publications regarding the formation and applications of carbon nanofibers kept on increasing exponentially. At present, a total of more than 1800 research articles are published and more than 150 research groups are working with carbon nanofibers with different research targets (B.-S. Lee et al., 2020). Figure 1.24, gives information in the form of a histogram where complete listing of publications related to electrospun carbon fibers is done

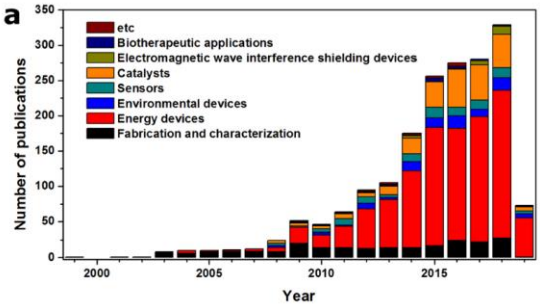

. Figure 1.24: Statistical analysis of 1828 publications related to electrospun carbon nanofibers. (a) Complete listing. (B.-S. Lee et al., 2020)

All the electrospinnable polymers cannot be used as carbon precursors for preparing carbon nanofibers. Only few polymers, that can form graphitic or turbostratic microstructures can be used for formation of carbon nanofibers. Some precursor molecules have linear structure and converted to aromatic structures via a thermal treatment. The sources like PAN, polyamide, silk and PVA falls in this category (Barakat et al., 2012; Karacan et al., 2018; Padmavathi et al., 2013; Q. Wang et al., 2017). Some precursors have aromatic backbones in their structure and form the graphitic or turbostratic structures during the heat treatment process. The sources like polyimide, phenolic resins and pitch fall in this category (Bui et al., 2009; Y. Huang et al., 2009; K. Yang et al., 2003). The other precursors used for preparation of electrospun carbon nanofibers are PVDF (Y. Yang et al., 2011), PVP (Dong et al., 2016), melamine (Yun et al., 2013), coal (M. Guo et al., 2015), tar (K. Song et al., 2015), propylene glycol mono methyl ether acetate (PGMEA; SU-8) (C. S. Sharma et al., 2010), cellulose, and lignin (Kumar et al., 2019).

The preparation of electrospun fibers from precursors involve three main steps, they include three steps (a) spinning step, (b) stabilization step and, (c) carbonization step. The typical process of PAN to carbon fiber along with the structure formation is illustrated in Figure 1.25. In the case of PAN, first the polymer is dissolved in a suitable solvent, and by optimizing the electrospinning parameters, these nonwoven polymer mats are prepared. In the later stage (stabilization), these mats are thermally treated at a temperature range between 200 °C to 350 °C, to obtain a ladder molecular structure. This ladder structure is formed due to the dehydrogenation and cyclization reactions that occur simultaneously. This can be confirmed by conversion of white PAN mat to darkish brown or black color. This step is called pre-carbonization step which is followed by subsequent carbonization at high temperatures. Carbonization is an important step usually taking place from 600 °C to 1500 °C in inert atmosphere, which transforms the pre-carbonized fiber to graphitic structures. This steps makes the stabilized fiber undergo crosslinking condensation and other chemical reactions and

results in the formation of integrated aromatic structure, forming a disordered graphitic carbon fiber. In order to improve the performance of carbon fiber, graphitization can be done at very high temperatures > 2000 ℃, to get fibers with better graphitic structures.

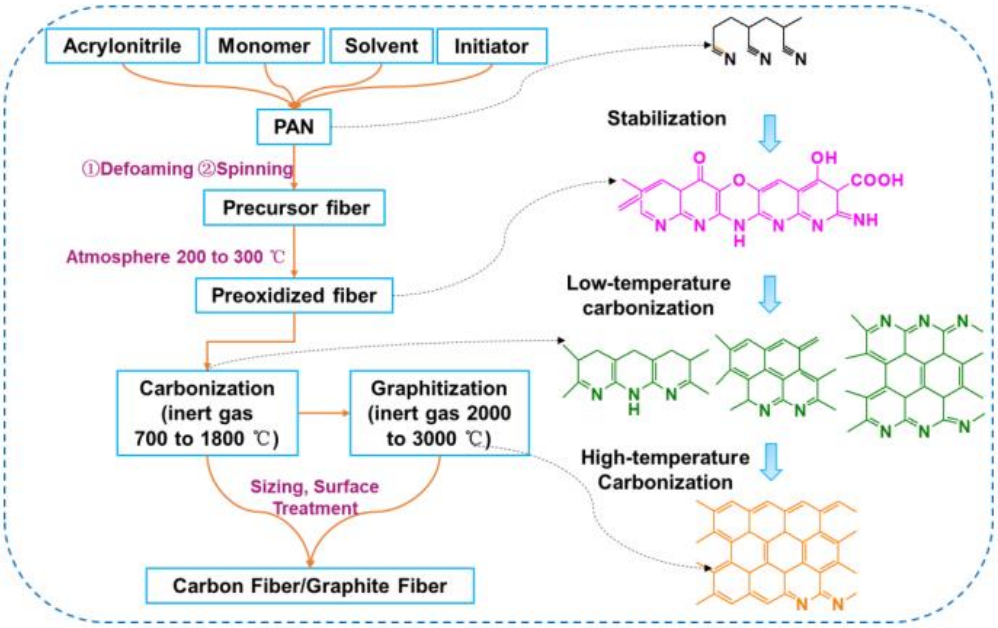

Figure 1.25: Carbon fiber production from PAN polymer (Y. Xu et al., 2020).

The properties of prepared carbon fibers generally depend on carbonization temperature, holding time and heating rate. Usually, high carbonization temperature, low heating rate and high holding time is preferred to produce carbon nanofibers with better quality. The order of importance among them is given as; heating rate > carbonization temperature > holding time (X. Ma et al., 2011; Y. Xu et al., 2020).

Morphology of carbon nanofiber reveals that they have sp^2 hybridization with turbostratic structures that falls in between amorphous structures and graphitic structures. Because of the microstructures, the properties of single CNF is equal or superior to amorphous carbon and lower to crystalline carbon. The electrical conductivity of PAN based CNFs falls between 1.95 to 7.69 S cm^{-1} and a thermal

conductivity of 0.012 W m^{-1} K (at 25 ˚C) is noticed (B.-S. Lee et al., 2020; B. Wang et al., 2011). The mechanical strength of CNFs is observed from carbonization temperature range of 800 ˚C to 1700 ˚C. When temperature increased from 800 ˚C to 1400 ˚C, an increase from ≈1.86 GPa to ≈ 3.52 GPa was observed. However, as the temperature increased to 1700˚C from 1400˚C, the mechanical strength decreased to ≈ 2.05GPa. This decrease is attributed to micro structural mismatch in-between the amorphous and crystalline and phases (Arshad et al., 2011). The microstructure and performance of CNFs can be tuned by micro structural tuning, surface tuning and cross sectional tuning of carbon nanofibers. The carbon nanofibers are incorporated with various non carbon fillers, metallic fillers, and carbonaceous fillers to increase their specific performance. The type of fillers, the loading and the morphologies of the fibers contribute to the overall applications of CNFs. In Figure 1.26, the cross sectional images of carbon nanotubes are presented.

Due to their distinctive characteristics, carbon nanofibers find applications in various fields. These fibers are used in energy storage and energy conversion, adsorption, catalysis, environmental devices, sensors, biotherapeutic applications, EMI shielding applications, multifunctional composites etc. There is a lot of potential to modify and manipulate the morphology, microstructure and properties of carbon nanofibers depending on the target applications. These CNFs are promising next generation materials with a lot of scope and potential in material science.

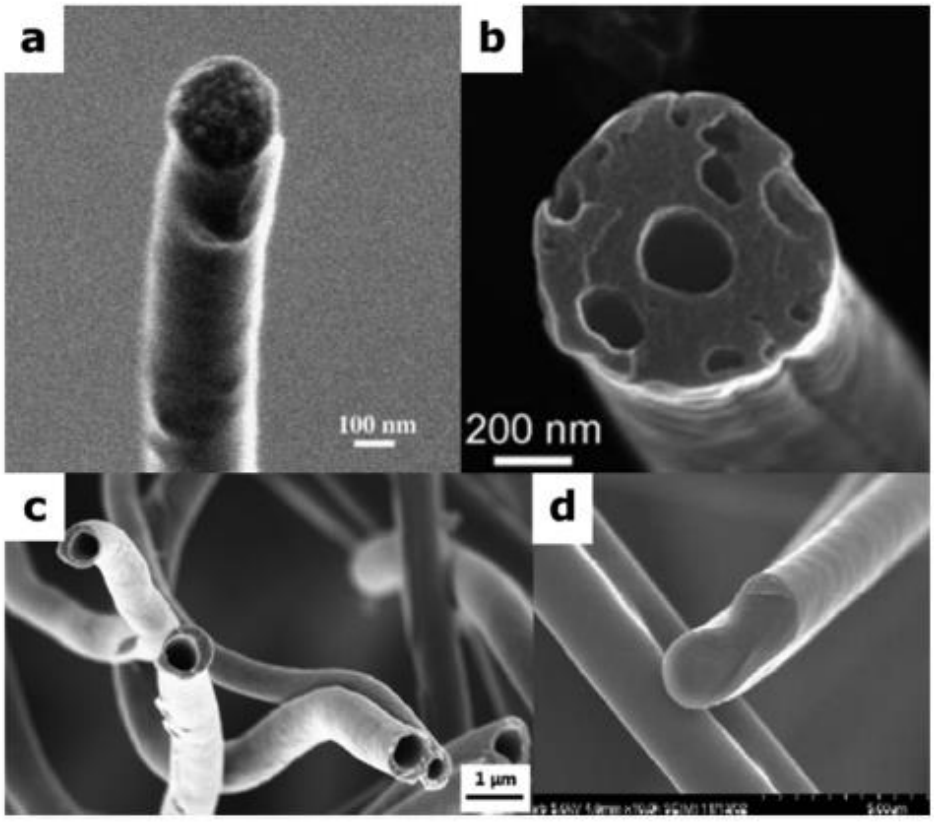

Figure 1.26: Cross-sectional scanning electron microscope images of various carbon nanofibers (CNFs). Circular or elliptical cross-sections: (a) solid CNFs (E Zussman et al., 2005) ,(b) Porous CNFs (Chan Kim et al., 2007), (c) Hollow CNFs (B.-S. Lee et al., 2012), (d) Cocoon-like cross-section of pitch-based CNFs (S. H. Park et al., 2003). (B.-S. Lee et al., 2020),

1.3.4. Electrospun Carbon Fibers (Derived from Precursor Polymer fibers) for EMI shielding

Electrospun carbon fibers find an excellent role in EMI shielding due to their ease of preparation, high conductivity, chemical inertness and environmental friendly nature (Inagaki et al., 2012). For EMI shielding, pure carbon fillers as well as composite carbon fibers can be used, where the latter is benefitted by significant mechanical

performance and enhancement. The common fillers used for making composite carbon fibers are electrically conductive fillers, magnetic fillers and ceramic fillers (H. Guo, Chen, et al., 2021). Bayat et al.(Bayat et al., 2014) in their work investigated the EMI shielding of pure carbon fibers and compared them with hybrid multi-functional Fe_3O_4/ carbon nanofiber composites. For this they used PAN as the carbon source and Fe_3O_4 (20-30 nm) nano particles, and followed electrospinning-stabilization-carbonization strategy for making composites. The carbonization was done at 700 °C and 900 °C. The results show that the electrical conductivity and EMI shielding behavior increased with increase in carbonization temperature (in Figure 1.27 a).

The Fe_3O_4 incorporated composites were prepared by maintaining its loading at 3 and 5 w% respectively. From the results, we can see that the SE of the composites increased with Fe_3O_4 loading and reached a maximum of 67dB, for composites of 5 w% Fe_3O_4 loading and 0.7mm thickness. The increment in the EMI SE is contributed to inclusion of magnetite filler inside conducting matrix which increased both the magnetic loss and dielectric loss in the material.

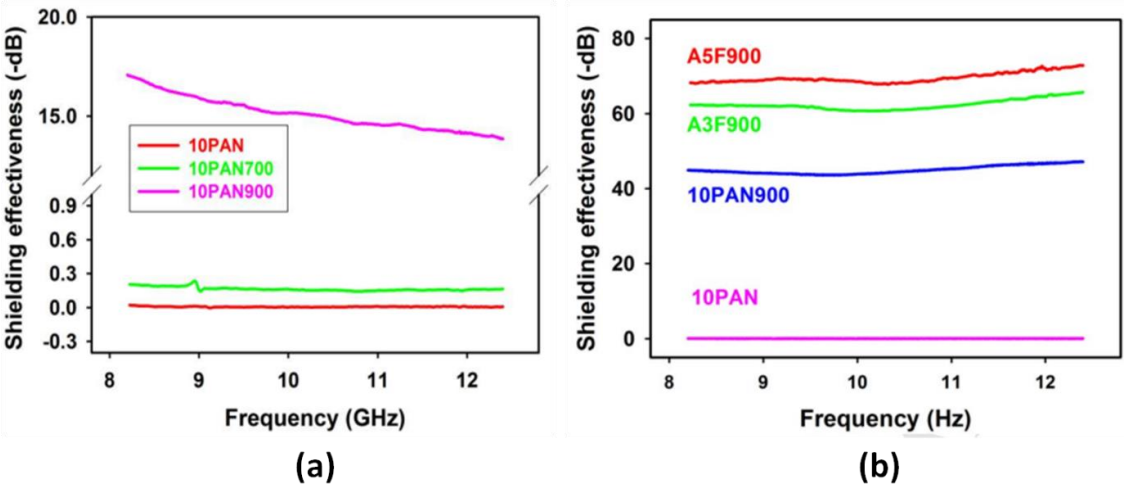

Figure 1.27: EMI SE of (a) PAN derived CNFs and (b) Fe_3O_4 incorporated CNFs.(Bayat et al., 2014)

In another work, carbon black loaded electrospun carbon fibers were fabricated (Im et al., 2009). For increasing the adhesion and dispersion, the carbon black was fluorinated and then used in PAN/DMF solutions. These solutions are electrospun and heat treated to obtain nano sized carbon fibers. From the results, the role of fluorination reaction in improving the electrical conductivity and EMI shielding effectiveness is observed, as there is better adhesion between the carbon black and carbon fibers. They reported an overall electrical conductivity of 38 S/cm and EMI shielding effectiveness of 50 dB for the prepared materials. In other work, an EMI shielding effectiveness of 20 dB is reported for carbon nanofibers heat treated at a high temperature of 2100 $^{\circ}$C (Im et al., 2011).

Chen et al.(I.-H. Chen et al., 2010) prepared carbon nanotubes incorporated carbon fibers via electrospinning and carbonization and studied its EMI shielding performance. For this they prepared acrylonitrile grafted CNTs and mixed them in PAN/DMF combinations for electrospinning. From the results, they concluded that these prepared carbon nanofibers displayed a low sheet resistance of 8Ω/sq and an EMI SE of 20 dB. In another work, composite carbon nanofibers with Fe_3O_4 were prepared and their role as microwave absorber was investigated (T. Zhang et al., 2013). For this they used a combination of PAN, DMF and acetyl acetone iron. The resultant carbon fibers have diameters in the range of 200 and 300 nm. The results show that there is enhancement in the magnetic properties and electrical properties, thereby enhancing the microwave adsorption property.

Song et al. (W.-L. Song et al., 2014) in their work prepared a novel all carbon CNF- graphene sheet- CNF heterojunction for efficient EMI shielding. In their work, they introduced graphene nanosheets inside the PAN fiber while electrospinning. These graphene sheets got attached to the fiber surface and these fibers were carbonized. The carbonization at 1000 $^{\circ}$C in nitrogen atmosphere, lead to the conversion of PAN to carbon nanofibers, finally leading to the generation of CNF-graphene sheet-CNF

heterojunctions. The scheme describing the formation of these heterojunctions is presented in Figure 1.28 a. The SEM images of neat carbon nanofibers show a smooth structure (in Figure 1.28 b), while the formation of heterojunctions increased with the graphene nanosheet loadings. In Figure 1.28 c & 1.28 d, the SEM images showing the formation of these heterojunctions are presented. The graphene loading in Figure 1.28 c is 17.2 w % and Figure 1.28 d is 31.9 w %.

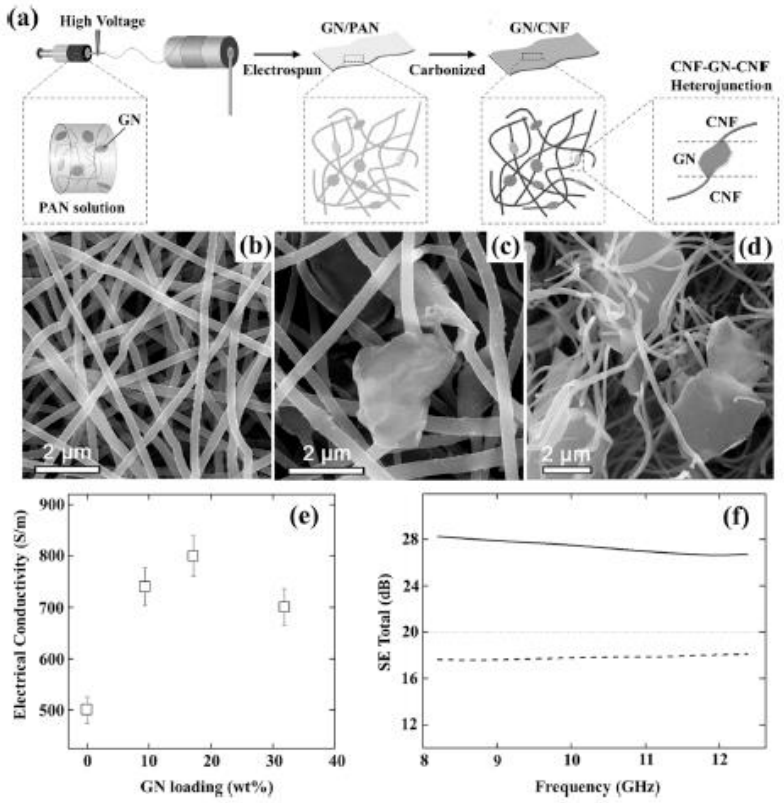

Figure 1.28: (a) Scheme for fabricating flexible networks and CNF- GN-CNF heterojunctions by electrospinning. SEM images of neat CNF networks (b) and GN/CNF composite networks with 17.2 wt%, 31.9 wt% GN (c and d). (e) Electrical conductivity of the samples with different GN loadings. (f) Total SE of the GN/CNF composite networks with 17.2 wt% GN (solid) were calculated based on the performance in neat CNF networks (H. Guo, Chen, et al., 2021; W.-L. Song et al., 2014)

In Figure 1.28 e, the electrical conductivity of prepared fibers is presented and we can observe that the conductivity of GN loaded samples at 17.2 w % performed well compared to unloaded samples and reached a value of 800 S/m, which is because of the formation of heterojunctions, that act as interface modifiers, thereby enhancing the property. For 31.9 w % graphene loaded samples, the conductivity decreased because of fiber fracture, due to excess graphene loadings. The EMI SE of these samples were tested and the results are presented in Figure 1.28 f. From the results, a total shielding effectiveness of almost 25-28 dB is observed which is 50-60 % more than the pure carbon nanofibers, at a sample thickness of 0.22–0.27 mm. So the authors concluded that these flexible all carbon systems are potential EMI shielding materials as they are having good SE and slim structure. They also forecasted that these materials play an important role in portable and flexible electronic devices.

In another work, the electrospun carbon fibers with Fe_2O_3/$BaTiO_3$/MWCNT were prepared for investigating the electromagnetic shielding performance (Im et al., 2010a). In this work, PAN/DMF solutions were prepared at 10 w% and additives FB (Fe_2O_3 and $BaTiO_3$) and FBC (Fe_2O_3, $BaTiO_3$ and MWCNTs) were added and electrospun to form fibers. In Figure 1.29 a & b, the SEM images of FB and FBC samples are presented, the average diameters of FB and FBC fibers are found to be 220 ± 70 nm and 280 ± 80 nm respectively. The electrical conductivity of FB and FBC samples are found to 3 S/m and 25 S/m, which indicates the positive role of CNTs in enhancing the conductivity. The EMI SE graph of FB and FBC samples are presented in Figure 1.29 c, which shows the high SE of these samples. An average of 37 dB is observed for samples added with Fe_2O_3, $BaTiO_3$ and MWCNTs, due to the enhanced permittivity and permeability. These authors recommended that the presence of additives inside carbon nanofibers is a potential strategy to developed novel EMI shielding materials.

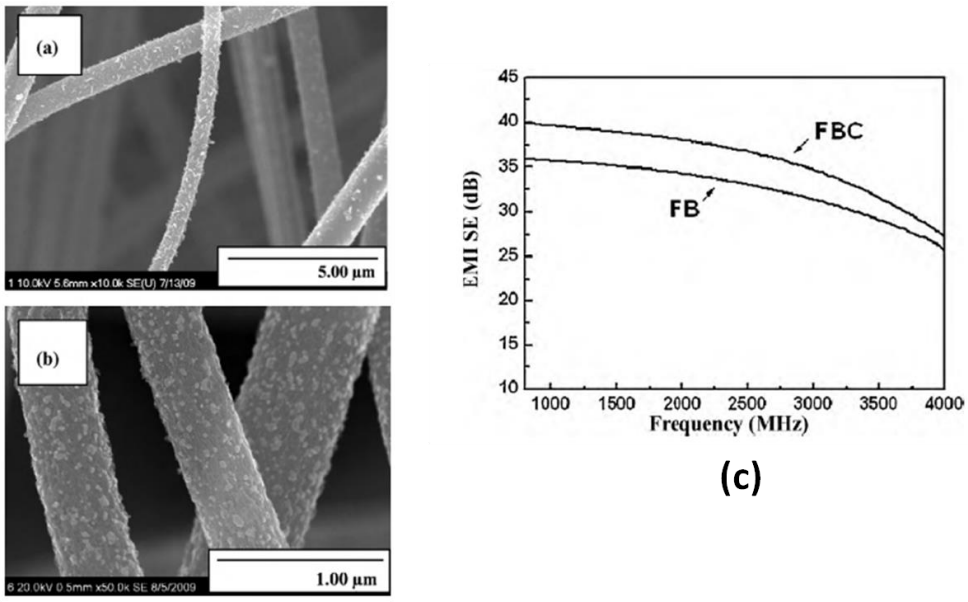

Figure 1.29: (a,b) SEM images of FB and FBC samples. (c) EMI SE of FB and FBC samples. (Im et al., 2010a)

Recently, Li et al.(Z. Li et al., 2021) in a study, prepared electrospun carbon nanofiber films by electrospinning- thermal stabilization-carbonization process and using silicone as the matrix, prepared carbon nanofiber/silicone composites with different CNF layers and evaluated the electromagnetic shielding performance. For this PAN is used as the carbon source, electrospun mats are stabilized at 260 °C and 1400 °C at a heating rate of 5 °C/min. The photograph of prepared carbon nanofiber films is presented in Figure 1.30 a. In Figure 1.30 b & c, the scanning electron microscope of these CNFs are presented.

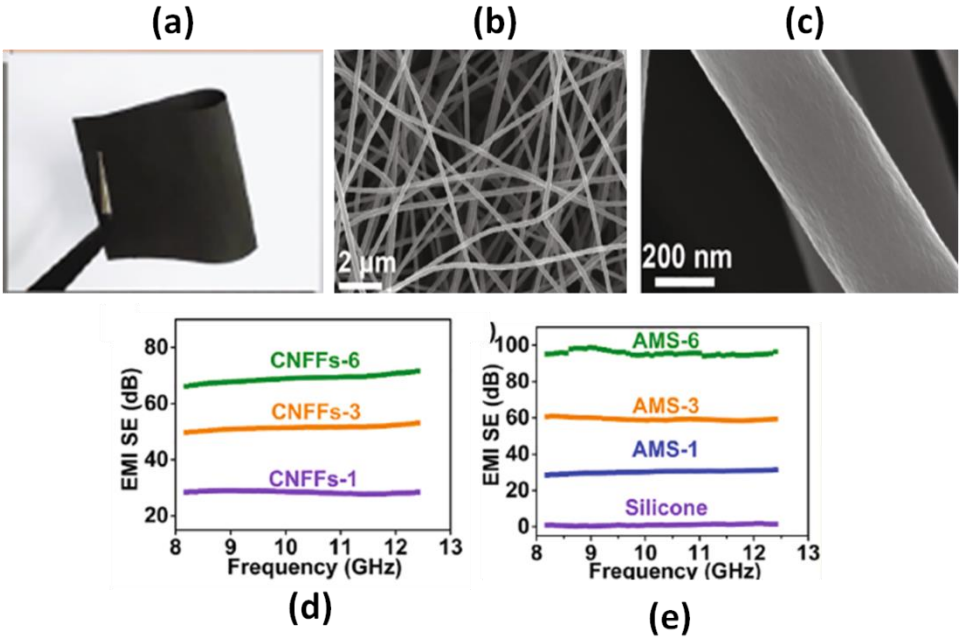

Figure 1.30: (a,b) SEM images of FB and FBC samples. (c) EMI SE (Z. Li et al., 2021)

Later, an alternating multi layer structure (AMS) is prepared by using silicone as matrix and varying the number of carbon nanofiber layers. The EMI SE results of carbon nanofibers and AMS structures with different layers are presented in Figure 1.30 (d) and (e). We can see that all the samples exhibited good EMI shielding performance with shielding effectiveness improving with the number of layers (thickness). In the case of AMS samples also, a good EMI performance was observed with SE increasing with number of layers, with AMS samples at 3 and 6 layers exhibited better SE than AMS with single layer. This sample exhibited a specific shielding effectiveness of 163 dB/mm. The sample AMS 6 displayed an EMI SE of almost 100 dB (at 0.6 mm thickness). The enhancement in EMI performance is attributed to the formation of micro-currents that can attenuate EM waves. Carbon nanofibers have active role in attenuating EM waves through reflections and scattering and the unique AMS structure leads to multiple wave reflections contributing to reflection loss. The authors reported

that 98% of EMI property is retained after 1000 bending cycles and they recommend the use of this material in advanced applications.

1.4. Scope and Objectives

Generally, Fiber reinforced composites are designed and prepared to obtain composite materials with enhanced mechanical properties for advanced structural applications. These materials are also potential candidates for multifunctional applications. When the size of these reinforcing materials is in the nano-scale, the composites will be benefited from both the nano size and high surface area, resulting in better performing composites. This thesis deals with one such material, electrospun fibers reinforced epoxy composites with comprehensive mechanical properties and electromagnetic shielding properties. The thesis investigates the use of short chopped electrospun fibers for enhancing the overall mechanical properties, and electrospun carbon fibers with and without additives for electromagnetic interference shielding properties. The major objectives of the present work are:

- To prepare electrospun fibers of SBC copolymer and develop electrospun SBC fiber/epoxy composites, and to study their mechanical, visco-elastic, fracture, rheological, and thermal performance.

- To successfully prepare polyimide fibers via electrospinning and to develop polyimide fiber/epoxy composites, and to evaluate their mechanical, visco-elastic, fracture, rheological, and thermal performance.

- To prepare carbon nanofibers from electrospun PAN fibers via electrospinning – stabilization-carbonization technique

- To prepare zirconia loaded electrospun carbon fiber/epoxy composites and to investigate their mechanical and EMI shielding performance.

- To develop titanium carbide @ titanium oxide loaded electrospun carbon fibers and use them as reinforcements in epoxy composites, and to evaluate their mechanical and EMI shielding performance.

1.5. Arrangement of Thesis

This thesis describes the work on electrospun fibers reinforced epoxy composites and evaluates their overall mechanical performance. Further, in a view to develop multi-functional materials, electrospun carbon fibers were developed with and without fillers and their effect on mechanical and EMI shielding performance of epoxy composites were investigated. The structure of thesis is presented in the following seven chapters

Chapter 1 contains a general introduction on electrospinning, parameters governing electrospinning, epoxy resins, electrospun fibers reinforced polymer matrices. It deals with an updated survey of different electrospun fiber reinforced composites especially electrospun fiber reinforced epoxy composites. In the latter part, details about electrospun carbon fibers, their preparation, applications and potential use in electromagnetic interference shielding is presented. A survey on previous literature on electrospun carbon fibers form EMI shielding is presented. The objective ad scope of the present investigation is presented at the end of this chapter.

Chapter 2 gives information about the materials used for this study. A general description about the experimental techniques used for the characterization is also presented

Chapter 3 deals with the preparation of SBC electrospun fibers and the development of SBC fiber/epoxy composites. The results corresponding to various characterizations are presented and compared with neat epoxy composites.

Chapter 4 gives details about the preparation of polyimide electrospun fibers from poly (amic acid) and the development of polyimide fiber/epoxy composites. The characterization results are presented and compared with neat epoxy composites.

Chapter 5 deals with the preparation of zirconia loaded carbon fiber and their epoxy composites. This chapter gives information about different characterization techniques especially EMI shielding capability of these prepared materials.

Chapter 6 deals with preparation of titanium carbide @ titanium oxide core-shell type carbon fibers and their epoxy composites. This chapter gives details of various characterization techniques with emphasis on EMI shielding properties.

Chapter 7 presents a summary of all the conclusions drawn from this research work and provide recommendations for future course of the work

CHAPTER 2

MATERIALS AND METHODS

This chapter gives details about all the materials used for the study. Alongside, it also provides information about the processing and testing equipments used in the study. A general description of sample preparation steps and characterizations is also presented briefly.

2.1. Materials

The materials used for the study are

- Epoxy resin: DGEBA based epoxy resin, trade name: Araldite® GY 250
- Hardener: Polyamidoimidazoline, trade name: Aradur® 140#
- Poly (styrene-co-butadiene): SBC, having a butadiene content of 4%
  Procured from Sigma-Aldrich, USA
- Poly amic acid: intermediate of Kapton®, PAA
- Polyacrylonitrile: PAN, having a molecular weight of M_w: 1,50,000 KDa
  Procured from Sigma Aldrich, USA
- Zirconia: ZrO_2, micron-sized
  Procured from Alfa Aesar, USA
- Titanium carbide: TiC, nano-sized < 200 nm
  Procured from Sigma Aldrich, USA
- The solvents, dimethylformamide (DMF), and tetrahydrofuran (THF) study are procured from Spectrochem Pvt. Ltd, India. All the chemicals used in this work are used as such without any further purification

2.2. Equipment Used

2.2.1. Electrospinning Unit

For this study, a horizontal electrospinning apparatus that was designed and supplied by ESPIN-NANO (Physics Instruments Co. Ltd; Chennai, India) was used. The apparatus consists of a high voltage supply unit, programmable pumping unit, and syringe holder. The pumps are arranged horizontally to the rotating collector. Aluminum foil (0.5 mm) was used as the substrate for collecting spun mats. The process parameters are adjusted to obtain the spun fibers on the foil during the electrospinning process. After the spinning process, the spun mats are removed from the foil and used.

2.2.2. Inert Furnace

An inert furnace with a continuous inert gas supply (nitrogen/argon) is used for carbonization. For this purpose, a high temperature furnace (Thermo systems, India) or a high temperature furnace (Vacuum Techniques Pvt. Ltd, India) was used. The electrospun fibers are placed on commercial carbon fiber and subjected to carbonization with a pre-designed program. The specific details are mentioned in respective chapters.

2.3. Characterization techniques

2.3.1. Light microscope

The morphology of the prepared electrospun fibers and nanofiber epoxy suspension was observed by polarized light microscope (PLS) (Leica DM 2500 P). All the samples were directly spun on a glass plate for electrospun samples, and the fibers are observed.

2.3.2. Scanning Electron Microscopy

The morphology of prepared fibers and fractured epoxy composites was observed by scanning electron microscopy at different magnifications, and SEM images were recorded. The samples were gold coated prior to SEM analysis to make them conducting. Scanning electron microscope (JEOL, 6390LA) and scanning electron microscope (ZEISS, EVO 18 model) are used for observing the samples. The specific details are presented in respective chapters.

2.3.3. Transmission Electron Microscopy

The high-resolution transmission electron microscopy (HRTEM) was done using JEOL JEM-2100 with an acceleration voltage of 200 kV. The samples were spun on a copper grid and observed in a microscope.

2.3.4. Atomic Force Microscopy

For AFM, a mica sheet was used as the substrate (Aligent 5500, SPM, non-contact mode). The samples were spun on a mica substrate and observed in a microscope.

2.3.5. Universal Testing Machine

The static mechanical properties of the neat and nanofiber loaded composites were investigated by Instron universal testing machine (UTM) (5984, USA). Dog bone shaped samples (165×13×3) were prepared and tested at a speed of 1 mm/min by keeping a gauge length of 100 mm. All the samples were analyzed as per ASTM D 638, and the average values were reported

Fracture Toughness of the samples was found using Instron UTM (5984, USA) at a head speed of 10 mm/min (as per ASTM D5045). The fracture toughness was expressed in stress intensity factor (K_{IC}), using the equation

$$\boldsymbol{K_{IC}} = \frac{\boldsymbol{L}}{\boldsymbol{Bw^{0.5}}}\boldsymbol{f(x)} \quad (2.1)$$

Where 0 < x < 1 and

$$\boldsymbol{f(x)} = \frac{\boldsymbol{6x^{0.5}[1.99 - x(1-x)(2.15 - 3.93x - 2.7x^2)]}}{\boldsymbol{(1+2x)(1-x)^{1.5}}} \quad (2.2)$$

L is the maximum load at crack initiation; B is the sample thickness; w is the width of sample; a is the crack length and variable x= a/w.

2.3.6. Dynamic Mechanical Analyzer

PerkinElmer dynamic mechanical analyzer (DMA 8000) was used to study the dynamic mechanical properties. The dynamic mechanical analysis of the neat, as well as nanofiber incorporated epoxy, was evaluated with an oscillating frequency of 1 Hz. The sample dimensions and temperature range are specified in respective chapters. The test was performed by heating the sample at a rate of 2˚ C/min

2.3.7. Rheological Studies

Dynamic rheological properties of unloaded epoxy and fiber loaded epoxy composites were performed using an Anton par Modular Rheometer (MCR102, USA), employing 25 mm circular parallel plates. The viscosity and the shear stress were investigated with respect to shear rate, and plots are presented. The storage modulus, loss modulus, and complex viscosity were investigated with respect to angular frequency. The specific details are presented in respective chapters.

2.3.8. Thermogravimetric Analyzer

Thermal stability of nanofiber loaded epoxy composites were tested using TA Instruments thermogravimetric analyzer (Q-50, USA). The samples were heated at a from room temperature to 800 ˚C in the presence of nitrogen, and the results were plotted. The specific details are presented in respective chapters.

2.3.9. Fourier Transform Infrared Spectrometry

Fourier Transform Infrared (FTIR) spectrometer (Spectrum 100, Perkin Elmer, USA) was used for testing the samples. The samples were tested in attenuated total reflectance (ATR) mode from wave number 4000 cm^{-1} to 600 cm^{-1}

2.3.10. AC Conductivity

Electrochemical measurements were carried out using EG&G (Princeton applied research, Model no. 263A) using symmetrical cell configuration. The AC conductivity of samples was calculated using the following equation.

$$\sigma_{ac} = 2\pi f \boldsymbol{\varepsilon}_0 \boldsymbol{\varepsilon}^{"} \qquad (2.3)$$

Where f is the applied frequency, ε" is the dielectric loss, and ε_0 is the vacuum permittivity (ε_0=8.8541878128×10^{-12} F·m^{-1}).

2.3.11. EMI Shielding Measurements

The total electromagnetic shielding effectiveness was measured using a vector network analyzer (VNA; Anritsu MS4642A) with a KEYCOM wave-guide adaptor in a

12–18 GHz frequency. The scattering parameters were recorded and were used to estimate the total shielding effectiveness using the input and output power.

2.3.12. X-ray Diffraction (XRD)

Powder X-ray diffraction (XRD) patterns were recorded using Philips Diffractometer (PAN Analytical with Cu-Kα, 45 kV and 30mA) and Bruker D8 Advance (40 kV and 30mA. The specific details are presented in respective chapters.

2.3.13. X-ray Photoelectron Spectroscopy (XPS)

The surface chemistry of the carbonized samples was analyzed using X-ray photoelectron spectroscopy (XPS, PHI 5000 VersaProbe II, ULVAC-PHI Inc., USA) equipped with micro-focused (200 μm, 15 kV) monochromatic Al-Kα X-Ray source (hν = 1486.6 eV). XPS data were processed using PHI's Multipak software.

2.3.14. Raman Analysis

Raman spectra were recorded using LabRAM HR Evolution, Horiba Jobin Yvon, France, using a laser of 532nm.

CHAPTER 3

PREPARATION AND CHARACTERIZATION OF ELECTROSPUN POLY (STYRENE-CO-BUTADIENE) FIBER /EPOXY COMPOSITES

This chapter deals with the successful preparation of electrospun styrene-butadiene copolymer mats and the use of these mats as reinforcement in epoxy matrix. At first the polymers were dispersed in suitable solvent system and that solution was spun into continuous fiber mats by electrospinning technique. These mats were chopped into specified dimensions and incorporated into the epoxy. Considerable improvements in toughness as well as mechanical strength were observed in the fabricated epoxy composites.

Part of this chapter has been published in Composites Part B: Engineering, (2019).

DOI: 10.1016/j.compositesb.2018.12.102

3.1. Introduction

Composite materials are combinations of two or more constituent materials that combine to form resultant materials with enhanced properties. Nanocomposites can be considered promising next-generation materials as they offer excellent properties. They can be prepared by varying the experimental conditions by simple approaches, resulting in novel material combinations (Zinatloo-Ajabshir et al., 2018; Zinatloo-Ajabshir et al., 2017). Specifically, polymer nanocomposites offer interesting properties due to their low weight and distinctive material combinations.

In a view to develop high performance polymer composite materials, the use of nano-scale inclusions is an emerging market trend (Potts et al., 2011; Zou et al., 2008). Specifically, the studies involving the electrospun nanofiber incorporated composites have become an exciting area of research as they possess definite advantages not shared by other nano level fillers, such as material choice, controlled diameter and structure, alignment, and so on (G. Wang et al., 2017).

Even at extremely low fiber loadings, nanofibers, owing to their very high aspect ratio and ultra-high surface area, helps in the attainment of high fiber/matrix interface, thereby resulting in superior performing composites (Cholake et al., 2015; Zucchelli et al., 2011). Even though, many techniques are available in literature for the preparation of nano sized fibers like phase separation (Zhang & Ma, 2001), template based synthesis (Long et al., 2011; Martín et al., 2012) and the self assembly (Hartgerink et al., 2002), electrospinning has drawn major attention due to its relative ease of processing and scale-up ability (Valizadeh & Farkhani, 2013). Electrospinning technique is a versatile method to prepare polymeric, ceramic and carbonaceous nanofibers from their solutions (Bhardwaj & Kundu, 2010; Dzenis, 2004; Garg & Bowlin, 2011; Greiner & Wendorff, 2007). The main phenomenon involved in electrospinning, is the fiber formation by electrostatic forces and whipping instability mechanism. Using this top-

down approach of electrospinning, we can obtain non-woven mats, and further purification is not needed when compared to other bottom up approaches or 1D materials(G. Wang et al., 2017). The major applications of spun fibers fall in the areas of bio-medical (Fong, 2004; Y. Gao et al., 2008), filtration (Bognitzki et al., 2000; Hajra et al., 2003), protective clothing (Schreuder-Gibson et al., 2002) , sensors (Bognitzki et al., 2001; X. Wang et al., 2001), composite reinforcement (Chen et al., 2009; Romo-Uribe et al., 2009) etc.,

On the other hand, epoxy resin is one of the most widely used thermosetting polymers with good mechanical strength, thermal and chemical resistance. The In-built brittleness of cured epoxy is a major concern that limits its usage at advanced levels (J. Gao et al., 2012). Usually, secondary phase materials like rubbers (Chikhi et al., 2002; Thomas et al., 2007), particulate fillers (McGrath et al., 2008) and engineered plastics (Mimura et al., 2000) were dispersed in epoxy to improve the toughness. But, this improvement in toughness in rubber filled composites is accompanied with a comprehensive decrement in mechanical modulus and glass transition temperature (T_g) (Konnola et al., 2015). So, the development of advanced epoxy composites with both improvement in fracture toughness and mechanical performance was the need of the hour. The investigation of electrospun fibers as reinforcement in the epoxy matrix to address this issue is thus a noteworthy study.

The effect of short-milled carbon fibers in the epoxy matrix was investigated by10 wt% loading of the fibers and an improvement of 3.5 times in fracture toughness was observed compared to the pure epoxy. The main reasons for toughness improvement is manifested as intensive de-bonding and pull-out (Cholake et al., 2015). The role of graphite nanofiber in reinforcing epoxy was done by Xu et al. (Xu et al., 2007) and an improvement of 30% in the strength was observed in fiber incorporated samples.In another work, poly(ethylene oxide) electrospun nanofibers (5 w%) were incorporated in DGEBA epoxy resin and the stress intensity factor, fracture toughness and fracture

energy, were evaluated under 3-point flexural load and it was found that there was improvement in all toughness parameters in fiber filled composites when compared to unfilled composites (Lee et al., 2004). Ozden et al. (Ozden et al., 2010) investigated the use of poly(styrene-co-glycidyl methacrylate) nanofibers as reinforcement and found that the storage modulus of fiber loaded composites was ten times higher than that of the unloaded epoxy. The improvement in performance was attributed to fiber cross-linking, which in turn resulted in better fiber-matrix interfacial bonding. The fracture toughness of epoxy based nanocomposites reinforced with nylon 66 nanofiber yarn was investigated and the subsequent improvement in fracture toughness turned out to be 49% (Ahmadloo et al., 2017). The influence of PMMA nanofibers (Al-Assafi et al., 2016), cellulose nanofibers (Jahanbaani et al., 2016) and polystyrene nanofibers (Demir et al., 2014) in epoxy has been investigated and reported. Styrene-butadiene copolymers are widely used materials with many applications. It can be used in many combinations such as styrene-butadiene rubber, tri block styrene- butadiene copolymers etc. Styrene-butadiene copolymers can be used in footwear, coatings, adhesives and sealants etc., the preparation of nanofibers from styrene-butadiene copolymers is an interesting way to improve its applications.

In this chapter, electrospun fibers of flexible amorphous thermoplastic polymer, poly (styrene-co-butadiene) (SBC) were prepared using electrospinning and their reinforcing effect in the DGEBA epoxy resin at different loadings was examined. To the best of our knowledge, there is no previous literature with respect to epoxy nanocomposites containing electrospun fibers of poly (styrene-co-butadiene), and hence our attempt is to bridge this gap in the literature. The morphology, mechanical performance, rheology, thermal and toughening behavior of these composites were also studied and reported. Theoretical modeling of the rheological and visco elastic properties was also done. This work presents SBC electrospun fibers as novel modifiers in epoxy thermosets with comprehensive improvement in toughness along with mechanical performance

3.2. Experimental details

3.2.1. Preparation of Electrospun (styrene-co-butadiene) Fibers

The Poly (styrene-co-butadiene) polymer pellets were procured from sigma Aldrich, India (with butadiene 4 wt. %). These pellets were dissolved in Tetrahydrofuran (THF): Dimethyleneforamide (DMF) co-solvent system of 75:25 (w/w %) to get 18 w % polymer concentrations by overnight stirring. THF is a very good solvent of both styrene and butadiene units and the DMF helps in maintaining the jet stability during spinning. The resultant homogenous polymer solution was electrospun in a horizontal electrospinning machine at 10 kV at 20 ml/hr flow rate. The distance between the drum collector and needle was maintained as 15 cms. The collector speed was maintained at 1000 rpm. Thus spun system fibers were collected on an aluminum foil and spun mats were obtained. For simplicity, the term SBC is used to mention poly (styrene-co-butadiene).

3.2.2. Preparation of Electrospun SBC/Epoxy Composites

The epoxy used was Diglycidyl ether of Bisphenol-A (DGEBA) with a trade name of Araldite®GY-250. The hardener selected for low temperature cure was Polyamidoimidazoline, with trade name Aradur®-140#. The mix ratio of DGEBA to hardener used is 100 to 50 parts per weight. The spun mat obtained after spinning was chopped into $1cmX\ 1cm$ square pieces. These pieces were incorporated into the epoxy resin (DGEBA) and composites were prepared at weight percentages of 0, 1, 2.5 and 5 w % fiber loading. The composites prepared as per the aforementioned procedure was subjected to subsequent characterization studies. The codes 0% nf, 1% nf, 2.5 % nf and 5% nf was used to determine the composition of nanofibers (in w %) dispersed in epoxy respectively.

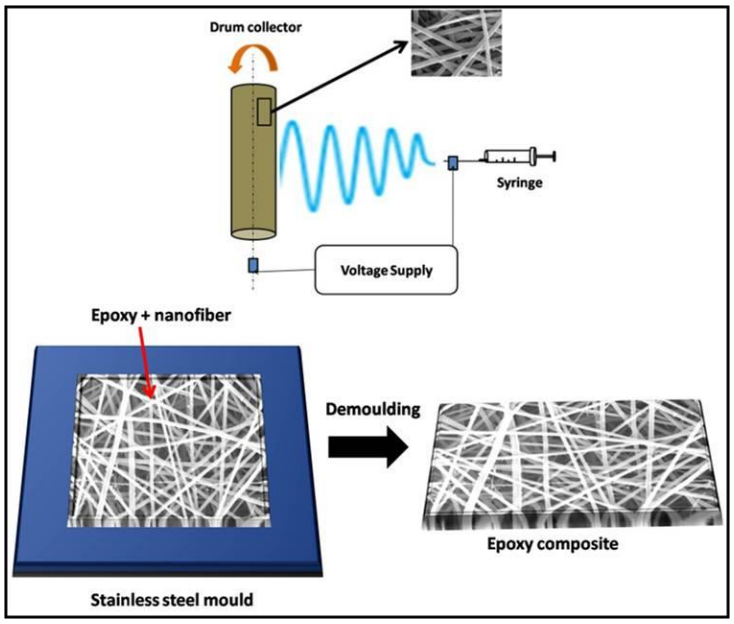

Figure 3.1: Schematic of electrospun set up for fiber fabrication and composite preparation

3.2.3. Characterization Techniques

The morphology of the prepared electrospun nanofibers and nanofiber epoxy suspension was observed by Polarized light microscope. The morphology of fractured epoxy composites was observed by scanning electron microscopy at different magnifications and SEM images were recorded. The dynamic mechanical analysis of the neat as well as nanofiber incorporated epoxy was evaluated in single cantilever beam mode with an oscillating frequency of 1 Hz. The sample dimensions were maintained as $50 \times 10 \times 3\ mm^3$.The test was performed at a heating rate of 2˚ C/min between room temperature to 180˚ C and the storage modulus data was plotted. Fracture Toughness of the samples was measured using UTM at a cross head speed of 10 mm/min (ASTM D5045). The static mechanical properties of the neat and nanofiber loaded composites were investigated by universal testing machine (UTM). Dog bone shaped samples (165×13×3) were prepared and tested at a crosshead speed of 1 mm/min by maintaining

a gauge length of 100 mm. All the samples were tested as per ASTM D 638 and the average of 5 values are reported. Dynamic rheology of unloaded epoxy and fiber loaded epoxy composites were performed using Modular Rheometer employing 25 mm parallel plate. The viscosity and shear stress was investigated as a function of shear rate and plots were presented. Thermal stability of nanofiber loaded epoxy composites was tested using a TA Instruments thermogravimetric analyzer (Q-50, USA). The samples were heated at a rate of 10˚C/min from room temperature to 800 ˚C

3.3. Results and Discussions

3.3.1. Morphology of Prepared Electrospun SBC Fibers

The morphology of the SBC electrospun fibers and fiber-epoxy system was observed by polarized light microscope and the images are depicted in Figure 3.2 (a). The electrospun fibers formed were porous, uniform and the diameter was observed to be in range of 400 nm- 900 nm. The average diameter of the fibers was observed to be around ~ 643 nm. The electrostatic potential force applied in between the syringe needle and collector helped the polymer solution to form a Taylor cone and thereafter yielded continuous fiber to form uniform non woven fibers. The polarized light microscope image of chopped SBC fiber mixed epoxy resin is shown in Figure 2(b). This image reveals that due to mechanical mixing, the fibers were separated out from the mat and got distributed in the epoxy matrix. This image also indicates that these chopped fibers are stable in the epoxy phase.

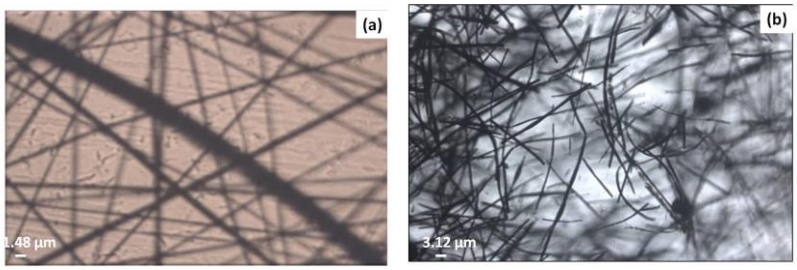

Figure 3.2: PLS images of (a) electrospun nanofibers as prepared, (b) nanofiber incorporated epoxy resin

The transmission electron microscopy images of SBC electrospun nanofibers are portrayed in Figure 3.3. From this image the porous nature of the fibers can be observed. Presence of styrene and butadiene blocks, lead to phase separation and has thus resulted in porous morphology of the fibers. As the wt % of butadiene in the copolymer is very less, pores of small size are obtained.

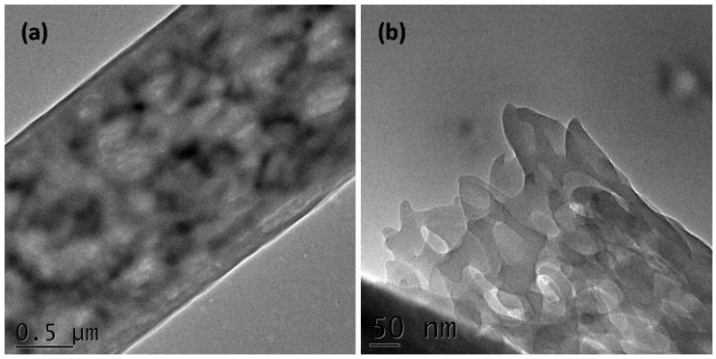

Figure 3.3: TEM images of SBC electrospun nanofibers as prepared (a) at low magnification and (b) at high magnification

3.3.1. Static Mechanical Properties

The mechanical properties of epoxy composites depend on the aspect ratio of the fillers, their volume fraction, dispersion of the fillers in the matrix and interactions between them. The effect of chopped SBC fibers on the tensile strength and tensile

modulus of the resultant composites is illustrated in Figure 3.4 (a & b). The average tensile strength of the nanofiber loaded samples (0,1,2.5 and 5w% samples) is observed to be 20.2 MPa, 20.5 MPa, 23.77 MPa and 14.09 MPa, while the tensile is observed to be 1206.67 MPa, 1343.33 MPa, 1503.33 MPa and 1509 MPa. In the case of composites with 1 w % and 2.5 w% loading, the tensile strength increased by ≈ 2% and ≈ 18% respectively and the increase in tensile modulus was noted to be ≈ 12% and ≈ 25% respectively. Even though the reinforcing effect is less at low loadings, it increased along with fiber loading. The increase in strength can be attributed to the high aspect ratio and large surface area to volume which in turn permits a greater stress transfer. This also shows that fiber /matrix interface helps in load transfer from matrix to the reinforcing fiber. At 5 w % fiber loading, the tensile strength and modulus decreased because of the lack of wettability and the presence of voids. The increased amount of fiber loading leads to a non-uniform distribution of fibers within the matrix and hence the fibers act as weak points for stress transferability.

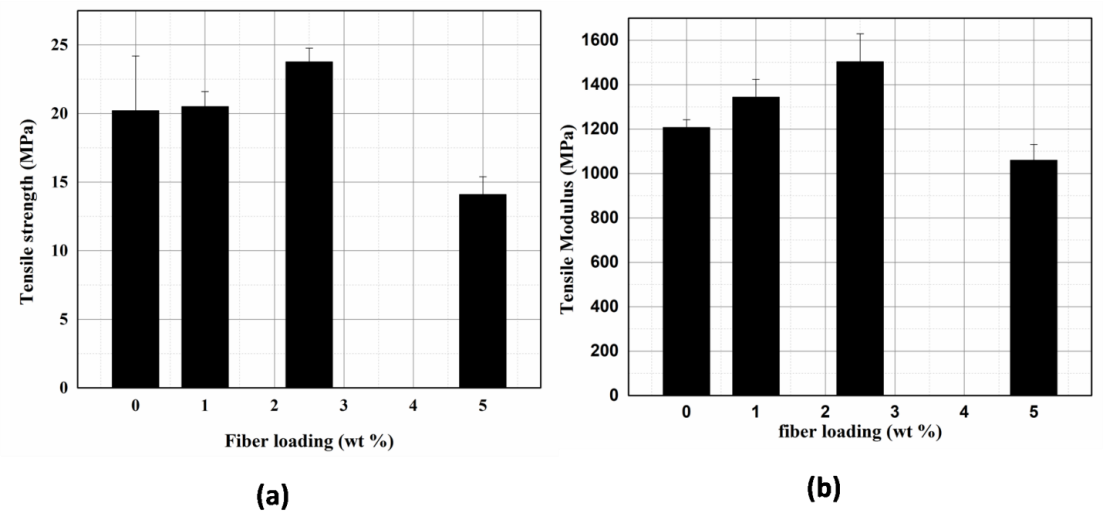

Figure 3.4: Variation of (a) tensile strength, (b) tensile modulus of nanofiber loaded epoxy samples with respect to fiber loading

3.3.2. Dynamic Mechanical Properties

Dynamic mechanical analysis is a conventional approach to investigate the interaction between the matrix and the reinforcing fibers. This analysis was carried out to evaluate the dynamic mechanical properties of neat and fiber loaded samples over temperature range of 30 ˚C to 180˚C and is presented in Figure 3.5(a). It can be seen that no substantial improvement in the modulus was noticed in the case of 1% filler loading. But, for 2.5% nf and 5% nf samples, there was a note worthy improvement of 1.5 times and 2 times respectively. So the incorporation of these SBC nanofibers lead to remarkable improvement in the modulus throughout the temperature range. This enhancement was due to the high aspect ratio, distribution and interactions of these fibers in the epoxy matrix.

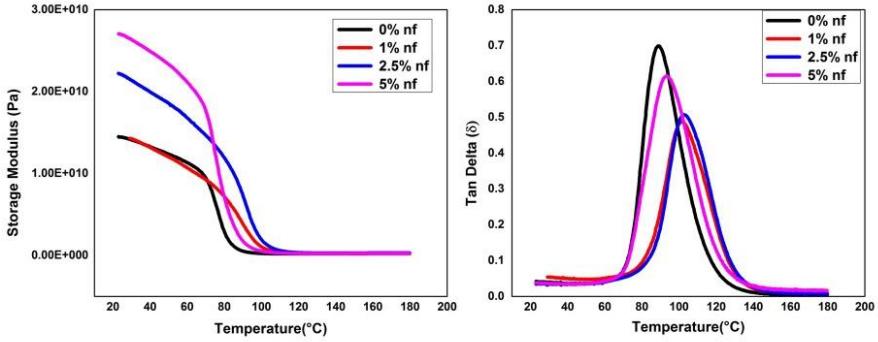

Figure 3.5: (a) Variation of dynamic storage modulus with temperature, (b) variation of tan δ with temperature

The tan δ of virgin epoxy and SBC/epoxy composites is shown in Figure 3.5 (b). The mechanical damping factor (tan δ) determines the glass transition temperature (Tg) of the polymeric system. In case of fiber loaded samples, a reduction in the damping factor and an improvement in the Tg is observed. These changes are attributed to the existence of a strong fiber matrix interface in the composite. The Tg is closely related to

the polymer segment mobility and volume fraction of the polymer. The mobility of the polymer chains near these fibers is restricted and so the occurrence of the relaxation behavior at the Tg region is obstructed. This leads to an improvement in the Tg of fiber loaded samples, when compared to the neat samples.

3.3.2.1. Theoretical Modeling of Dynamic Mechanical Properties

Several theoretical models have been used to estimate the variation in modulus of the epoxy matrix with respect of the reinforcement composition. The theoretical prediction of the properties of composite materials is essential in order to assess the contribution of each component properties such as matrix modulus and reinforcement modulus, volume fraction of reinforcement, reinforcement aspect ratio, reinforcement orientation etc. The most important models for filled composite systems include Einstein model, Guth model and Quemada models

A simple model for the filler incorporated polymeric materials was introduced by Einstein. As per the model, the equation is denoted by,

$$\frac{E_c}{E_p} = \left(1 + 2.5V_f\right) \tag{3.1}$$

Where, E_c and E_p are the modulus of reinforced composite and matrix polymer respectively and V_f is the volume fraction of reinforcing filler. The Einstein model is applied to polymers reinforced with less concentration of spherical particles.

Guth equation for filler reinforced polymer is expressed by

$$\frac{E_c}{E_p} = \left(1 + 2.5V_f + 14.1{V_f}^2\right) \tag{3.2}$$

This equation considers the interactions between the particles even at higher concentration

The Quemada equation is given by

$$\frac{E_c}{E_p} = 1/(1 - 0.5K_6V_f)^2 \tag{3.3}$$

This equation employs a variable term that signifies the particle interaction and the geometric aspects (where, K_6 =2.5).

It is observed from Figure 3.6 that the experimental data is close enough to the estimated theoretical data in the glassy and rubbery regions. From the theoretical calculation, it can be observed that the experimental results show closeness to all the three different models at low loadings. At higher loading, there is a variation of experimental data from theoretical models.

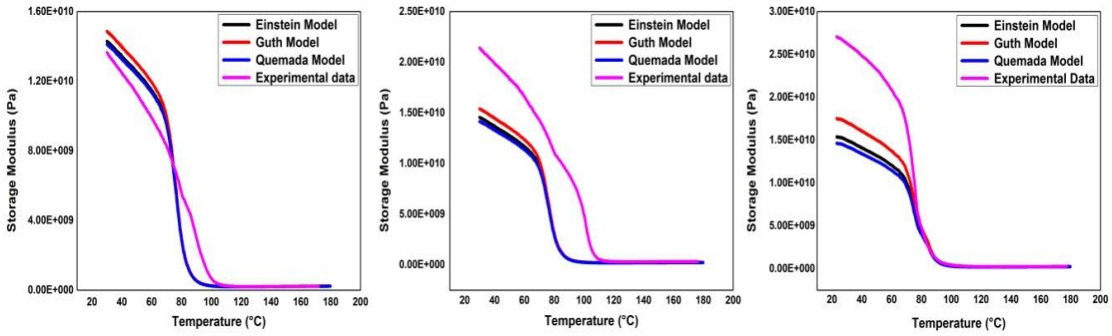

Figure 3.6: Visco elastic modeled plots of (a) 1% nf, (b) 2.5% nf and (c) 5% nf composites

3.3.3. Fracture Toughness

The fracture toughness of single edge notched samples were evaluated and reported in Figure 3.7. By addition of 1 wt % fibers to epoxy, an improvement of around

43% in K_{IC} was observed. When the loading increased to 2.5 wt % fibers an improvement of around 103% in K_{IC} was observed. During fracture, the crack propagation through the fiber matrix interface consumed higher energy and traced a prolonged path. When the fiber loading was 5%, the improvement in K_{IC} was found to be 63%, which might be attributed to improper wettabilty and lack of dispersion of fiber at higher loading.

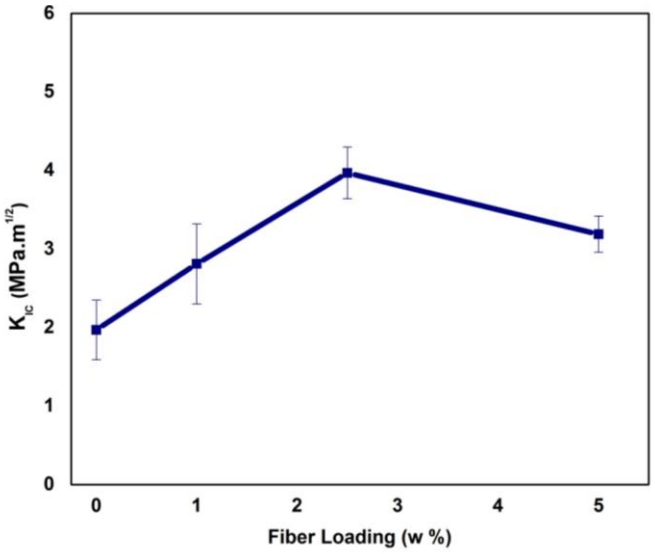

Figure 3.7: Fracture toughness of nanofiber loaded epoxy composites with fiber loading.

The fractured surfaces of neat epoxy and filled epoxy composites were investigated by scanning electron microscope and the images are presented in Figure 3.8. The fracture surface of pure epoxy depicts a glassy and smooth surface, because of the brittleness with no plastic deformation as shown in Figure 3.8(a). In the nanofiber loaded epoxy composites, crack deflection Figure 3.8(b), fiber pull-out Figure 3.8(c) & fiber breakage Figure 3.8(d) is observed as the main toughening mechanisms. Due to the presence of fibers, higher load and a lengthy path is required for the crack to propagate further thereby increasing the toughness. In addition to this, in the case of fiber loaded epoxy systems, crack pinning and shear banding also helped in improvement of toughness. Table 3.1 shows a comparison of the fracture toughness of the present study

with the already reported works in literature. It is clear from the table that the electrospun fibers employed in the present work act as superior toughening agents in the epoxy matrix.

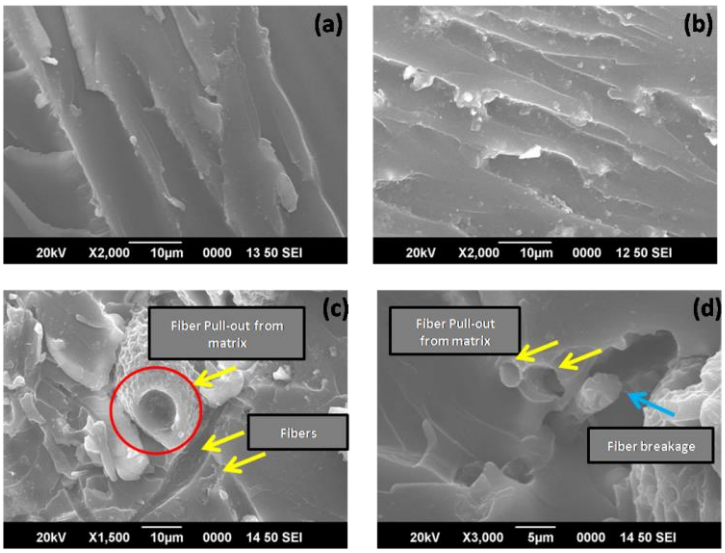

Figure 3.8: SEM Micrographs of the fractured surfaces (a) neat epoxy, (b), (c) and (d) are nanofiber loaded epoxy samples

Table 3.1: Comparison of properties of various Epoxy nanocomposites

Reinforcement	**Matrix**	**Property (improvement)**	**Reference**
Short milled carbon fibers	Epoxy	Fracture toughness(3.5 times)	(Cholake et al., 2015)
PA 66	Glass/epoxy laminated composites	Mode I energy release (62%) Mode II energy release (109%)	(Saghafi et al., 2014)
PA 66 nanofiber yarn	Epoxy	Fracture Toughness (29 %)	(Ahmadloo et al., 2017)
SBC	Epoxy	Fracture Toughness (104%)	Present work

3.3.4. Rheological Properties

Figure 3.9(a) shows the variation in the behavior of nanofiber reinforced epoxy composite and neat epoxy resin with respect to the shear rate. As per the Figure, neat epoxy shows a near Newtonian behavior with almost constant viscosity throughout the shear range. In the case of fiber loaded samples, a drastic improvement in the viscosity is observed. The viscosity increase is found to be consistent with increase in filler loading and a maximum is observed in 5 w % nf system. It can be inferred that these dispersed nanofibers have a constructive effect on viscosity. This implies that viscosity strongly depends on fiber loading and that electrospun fibers have a significant effect in stiffening the system. These electrospun fiber loaded epoxy systems display a shear thinning behavior.

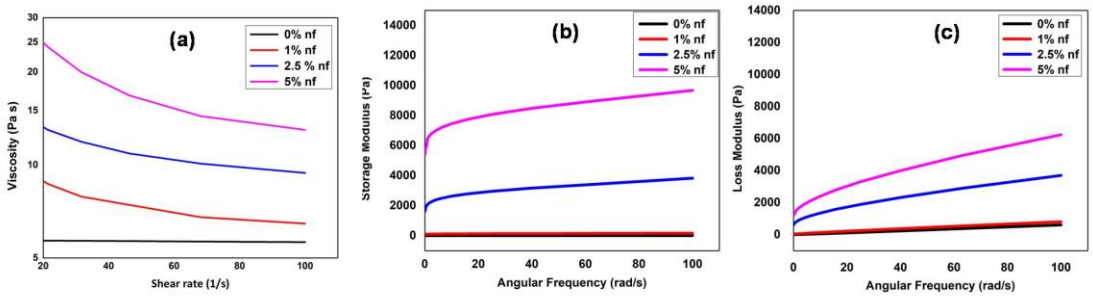

Figure 3.9: Variation of (a) Viscosity with respect to shear rate, (b) Storage modulus with respect to angular frequency, (c) Loss modulus with respect to angular frequency.

The storage modulus and loss modulus of neat epoxy and fiber loaded systems are illustrated in Figure 3.9 (b) & 3.9(c) respectively. The contribution of the nanofibers in the improvement of the modulus of the system can be clearly observed from the Figure. Hence these fibers contribute to both the elastic as well as viscous nature of the system and the increase in the modulus is directly proportional to fiber weight percentage. This fiber dispersion in the matrix contributed more to elastic properties than the viscous properties.

3.3.4.1. Rheological Flow Models

A flow model is the mathematical expression that interprets rheology based data, like strain sweep, in an illustrative way and provides a more convenient manner of presenting the data. These models involve two or three parameters for describing the rheological data and are mostly used (Rao, 2014). Few of these models were used here to fit the obtained experimental data and the parameters were evaluated.

Powers law model (Ostwald's model)

In this model, The plots of shear rate and shear stress were plotted on logarithmic axis and describes thinning and thickening behavior of fluids(Casson, 1959; Folayan et al., 2017)

$$\sigma = K\gamma^{n} \tag{3.4}$$

Where σ is shear stress, γ is shear rate , n is the fluid flow index parameter which describes the fluid tendency to shear thin and it is dimensionless, and k is consistency coefficient .When $n < 1$,the fluid is thinning in nature and when $n > 1$,the fluid is thickening in nature. The power law model gives a better information in the low shear rate condition but has disadvantage in high shear rate conditions

Considering logarithms of both the sides of Equation 3.4:

$$log\sigma = logK + nlog\gamma \tag{3.5}$$

Equation 3.5 can be rewritten as,

$$log\eta = logK + (n-1)log\gamma \tag{3.6}$$

Where, η is the viscosity. The Powers law model fit of epoxy and fiber loaded samples are depicted in Figure 3.10. The values of the parameters obtained are tabulated in table 3.2.

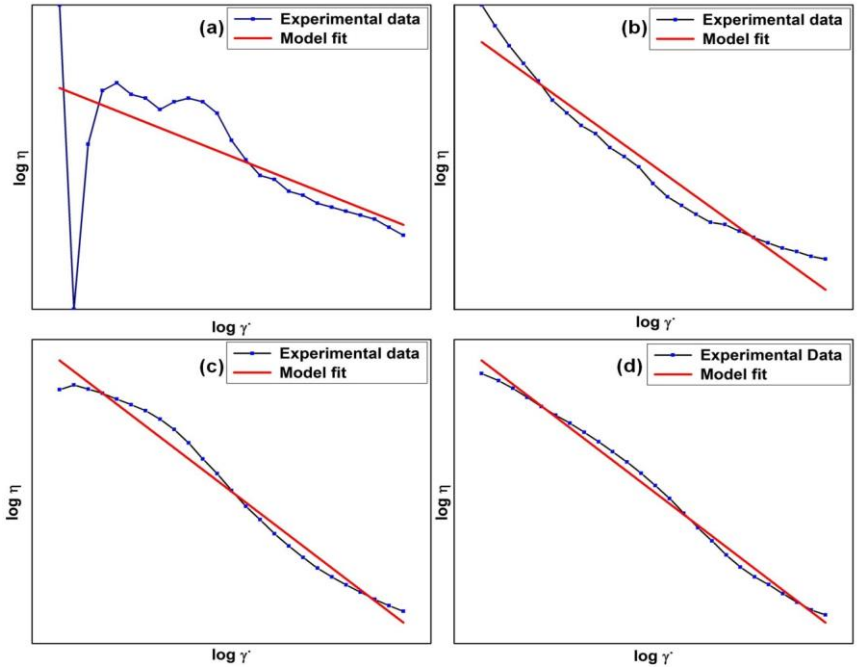

Figure 3.10: Powers law model fit for (a) neat epoxy, (b) 1w % nf, (c) 2.5 w % nf and (d) 5 w% nf samples

Table 3.2: Powers law model parameters

	Consistency co-effient (K)	**Flow Index (n)**	**Regression co-effient (R^2)**
Neat Epoxy	2.1502	0.99347	0.36746
1 w% nf	4.74788	0.50383	0.95075
2.5 w% nf	4.97272	0.65562	0.97811
5 w% nf	8.96205	0.42663	0.99291

Bingham Model

The Bingham rheological model is basically a two parameter model that is widely used to analyze the flow characteristics. Mathematically, it can be represented as(Folayan et al., 2017; Hemphill et al., 1993):

$$\sigma = \sigma_0 + \mu_p \gamma \tag{3.7}$$

Where σ is shear stress, γ is shear rate, σ_0 is yield point and μ_p is plastic viscosity. Fluids having Bingham Plastic nature are featured by a yield point (σ_0) and a plastic viscosity (μ_p). However, it does not represent accurately the behaviour of the drilling fluid at very low shear rates or at very high shear rate

The Bingham model fit of the epoxy and the fiber loaded samples are depicted in Figure 3.11. The parameters obtained are tabulated in Table 3.3.

Table 3.3: Bingham Model parameters

	Yield point(σ_0)	**Plastic viscosity (μ_p)**	**Regression co-effient (R^2)**
Neat Epoxy	0.34645	5.64193	0.99998
1 w% nf	20.37399	6.53365	0.99117
2.5 w% nf	29.53475	9.64519	0.98771
5 w% nf	128.82	12.8	0.93834

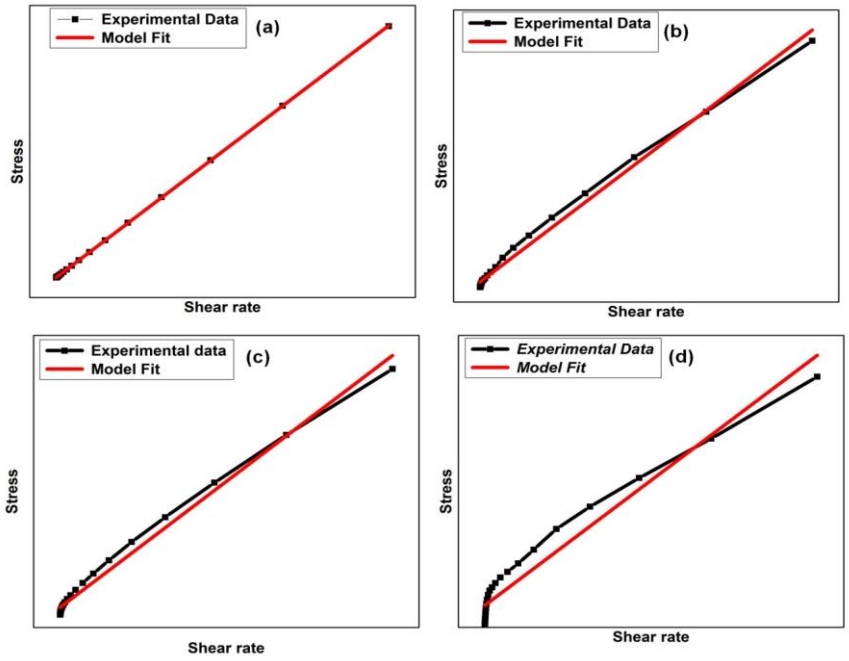

Figure 3.11: Bingham model fit for (a) neat epoxy, (b) 1 % nf, (c) 2.5% nf and (d) 5% nf samples

Casson Model

The Casson rheological model is widely used to describe the flow of visco-elastic fluids. This model has transition from Newtonian region to the Yield region. Mathematically, it is expressed as(Folayan et al., 2017; Herschel & Bulkley, 1926)

$$\sigma^{0.5} = K_{0c}^{0.5} + K_c^{0.5}\gamma^{0.5} \tag{3.8}$$

Where σ is shear stress, $\boldsymbol{\gamma}$ is shear rate, k_{oc} is Casson yield stress (Pa.s), k_c is Casson plastic viscosity in mPa.s. The Casson model fit of epoxy and fiber loaded samples are depicted in Figure 3.12. The values of the parameters obtained are tabulated in Table 3.4. From the models Bingham model and Casson model seems to be the best fit.

Table 3.4: Casson model parameters

	Yield Stress (K_{0c})	Plastic viscosity (K_c)	Regression co-effient (R^2)
Neat Epoxy	0.002	5.64067	0.99999
1 w% nf	6.8027	5.41223	0.99817
2.5 w% nf	6.96854	8.585134	0.98797
5 w% nf	62.6454	9.09655	0.93841

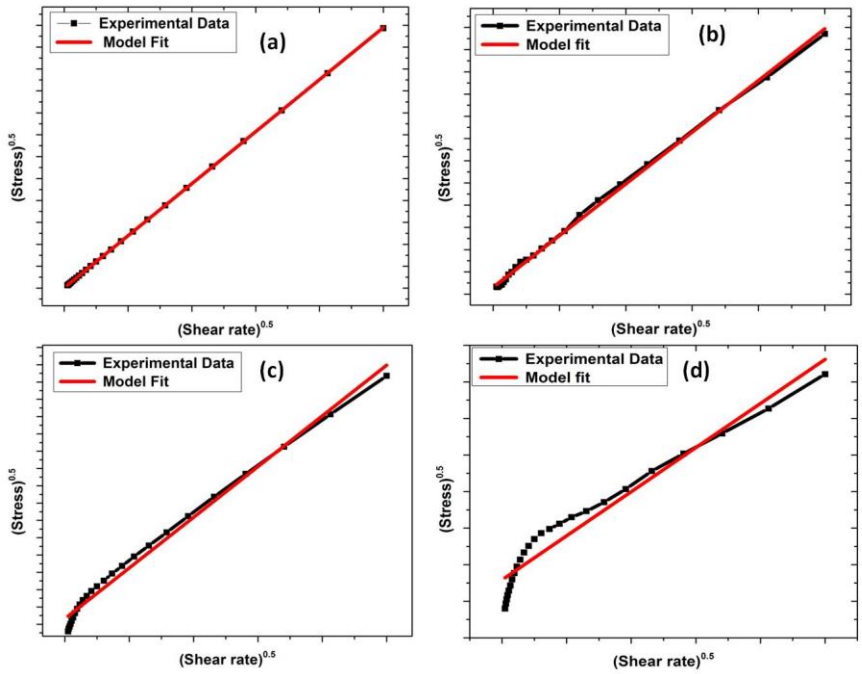

Figure 3.12. : Casson model fit for (a) neat epoxy, (b) 1% nf, (c) 2.5 % nf and (d) 5 % nf samples

3.3.5. Thermal Properties

The thermal properties of the composite materials play a crucial role in dictating the application temperature of the composite material. The thermal stability of unfilled

and filled epoxy systems was observed using thermogravimetric analyzer (TGA). Figure 3.13 shows the difference in thermal stabilities of nanofiber loaded epoxy systems and the neat epoxy system. There is no detectable difference observed in the overall stability and degradation temperature of all the composites. A small improvement in the char yield observed in the filled composites is because of the presence of nanofibers, which indicates that the added fibers did not influence the thermal stability of epoxy.

In the case of DGEBA resin, the thermal degradation happens in concurrent ways in a single step. i.e., (a) homolytic and heterolytic cleavage of bisphenol A to yield different phenol-based products, (b) cyclization of glycidyl ether side chain to yield C_6H_4-O-C_3O_4 or C_6H_5-O-C_3H_3 and uncured resin distillation. In case of cured epoxies, the degradation is in a single step but at a high temperature than uncured DGEBA epoxy (Remiro et al., 2002). Finally leaving char yield after all the by-products are left. In our case, we observe the onset temperature of degradation is significantly affected by the nanofiber loading. Further, these amorphous thermoplastic fibers are stable until the epoxy chains surrounding them are stable. Once the epoxy chains start to degrade by breaking of backbone chain, the inside amorphous thermoplastic degraded faster randomly at 300-400 °C temperature, which is very high for an amorphous thermoplastic. Hence, we can see nanofiber loaded samples have lesser char yield the neat epoxy samples.

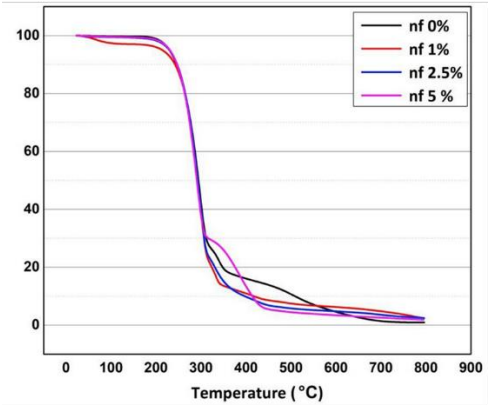

Figure 3.13: TGA curves of SBC/epoxy systems

3.4. Conclusions

By optimizing the electrospinning parameters, electrospun fibers from poly (styrene-co-butadiene) were successfully prepared at 18 wt% polymer concentration. These chopped fibers were loaded in the epoxy matrix at 0, 1, 2.5 and 5 w% loadings and nano composites were developed. The mechanical strength and modulus increased around 18% and 25% at 2.5 w% fiber loaded composites. The visco-elastic properties showed excellent enhancement in storage modulus and T_g. This enhancement in T_g was because of the hindered molecular mobility at the interface area. The fracture toughness of composites increased significantly and there was around 104 % improvement at 2.5% loading. The crack propagation was limited by crack bifurcation, fiber pull-out and fiber breakage as observed from SEM images. The rheological analysis showed a tremendous increase in the viscosity of fiber loaded epoxy composites. The theoretical modeling of visco-elastic properties and the flow behavior was done. The TGA showed that the presence of the Poly (styrene-co-butadiene) nanofibers did not deteriorate the stability of the epoxy composites. To conclude, the incorporation of nanofibers into epoxy matrix has marked an improvement in rheological, visco-elastic and mechanical performance of composites and leads to the development of a new class of high performance composite materials.

CHAPTER 4

PREPARTION AND CHARACTERIZATION OF ELECTROSPUN POLYIMIDE NANOFIBER / EPOXY COMPOSITES

This chapter deals with preparation of electrospun polyimide fibers from poly amic acid and thereafter developing chopped PI fiber epoxy composites. The morphology of prepared fibers is presented. The mechanical, fracture, rheological and thermal properties of these composites were investigated and reported. This chapter also presents theoretical modeling of the dynamic mechanical and rheological properties in comparison with the experimental data

Part of this chapter has been published in Nano-structures and Nano-objects (2020). DOI: 10.1016/j.nanoso.2019.100421

4.1. Introduction

Epoxy, an important thermosetting polymer, is the widely studied material owing to its good mechanical performance, wear and chemical resistance, and a wide array of applications (Biolley et al., 1994; Gonçalves et al., 2014; F.-L. Jin et al., 2015; Reis et al., 2015; Zheng et al., 2003). Epoxy curing causes irreversible physical and chemical changes in both the epoxy and hardener. During curing, the molecules form cross-links and grow as a three-dimensional network finally forming a solid epoxy resin. The resulting three dimensional cured systems are usually fragile and brittle (Dittanet et al., 2012; T. Jiang et al., 2013; Olmos et al., 2005; Roşu et al., 2002; Shadlou et al., 2013; Wetzel et al., 2006). The low impact resistance and poor resistance to crack propagation limit their use in advanced applications such as the aerospace industry. Hence, improving the fracture toughness is an indispensable requirement in epoxy-based systems. Incorporating rubbery particles to improve the fracture toughness of epoxy resins is quite known. However, the modification by the incorporation of rubbery inclusions with a low glass-transition temperature (T_g) results in a decrease in both the modulus and Tg of the resultant cured systems. Thus, engineering thermoplastics, such as polyamide, poly(methyl methacrylate), poly(ether sulfone), poly(ether ether ketone), poly(ether imide), and polyimide, are used as advanced modifiers for epoxy resins to overcome this problem (Choe et al., 2003; Galante et al., 2001; Gan et al., 2009; Huang et al., 1997; F. L. Jin et al., 2006). Other strategies like nanoparticle grafted polymer systems (Konnola et al., 2016), electrospun nanofibers (Ahmadloo et al., 2017) and block copolymers additives (Jayan et al., 2018) in epoxy to enhance its performance has also been investigated.

Polyimides (PIs) are an advanced class of high-performance polymers possessing cyclic imide group along with stiff aromatic groups in the chain backbone. These aromatic polyimides have been broadly investigated due to their excellent mechanical properties, thermal stability, combined with their good chemical resistance and dielectric

properties. Its excellent properties like heat and chemical resistance in addition to relatively facile processability, enables it to be used in electronic devices, hot gas filtration applications for spacecraft and in satellites. Polyimides finds applications in Li-ion batteries, sensors, exchange membranes, hydrophobic surfaces etc. The spectrum of its applications can be increased by the formation of micro and nanofibers (D. Chen et al., 2009; Ding et al., 2016; Liaw et al., 2012; Watson et al., 2002).

For spinning polyimide into fibers many traditional methods including dry jet wet spinning has been used earlier (Cheng et al., 1991; Gagliani, 1981a, 1981b; Park et al., 2001). A typical way of preparing PI fibers by wet spinning process of poly amic acid solution and thereafter by thermal imidization was reported (Park et al., 2001). They reported that the prepared poly amic acid (PAA) fibers have ultimate stress and modulus of 268 MPa and 4.1 GPa, respectively. However, after imidization reaction at temperature of 350 °C for about 30 min in N_2 atmosphere, the resultant PI fibers displayed a stress and modulus of 399 MPa and 5.2 GPa, respectively. Generally, traditional PI fibers have fiber diameter in several hundred micrometer range and are utilized for preparing exhaust gas filters, protective clothing and aircraft interior components (Chung et al., 1992; Krol et al., 2001; Weinrotter et al., 1993). In case of energy storage/conversion, environmental protection and allied fields, PI fibers with very small diameters are required (Gong et al., 2012; Maceiras et al., 2014).

Many techniques like template synthesis, self-assembly, phase separation etc., are available for obtaining nanostructured inclusions,. But now-a-days, electrospinning is one of the most commonly used technique for preparing nonwoven fabrics of submicron or nano-scale dimension. Electrospinning is a quite simple, relatively inexpensive technique and has easy scale up ability. The unique features of such spun nanofibers are one-dimensional morphology, high porosity, high surface-to-area ratio, small pore size between depositing fibers of the electrospun mats, and great possibility for fiber functionalization (Dai et al., 2011; Deitzel et al., 2001; Fong, 2001). Owing to

these distinctive properties, electrospun polymer fibers are progressively being used as reinforcement in the polymer matrices (Ahmadloo et al., 2017; Daelemans et al., 2016; Ozden et al., 2010).

Epoxy resin with polyimide is one of the important systems being investigated for high temperature applications (Gaw et al., 1997; Gaw et al., 1996). The use of polyimide electrospun nanofibers as a reinforcement in epoxy matrix is a good idea to develop high performance composites. Polyimide, because of its excellent mechanical and thermal stability forms a stiff system with epoxy matrix, thereby improving the life of the composite system. Moreover, the fibers also possess the additional benefit of the improved aspect ratio and better interfacial surface area resulting from their nano sized structure which leads to better adhesion between the filler and the matrix.

The use of electrospun polyimide fibers in PA6 composites was evaluated and reported (Y. Chen et al., 2012). Chen et al. (D. Chen et al., 2011) reported self-reinforced polyimide nanocomposites in which PI is the reinforcing material and matrix material. In another work, short PI fibers are used for self-reinforcement composites (S. Jiang et al., 2013). Recently, Chen et al. (Y. Chen et al., 2019) investigated the properties of polyimide reinforced epoxy composites by varying the fiber alignment and nanofiber loadings. They reported that the prepared PI/epoxy composites displayed excellent mechanical properties.

In this chapter, chopped electrospun polyimide nanofiber mats were incorporated in DGEBA epoxy at various loadings and epoxy nanocomposites were prepared. The dynamic mechanical properties were evaluated to investigate the reinforcing ability of these nanofiber mats in the embedded epoxy composites. The rheological properties of the nanofiber mat/epoxy systems were tested to find the effect of the PI nanofiber mat on the flow behavior of the systems. The fracture toughness of the PI nanofiber reinforced epoxy systems was tested and compared with the virgin epoxy systems.

Thermogravimetric analysis (TGA) was done to study the thermal stability and char yield of the PAA systems.

4.2. Experimental details

4.2.1. Preparation of Polyimide Electrospun Fibers

Polyamic acid (intermediate of classical polyimide Kapton®) with weight average molecular weight (M_w) 10000 KDa was used for the formation of polyimide. The PAA was filled in a 10 ml syringe and electrospun fibers were prepared in a horizontal electrospinning setup. The processing conditions optimized were 11 KV acceleration voltage, 1000 rpm collector speed, 15 cm distance and 1 ml/hr flow rate. These electrospun mats were collected on aluminum foil. These mats were thermally treated at 70 ˚C for 1hr, 120 ˚C for 1hr, 180 ˚C for 1 hr and 220 ˚C for 1 hr for imidization process to occur and form the polyimide. Thus prepared mats were further characterized and used for the preparation of the epoxy composites.

4.2.2. Preparation of Polyimide/Epoxy Nanocomposites

The electrospun mat was manually chopped into 0.5 mm X 0.5 mm pieces. These chopped pieces were incorporated in DGEBA epoxy (Trade name: GY 250) at weight percentages of 0, 0.5, 1, 2, and 3 respectively by mechanical mixing. Later, sufficient amounts of polyamidoimadazoline hardener (Trade name: AR 140) was added to the system (epoxy to hardener ratio is maintained to be 2:1) and kept for thermal curing After curing, the final products were tested and the properties were evaluated. The schematic representation of PI/epoxy composites are presented in Figure 4.1.

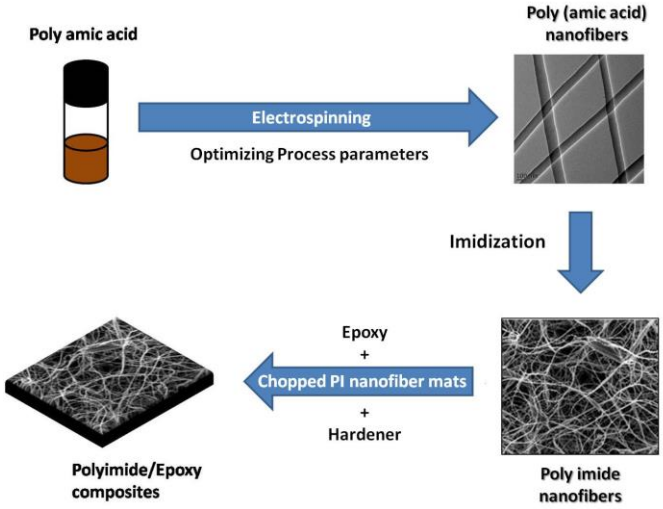

Figure 4.1: Schematic diagram for preparing electrospun fibers and epoxy composites

4.3. Characterization Techniques

The morphology of the nanofibers produced was observed by SEM, TEM and AFM. The samples were gold coated to make them conducting for SEM. These fibers were deposited on the copper grid and the TEM images were taken using HRTEM. For AFM, mica sheet was used as the substrate (Aligent 5500 SPM non-contact mode)**.**The samples were tested in ATR mode from wave number 4000 cm^{-1} to 600 cm^{-1} in a Perkin Elmer Fourier transform infrared spectrometer. The visco elastic properties of PI loaded epoxy thermosets and neat epoxy was analysed using a DMA analyzer from temperature 30 ˚C to 150 ˚C at a ramp rate of 2 ˚C and the modulus and damping factor was plotted. The specimen size maintained was $30 \times 5 \times 1\, mm^3$ and testing was done in tension mode. Fracture Toughness of the epoxy samples was performed using universal testing machine (Instron 5984) as per standards (ASTM D 5045).

The flow characteristics of the neat epoxy and chopped fiber incorporated epoxy systems were tested using Modular Rheometer (MCR 102) using parallel plate mode.

The storage modulus and loss modulus were investigated with respect to angular frequency from angular frequency 0.01 rad/s to 200 rad/s. The viscosity and shear stress of the samples were measured using the same set up with-in the angular frequency range of 1 rad/s to 200 rad/s. The thermal stability of neat epoxy and PI loaded epoxy samples were tested from a temperature range of RT to 800 ˚C by employing a heating rate of 20 ˚C/min in presence of nitrogen.

4.4. Results and Discussion

4.4.1. Morphology

The polyamic acid (PAA) solution was filled in a 10 ml disposable syringe and an electrical voltage was applied between the syringe needle and the drum collector. At a particular voltage, the repulsive force of the droplet exceeds the surface tension holding it. Hence it forms a Taylor cone at the needle tip, which subsequently tends to form fibers and moves towards the collector to satisfy the surface tension. The Transmission electron microscope and Atomic force microscope images of the polyamic acid electrospun nanofibers were taken and are depicted in Figure 4.2. The fiber diameters were measured using the available image processing software's and the diameter range was found to be between 70nm to 500 nm. By measuring the diameters of fibers at different places, the average fiber diameter was found to be about 280 nm.

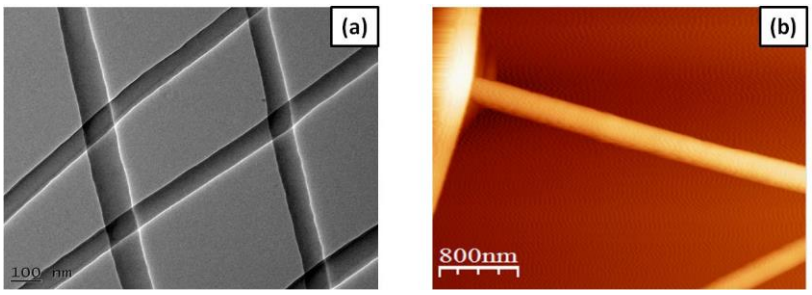

Figure 4.2: (a) TEM and (b) AFM images of electrospun PAA fibers

The obtained PAA electrospun mat was then kept in an air oven and subsequent thermal treatment was given at pre-mentioned temperatures for the imidization reaction to occur and thus converting polyamic acid to PI fibers. The SEM micrographs and optical microscopic images of PI fibers are presented in Figure 4.3. From the images we can observe fine nanofibers of the polyimide.

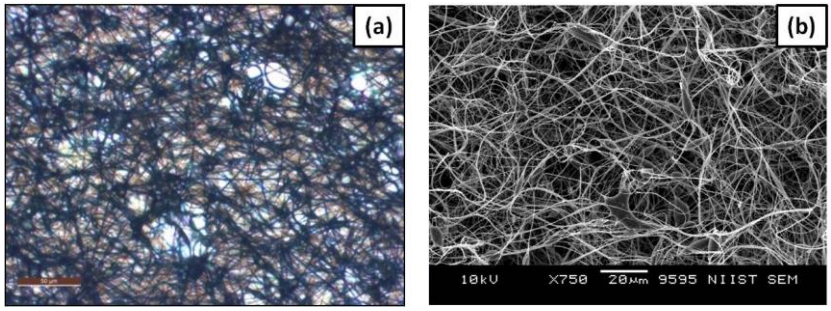

Figure 4.3: (a) Light microscope and (b) SEM images of PI fibers after imidization

4.4.2. Fourier Transform Infrared Spectroscopy

Fourier transform Infrared Spectroscopy (FTIR) spectra of the electrospun PAA fibers, electrospun PI fibers and casted PI fibers are presented in Figure 4.4. the curves reveal that, thermal treatment of poly(amic acid) at 70 ˚C for 1hr, 120 ˚C for 1hr, 180 ˚C for 1 hr and 220 ˚C for 1 hr results in the transformation of electrospun poly(amic acid) fibers to electrospun polyimide fibers. The peak at ~1627 cm $^{-1}$ can be accredited to the absorption of carbonyl stretching (C=O) of the amide group and the peak at 1505 cm $^{-1}$ is due to C-NH stretching vibration. The peak around ~3500 cm $^{-1}$ is associated with N-H and O-H stretching in polyamic acid. The vanishing of this peak after imidization indicates successful cyclisation of N-H and O-H to the corresponding imide group. Now, considering the polyimide spectra, the peak at ~1780cm $^{-1}$ and ~1722 cm $^{-1}$ corresponds to C=O symmetric stretching vibration and C=O asymmetric stretching vibration respectively. The peak at ~1372 cm $^{-1}$ can be credited to C=N stretching vibration, and ~725.5 cm $^{-1}$peak can be due to C=O bending. In the Figure, the prepared PI Electrospun

mat is also compared with casted PI film and both have identical FT-IR spectra, which confirm the formation of polyimide conclusively.

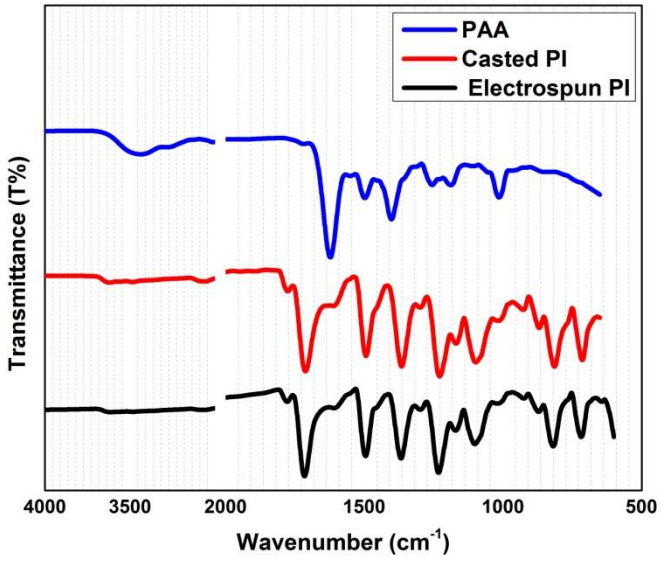

Figure 4.4: FTIR spectra of fibers (a) polyamic acid, (b) electrospun polyimide and (c) casted polyimide

4.4.3. Dynamic Mechanical Properties

The storage modulus of neat epoxy and PI nanofiber incorporated samples were analyzed and the graphs are presented in Figure 4.5 a. We can observe that the dynamic storage modulus of PI fiber incorporated composites increase with loading percentage and tan delta undergoes a positive shift. When compared to neat epoxy system, the storage modulus of PI loaded samples exhibit a hike at low temperatures until a point, after this point the modulus tends to decrease. This point has a significant thermal relaxation in the tan delta, which may correspond to the Tg of the polyimide. This increase in the modulus is indicative of the reinforcement effect of the nanofiber mat in epoxy systems. These mats while dispersed in epoxy constitute an isotropic stiffening system and so contribute to the high strength of the composites. The effect of the

nanofiber mat loading showed a constructive positive effect in the mechanical performance of the composites. This increase is due to the effective stress transfer, good interfacial surface area and reinforcing strength of the mat. In case of tan delta (Figure 4.5 b), the positive shift in the peak is due to the change in cross-linking density of the systems because of the presence of PI mats. The Tg of neat epoxy was found to be 92.7 ˚C, while Tg of all PI loaded epoxy composites were found to be more than 104˚C, which signifies the positive role of PI fibers in enhancing the glass transition temperature.

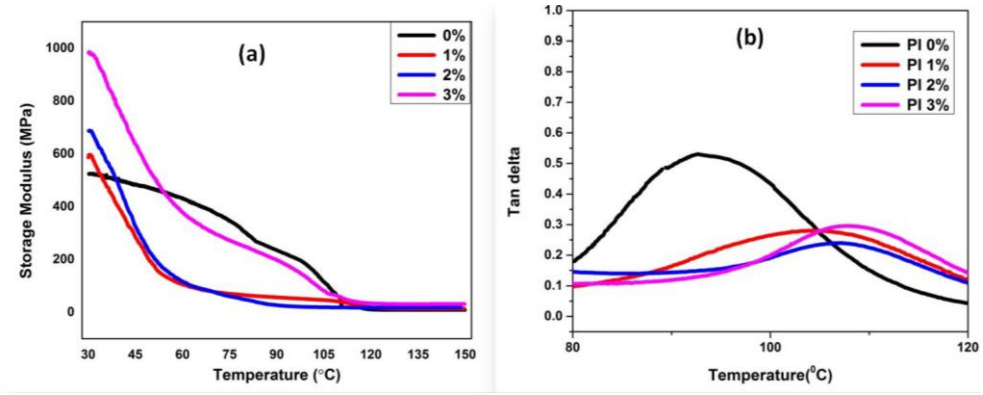

Figure 4.5: Dynamic mechanical properties of PI nanofiber reinforced epoxy composites

The dynamic mechanical properties of the PI loaded epoxy composites was modeled using Einstein, Guth and Quemada models to assess the change in storage modulus of the epoxy matrix with increase in loading. Einstein proposed a simple theoretical model to estimate the modulus of filler reinforced polymer matrices. It is mathematically denoted as

$$\frac{E_c}{E_p} = \left(1 + 2.5V_f\right) \tag{4.1}$$

Where, E_c and E_p are the storage modulus of resultant composite and matrix and V_f is the reinforcement volume fraction. This model is applied to polymeric systems reinforced with less concentration.

Guth equation for fiber reinforced polymeric systems is expressed by the equation

$$\frac{E_c}{E_p} = \left(1 + 2.5V_f + 14.1{V_f}^2\right) \quad (4.2)$$

This equation takes into account the interactions between the particles even at higher concentration

The Quemada equation for polymeric systems is given by

$$\frac{E_c}{E_p} = 1/(1 - 0.5K_6V_f)^2 \quad (4.3)$$

This equation uses a variable that implies the interaction between particles and the geometry (variable, K_6 =2.5). The experimental values were found to be higher than the theoretical model values.

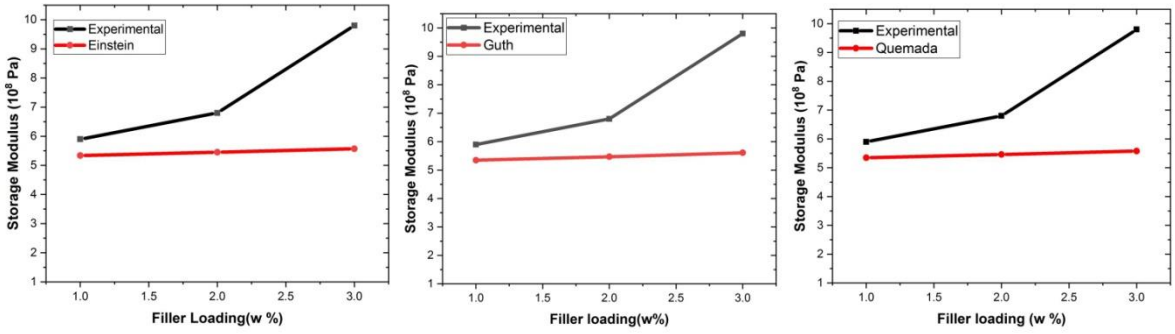

Figure 4.**6**: Visco-elastic properties comparison between experimental values and theoretical models (at room temperature)

4.4.4. Fracture Toughness

In epoxy composites, fracture toughness is one of the major challenges that need to be addressed. Cured epoxy being highly brittle tends to break with the slightest crack. This drawback of epoxy systems need to be overcome for its industrial applications and

can be done by the introduction of suitable reinforcements. The PI nanofiber mat loaded epoxy samples at different compositions were tested and the stress concentration intensity is depicted in Figure 4.7. The fractured samples were also observed using SEM and the images are illustrated in Figure 4.8. From the Figure 4.7, we can observe that 0% nanofiber mat loaded samples (neat epoxy) have a K_{IC} of 1.06 ± 0.37 MPa.m$^{1/2}$. This increased to 18% and 20% at 0.5 w % and 1 w % respectively. Upon further increase in loading of 2 w% and 3 w%, the toughness decreased gradually. At low loadings, the crack propagation is obstructed by the incorporated PI nanofiber mat and different crack propagation mechanisms like crack deflection, fiber pull out and fiber bridging can be observed. But at higher loadings, the system becomes highly brittle and hence fracture toughness decreases. So, at higher concentrations, the PI loaded epoxy composites might have developed "secondary cracks" that are formed parallel to the mat surface, thereby making the entire composite brittle and so, the toughness decreases. Similar decrease in flexural properties was observed in the PMMA nanofiber/epoxy systems (Al-Assafi et al., 2016). Hence, based on the results we can state that PI nanofiber mats being stiff can only be used at low loadings to toughen the epoxy systems. So, further loadings were not tested as the experimental trend shows a decrement in the toughness.

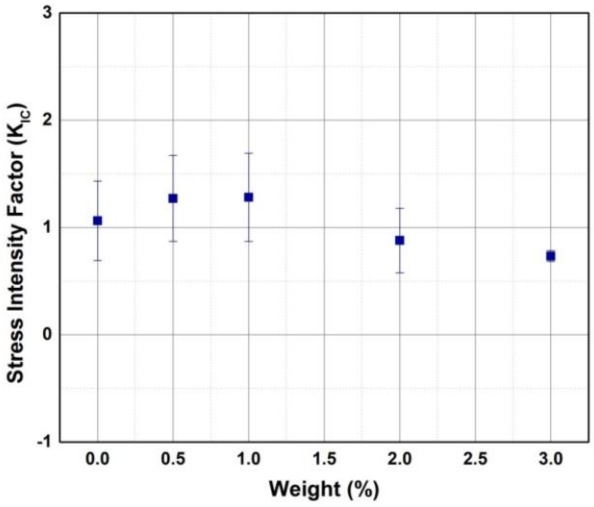

Figure 4.7: Variation of stress intensity factor with PI loading (w %)

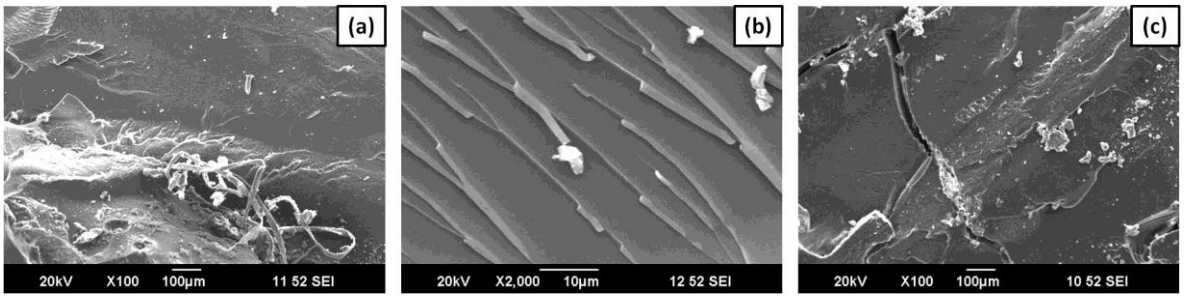

Figure 4.8: Fractured surface topography of polyimide/epoxy composites at (a) 1 w% and (b), (c) 3 w% PI loading

4.4.5. Rheological Properties and Theoretical Modeling

The storage and loss modulus of the neat epoxy and PI mat incorporated epoxy systems were estimated with respect to fiber content and are presented in Figure 4.9. As per the Figure, we can observe an increasing trend in modulus with respect to the fiber loading. The result conclusively proves that these nanofiber mats have a good influence in flow dynamics of the systems. Figure 4.10 depicts the change of viscosity with shear rate. We can observe from the Figure that viscosity depends on filler loading. The difference in viscosity is more significant in the lower frequencies than at higher frequencies.

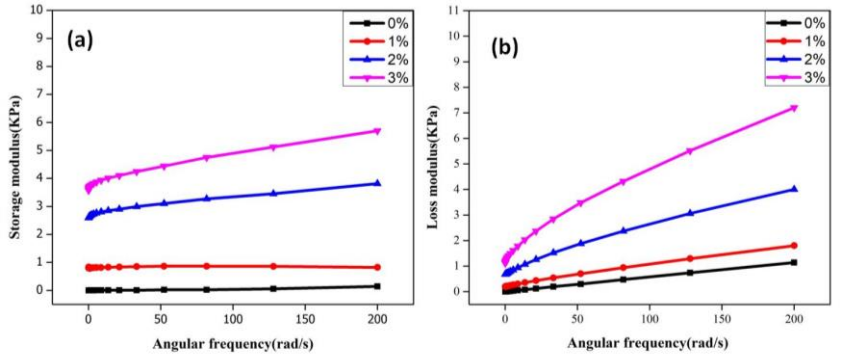

Figure 4.9: Variation of rheological properties, (a) storage modulus & (b) loss modulus with PI loading (w %)

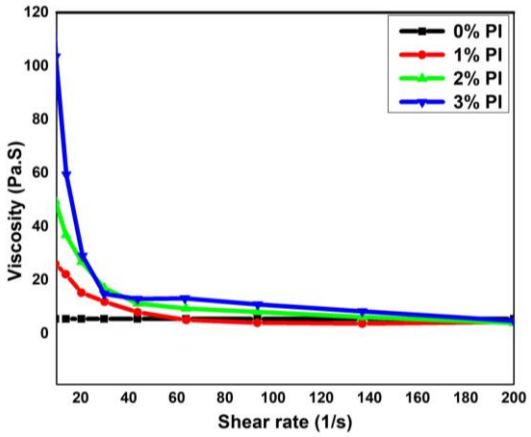

Figure 4.10: Variation of viscosity with respect to shear rate

Usually flow models are employed to estimate the type of flow followed by the system based on the experimental data. Here, PI/Epoxy rheology experimental data was modeled using available power's and Casson's models.

4.4.5.1. Power's Model

In this model, the shear stress and shear rate are plotted on logarithmic axis and it expresses shear thinning and thickening behavior of fluid (Folayan et al., 2017)

$$\sigma = K\gamma^{n} \tag{4.4}$$

Where σ and γ are shear stress and shear rate respectively, n is the flow index parameter which describes the tendency of fluid to shear thin , and k is consistency coefficient .When $n < 1$,the fluid is thinning in nature and when $n > 1$,the fluid is thickening in nature. The power law model holds better in the low shear condition

Applying logarithms on both the sides of Eq 4.4:

$$log\sigma = logK + nlog\gamma \tag{4.5}$$

Equation 4.5 can be expressed as,

$$log\eta = logK + (n-1)log\gamma \tag{4.6}$$

Where, η is the viscosity. The Powers law fit data of neat epoxy and loaded samples are depicted in Figure 4.11. The parameters obtained are tabulated in table 4.1.

Table 4.1: Powers law parameters

Sample	Slope	Intercept	Regression co-efficient
Neat epoxy (0% PI)	0.94501 ± 0.01123	0.80268 ± 0.01496	0.99634
PI 1%	0.44949 ± 0.02262	1.74934 ± 0.03013	0.93807
PI 2%	0.29772 ± 0.02692	2.32942 ± 0.03586	0.82351
PI 3%	0.31892 ± 0.04006	2.52892 ± 0.05337	0.70577

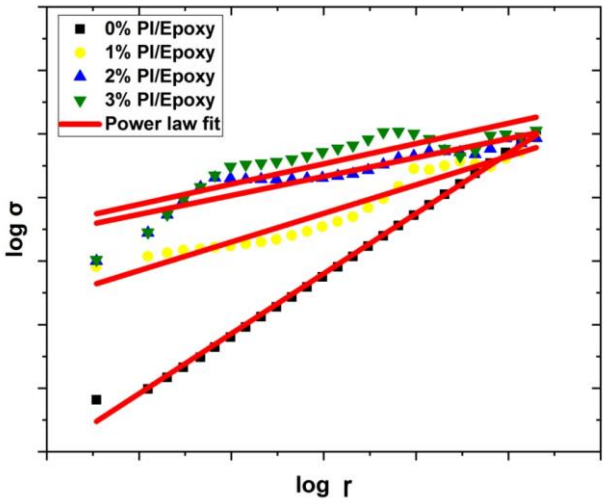

Figure 4.11: Powers law rheological model fitting

4.4.5.2. Cassons Model

The Casson rheological model is used to estimate the flow of visco-elastic fluids. Mathematically, it is expressed as(Folayan et al., 2017; Herschel et al., 1926)

$$\sigma^{0.5} = K_{0c}^{0.5} + K_c^{0.5}\gamma^{0.5} \quad (4.6)$$

Where σ is shear stress, **γ** is shear rate, k_{oc} is Casson yield stress (Pa.s), k_c is Casson plastic viscosity in mPa.s. The Casson model fitting data of neat epoxy and fiber loaded samples are presented in Figure 4.12 and the parameters obtained are presented in Table 4.2. From the models, powers law seems to be better fit.

Table 4.2: Cassons law parameters

Sample	Slope	Intercept	Regression co-efficient
Neat epoxy (0% PI)	2.33069 ± 9.15054E-4	0.07434 ± 0.00443	1
PI 1%	1.83234 ± 0.12928	4.80946 ± 0.62557	0.88489
PI 2%	1.50431 ± 0.17866	12.39152 ± 0.86452	0.72887
PI 3%	1.42839 ± 0.35548	17.54646 ± 1.72012	0.3681

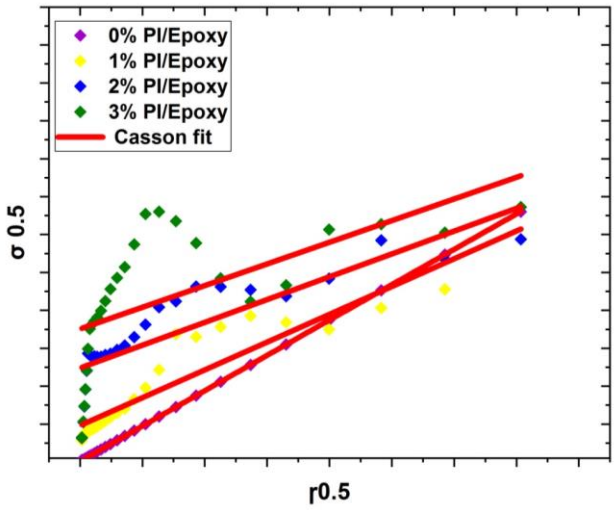

Figure 4.12: Cassons law rheological model fitting

4.4.6. Thermogravimetric Analysis

The Thermogravimetric analysis (TGA) profiles of PAA and electrospun PI are presented in Figure 4.13. From the profiles, it is seen that PI is mostly stable until 550 ˚C, and after complete degradation quite high char yield is present. However, in case of

PAA, most of the degradation takes place at low temperature, which is accompanied with a small peak at 550 ˚C and very less char yield at the end.

The thermal stability of PAA and PI systems are investigated by several researchers (Haghighi & Cotton, 2019; Tsimpris & Mayhan, 1972; Varma et al., 1977; Wang et al., 2022) . From the Figure, we can see that a lot of weight loss happened for PAA in lower temperature range indicating the evaporation of solvent and removal of water while formation of PI. And at 550 °C there is loss step corresponding the degradation of PI, which is profound in PI sample. In the case of PI sample we observed a excellent thermal stability until 550 °C and later a single degradation step with formation of char. This is the reason why polyimide can be used for making carbon fibers as it results in high carbon yield. Polyimide degradation is a one stage reaction. Detailed studies indicates that primary breakage in polyimide is because of breakage of C=O group to give out carbon dioxide (CO2) and carbon monoxide (CO). the CO2 and CO will continue with increase in temperature and alongside at high temperatures oxygen-nitrogen group will get cleaved to form nitrogen oxide and nitrogenous substances

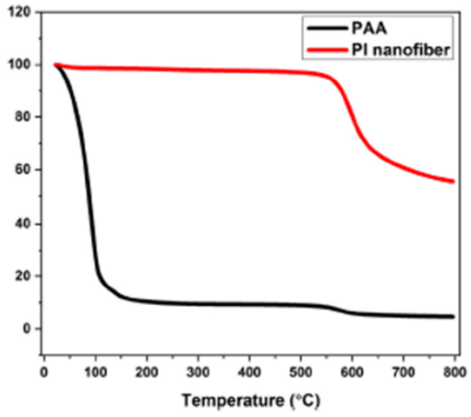

Figure 4.13: TGA thermograms of PAA and PI nanofibers

The stability of polyimide incorporated epoxy samples was tested and is presented in Figure 4.14. From the TGA thermograms, it is clear that PI mats affect the thermal stability of epoxy by improving the degradation temperature and further there is an improvement in the char yield compared with the neat cured epoxy. These PI mats positively improved degradation temperature of epoxy, so these materials can be used for applications requiring high thermal stability.

As from the previous discussions we can see the decomposition in cured epoxy and polyimide is a single step process. When a highly temperature stable PI is introduced inside the cured epoxy system, the high temperature PI is expected to prevent the epoxy chains from degradation at its virgin temperature. i.e., with improvement in PI content in the system the more will be the temperature needed to start the degradation. Hence the thermal stability of the composites improved. Further we can see that as the PI content is increased the char yield is improved than that of need composites as PI have high thermal stability, unlike the case where the SBC fibers did not contribute in improving the thermal stability

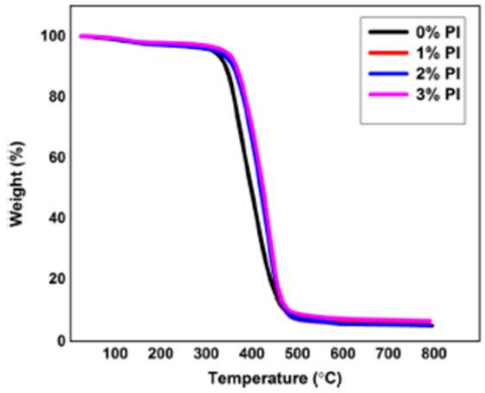

Figure 4.14: TGA thermograms neat epoxy and PI loaded epoxy thermosets.

4.5. Conclusions

Electrospun nanofibers of polyimide were successfully prepared by spinning poly amic acid, followed by thermal imidization of poly (amic acid) electrospun mat. PI nanofiber mat/epoxy composites were prepared at different mat loadings. The morphology of the fiber was confirmed by Transmission electron microscope and Atomic force microscope images. The completion of imidization reaction was confirmed by FTIR and the corresponding peaks. The dynamic mechanical testing results showed an increase in the modulus for the polyimide mat loaded samples than neat epoxy composites at room temperature. The fracture toughness of the epoxy systems exhibited a 20% increase at 1% loading and thereafter decreased with increase in loading. The dynamic rheology studies reveal the increased effect of these fibers on the visco elastic flow properties of the composite. The TGA of the systems were done and thermal stability was analyzed and it is observed that PI loading improved the thermal stability of epoxy composites. Thus polyimide nanofiber mat reinforced epoxy composites could be utilized for advanced applications at relatively low loadings of PI nanofiber mats. Thus the developed PI incorporated epoxy composites are having advanced performance than neat epoxy samples and have potential use as structural composites and in circuit boards.

CHAPTER 5

ELECTROSPUN ZIRCONIA INCORPORATED CARBON FIBER AND THEIR EPOXY COMPOSITES FOR EMI SHIELDING APPLICATIONS

These chapters deal with the preparation and characterization of electrospun carbon fibers from electrospun PAN fibers. Zirconia loaded carbon fibers were prepared and characterized. In the later stage, these mats are used as reinforcements in epoxy and epoxy composites are developed. These epoxy composites are observed to have superior mechanical performance and EMI shielding effectiveness than neat epoxy composites

Part of this chapter has been published in Materials Research Bulletin (2021). DOI: 10.1016/j.materresbull.2021.111477

5.1. Introduction

Electrospinning has proved its worth as an exceptional technique to prepare polymeric fibers in nano/sub-micron dimensions from their respective solutions. Based on the end-use and final requirements, even ceramic and carbonaceous fibers can be prepared using the electrospinning process (Dzenis, 2004; D. Li, Babel, et al., 2004; Xie et al., 2008). The selective use of proper experimental setup and conditions will yield various fiber morphologies like core-shell fibers (Guo et al., 2014; Sun et al., 2003; Yarin, 2011), nanofiber yarns (Ahmadloo et al., 2017; Smit et al., 2005), hollow fibers (D. Li et al., 2005; D. Li & Xia, 2004). The assets of the electrospinning process include the ability to achieve different morphologies, ease of fiber functionalization, and a wide range of material choices. These advantages, coupled with the unique properties of the electrospun fibers (like high surface area, excellent aspect ratio), make electrospinning a distinguished nanofiber production technique. Electrospun nanofibers find lots of attractive applications in the bio-medical field (Liang et al., 2007), protective clothing (Faccini et al., 2012; Liang et al., 2007), composite reinforcement (Bergshoef et al., 1999; Tian et al., 2007), sensors (Ding et al., 2010; Ding et al., 2009), energy storage/conversion (Dong et al., 2011; Mao et al., 2013), EMI shielding (Im et al., 2010a, 2010b; H.-R. Kim et al., 2012; Sonehara et al., 2008).

For the preparation of carbon fibers, melt spinning, and chemical vapor deposition (CVD) processes are widely and commonly used. Many researchers have started preparing carbon nanofibers by carbonizing electrospun polymer mats and exploring their applications (Cai et al., 2018; Inagaki et al., 2012; Q. Li et al., 2019; Wei et al., 2019; Zhou et al., 2009). Even though many polymers have been reported for their ability to produce nanofibers from the electrospinning technique, only a few polymers like polyacrylonitrile (PAN) (Alarifi et al., 2018; De Oliveira et al., 2018; Y. Wang et al., 2002), pitch (Park et al., 2003), poly (vinyl alcohol) (Gupta et al., 2017; Zou et al., 2010), polyimide (PI) (Chan Kim et al., 2004; Xuyen et al., 2007) and poly

(vinylidene difluoride) (Yang et al., 2011), were used extensively to produce carbon nanofibers due to their low cost, ease of availability and properties of the final carbon produced. These carbon nanofibers have lot of applications, which include electrochemical capacitors (C Kim et al., 2003; Wee et al., 2010), composite fibers (Ge et al., 2004), Lithium-ion batteries (Hwang et al., 2012; L. Wang et al., 2008), electromagnetic interference shielding (Im et al., 2011).

The growth and process in technology have led to the broad use of electronic devices in society, and consequently, electromagnetic interference (EMI) associated with it, too has increased rapidly. These interferences cause a glitch to the usual operations of other electronic devices and may adversely affect human health. Hence, the development of materials that has the ability to shield electronic components from these unwanted interferences is an exciting and vital area of study (Baker et al., 1988; Y.-Y. Kim et al., 2011). Such materials are known as EMI shields, and the usual shielding mechanism is either reflection or absorption of electromagnetic waves. By totaling the amount of shielding by reflection and absorption of the material, the total effective shielding performance of particular shielding material can be found by adding the amount of shielding by reflection and absorption together. Materials having high permittivity and permeability are the best choice for EMI shielding applications. The electrical and magnetic states of those materials can vary with incoming electromagnetic waves, and thereby attenuating them. When reflection is the primary shielding mechanism of an EMI shielding material, then there is a chance for the reflected wave to interact with other electronic equipment causing secondary EMI (Håkansson et al., 2007; Im et al., 2011; Meena et al., 2010). This secondary EMI is unintentional and further creates electronic abnormalities. So, developing absorption dominant EMI shields are mostly preferred in the current scenarios.

Metallic materials and their allied combinations were the primary choices for EMI shields until a few years back, but their primary shielding mechanism being

reflection and their inherent heaviness has restricted its widespread usage nowadays (Zhiming Zhang et al., 2003). Carbon nanomaterials are another class of materials that are being extensively used and researched for EMI shielding applications because of their excellent ability to absorb incoming electromagnetic waves (Hong et al., 2017). Carbon nanotubes (single-walled and multiwalled), graphene, reduced graphene oxide, and carbon fibers are the most commonly used in this category. Compared to other carbon structures, the utilization of carbon fibers for EMI shielding is preferred to some extent since it is cost-effective, and the problem of agglomeration is minimal in carbon fibers than in other counterparts. Electrospun carbon nanofibers and their combinations are potential and efficient candidates for EMI shielding applications.

Zirconia is corrosion and chemical-resistant ceramic with low brittleness, high density, hardness, and permittivity. Zirconia has a dielectric constant in the range of 10-25, making it an interesting material for EMI shielding applications. Chen et al. developed zirconia doped electrospun carbon fiber/epoxy composites and investigated the mechanical and corrosion resistance properties of those composites, and found improvement in both static mechanical properties and corrosion resistance(C. Chen et al., 2018). Submicron level zirconia of distinct sizes were synthesized and used as reinforcement in the epoxy resin (at 1, 3, and 5 wt%), and elastic modulus were also investigated. They found an improvement in modulus in both cases compared to unfilled epoxy (Bondioli et al., 2006). Zirconia-loaded carbon nanofibers act as very effective wave absorbing materials with high permittivity that absorbs incoming EMI waves. Im et al. investigated the effect of heat treatment on EMI shielding properties of ZrO_2/carbon fiber mats in the frequency range of 0.8 GHz to 8.5 GHz by carbonizing at different temperatures. Their studies revealed that the mats carbonized at 900 $^{\circ}$C and a sample with zirconia loading of 1.5 g exhibit EMI shielding effectiveness (SE) of ~15dB, and the maximum SE obtained was 31.79 dB at 2100 $^{\circ}$C (Im et al., 2011). Recently, Naresh et al. (Naresh et al., 2022) prepared zirconia added carbon nanotubes/epoxy composites and studied their EMI performance and concluded that the

composites showed improved absorption thereby increasing EMI shielding effectiveness due to incorporated zirconia. On the other hand, Rohini et al., investigated the effect of branched poly(ethyleneimine) functionalized multiwalled carbon nanotubes on commercially available carbon fiber/epoxy composites (having less thickness of 0.5 mm) and found maximum shielding effectiveness of absorption (SE_A) of -49 dB at 17 GHz (Rohini et al., 2018).

In this chapter, zirconia embedded PAN electrospun mats are prepared by optimizing the electrospinning process parameters. These PAN mats are then converted to carbon nanofiber mats by carbonization in a furnace. The surface morphology of electrospun fiber and carbonized fiber mats were observed and compared using SEM analysis. The XRD, Raman, and AC conductivity studies on carbon fiber mats were done and are reported in the following sections. The EMI shielding capability of these carbon mats were also investigated in the important satellite/aircraft communication Ku band. The effect of the number of layers (thickness) on the total shielding effectiveness was tested to investigate the dependence of absorbance on EMI shielding. Also, to demonstrate the application of electrospun zirconia embedded carbon fibers, ZrO_2/carbon fiber/epoxy composites were prepared by a facile and economical hand layup technique. The dynamic mechanical properties of ZrO_2/ carbon fiber /epoxy laminas were also performed and reported herein, which are not available in the literature at present to the best of our knowledge. In the current work, we have attempted to simultaneously improve EMI shielding and mechanical properties of ZrO_2/ carbon fiber / epoxy composites to develop multifunctional composites with comparable properties of commercial CF/epoxy systems.

5. 2. Experimental Details

5.2.1. Preparation of Zirconia Incorporated PAN Electrospun Nanofibers

The polymer used as a carbon source, polyacrylonitrile (PAN) (M_w: 1,50,000 KDa), was procured from Sigma Aldrich. Zirconia powder (micron-sized) was procured from Alfa Aesar. The solvent used N, N-dimethylformamide (DMF), was supplied by Spectrochem Pvt. Ltd and was used as such. The particle size of micron-sized ZrO_2 was reduced to the sub-micron level using the planetary ball milling process (conditions: 200 rpm for 18 hrs). Thus obtained ZrO_2 particles at different compositions were mixed with PAN polymer solution of 9 wt% concentration. The solutions were kept for overnight stirring, and the obtained homogenous solution was used for preparing electrospun nanofibers.

Table 5.1: Electrospinning parameters optimized for PAN/ZrO_2 combinations.

Sample Code	PAN/ZrO_2 (w%: w %)	Acceleration Voltage(KV)	Flow rate (ml/hr)	Distance (in cms)	Collector Rotation
A	PAN alone	9	1.5	16	1100 rpm
B	1:1	10	1.5	15.5	1150 rpm
C	2:1	10	1.5	15.5	1100 rpm
D	2:3	10.5	1.5	15.5	1200 rpm

The solution was taken in a 10 ml syringe in a horizontal electrospinning setup and spun on an aluminum foil. The optimized electrospinning parameters for each

combination are tabulated in Table 5.1. The sample code A, B, C, and D are given for PAN/ZrO_2 combinations as presented in the table and used throughout the chapter.

5.2.2. Preparation of ZrO_2 Loaded Carbon Fibers

The obtained nanofiber mats incorporated with zirconia from the electrospinning process were then subjected to oxidation stabilization in an air oven at 220 ˚C for 1 hr. After that, the samples were carbonized in a furnace under a nitrogen atmosphere at 1000 ˚C at a heating rate of 1 ˚C/min. The samples were held for 4 hrs at 1000˚C, and subsequently, the furnace was cooled down to room temperature. These mats were carefully taken out from the furnace, stored safely, and further characterizations were done. Polyacrylonitrile (PAN) (a high carbon yield precursor) in the form of a fibrous mat produced by electrospinning technique when subjected to stabilization and high-temperature treatment will be converted to carbonaceous fibers. Stabilization is a vital step to avoid the fusing of fibers during the carbonization step, as the carbonization process involves both physical and chemical reactions like dehydrogenation, cyclization. The carbonization process was done in a nitrogen atmosphere to remove heteroatoms and prevent oxidation during the process. During this process, the morphology of smooth PAN fibers will be lost, and wrinkled types of carbon fibers will be obtained, with an increase in surface area and a decrease in fiber diameter (Mao et al., 2013).

5.2.3. Preparation of ZrO_2/CNF/Epoxy Composites

For the preparation of epoxy composites, DGEBA epoxy resin with the trade name GY 250 was used with a hardener combination of AR 140 at a weight ratio of 2:1. The carbonized mats were then impregnated using this epoxy/hardener mixture, and composites were prepared by curing them at 60 ˚C and 80 ˚C. The mass of fibers in the composite is found to be ≈ 0.021, corresponding to 0.21% fiber weight fraction. The sample codes AE, BE, CE, and DE represents epoxy laminas prepared from samples A,

B, C & D. The schematic representation of electrospinning process and composite preparation is presented in Figure 5.1.

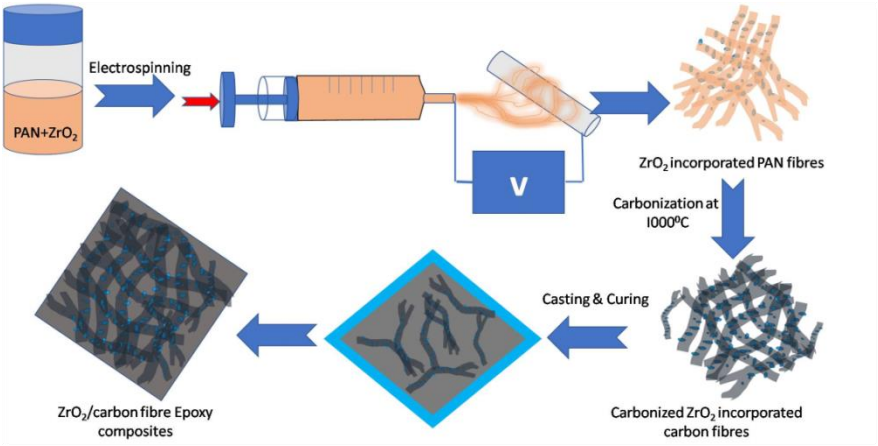

Figure 5.1: Schematic representation of electrospinning process and composite preparation

5.3. Characterization Techniques

The morphology of the neat PAN nanofibers and zirconia-loaded PAN nanofibers was observed and studied using a transmission electron microscope (JEOL, JEM 2100). On the other hand, a scanning electron microscope (JEOL, 6390LA) was utilized to study the change in morphology of PAN nanofibers before and after carbonization. The samples were gold-coated before observing in the scanning electron microscope to make the surface conducting in nature. Powder X-ray diffraction (XRD) patterns were recorded from 5˚ to 90˚ at 45 kV and 30mA. Raman spectra was recorded using LabRAM HR Evolution, Horiba Jobin Yvon, France, using a laser of 532nm. Electrochemical measurements were carried out using EG&G (Princeton applied research, Model no. 263A) using symmetrical cell configuration. The AC conductivity of samples was calculated using the following equation (Elimat et al., 2008).

$$\sigma_{ac} = 2\pi f \varepsilon_0 \varepsilon^{"} \quad (5.1)$$

Where f is the applied frequency, ε" is the dielectric loss, and ε_0 is the vacuum permittivity (ε_0=8.8541878128×10^{-12} F·m^{-1}). The total electromagnetic shielding effectiveness was measured using a vector network analyzer (VNA; Anritsu MS4642A) with a KEYCOM wave-guide adaptor in 12–18 GHz frequency. The scattering parameters were recorded and were used to estimate the total shielding effectiveness using the input and output power. The viscoelastic nature of the epoxy composites was investigated by PerkinElmer dynamic mechanical analyzer (DMA 8000) in tension mode. Rectangular specimens ($25 \times 10 \times 0.5\, mm^3$) were taken, and the test was performed from a temperature range of -30 ˚C to 150 ˚C, at a heating rate of 2 ˚C/min.

5.4. Results and Discussion

5.4.1. Morphological Development

In Figure 5.2, the morphology of the electrospun PAN nanofibers and zirconia incorporated PAN nanofibers observed in the transmission electron microscope are presented.

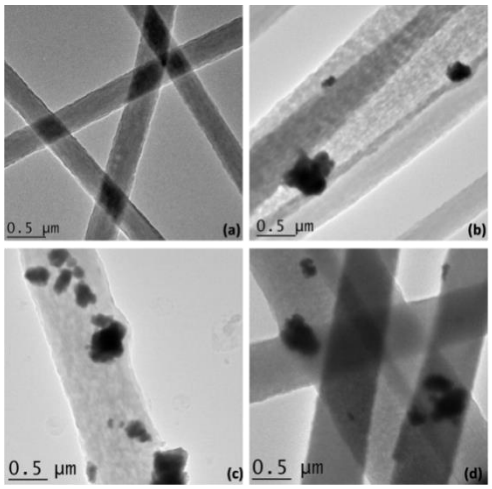

Figure 5.2: TEM Micrographs of PAN/ZrO_2 electrospun fibers coated on copper grid (a) PAN alone, (b) PAN/ZrO_2 (2:1) (c) PAN/ZrO_2 (1:1) and (d) PAN/ZrO_2 (2:3)

Table 5.2: Average diameter of nanofibers with respect to concentration

Sample code	Average diameter as spun (in nm)	Average diameter after carbonization step (in nm)
A	540±79	398±77
B	702±38	566±91
C	521.6±113	496±91
D	821.6±153	726.6±84

Scanning electron microscope images clearly disclose that the carbonized mats retained their fibrillar morphology and the size of the carbonized mat decreased compared to the original mat. The diameter of the fiber was measured in the instrument software. Using the ImageJ software, at least ten fiber diameters were measured, and the average value is presented in table 5.2. Further, the elemental spectrum (EDAX) of carbon nanofibers was taken to see the elemental composition and presented in Figure 5.3. The carbon fibers obtained after carbonization step are depicted in Figure 5.4.

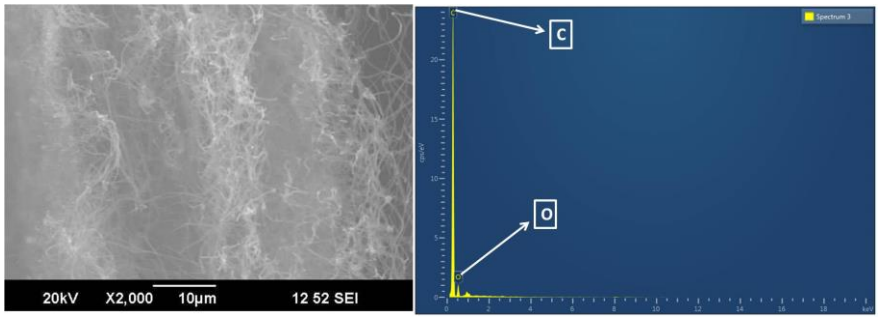

Figure 5.3: SEM and EDAX Spectrum of neat carbon nanofibers after carbonization

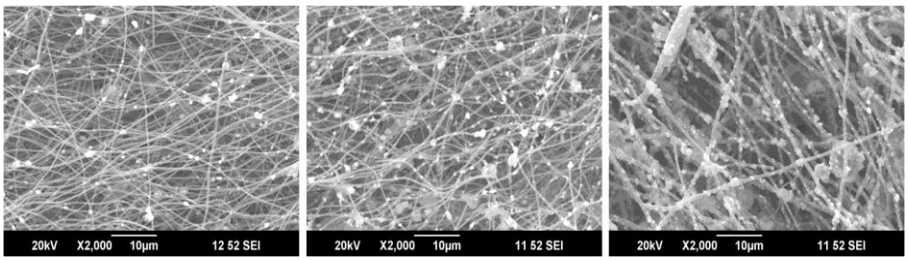

Figure 5.4: SEM Micrographs of ZrO_2 loaded Carbon nanofiber mats of, (a) PAN/ZrO_2 (2:1) (b) PAN/ZrO_2 (1:1) and (c) PAN/ZrO_2 (2:3)

5.4.2. X-ray Diffraction Analysis

XRD of neat carbon nanofiber mat and ZrO_2 incorporated carbon fiber mats were performed to study the phase transformations after the carbonization process at 1000 °C, and the patterns are illustrated in Figure 5.5. For sample A, the carbon peaks were observed at 2θ ~ 25°, which depicts the crystallographic plane (0 0 2) of the graphitic structure, thereby proving that the carbonized mat at 1000 °C has a graphitic structure (Aboagye et al., 2015; Zhaobao Zhang et al., 2017). In samples B, C, and D, along with the carbon peaks at ~25°, the existence of other peaks is also clearly observed because of the presence of embedded zirconia (G. Wang et al., 2010). The intensity of sample D is more than any other sample because of the increased zirconia content.

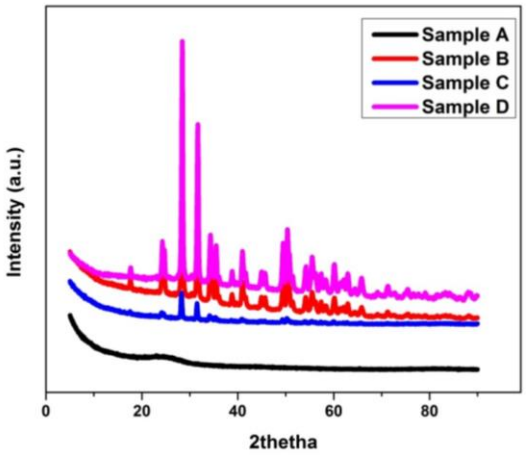

Figure 5.5: XRD Spectrum of Zirconia loaded carbon nanofiber mats (samples A, B, C & D).

5.4.3. XPS analysis

For investigation, the elemental compositions and their chemical state XPS analysis was carried out. The XPS spectrum of carbonized carbon nanofiber mat and zirconia embedded carbon fiber mats are depicted in Figure 5.6 and Figure 5.7 respectively. For neat carbon nanofiber mats, the survey spectra displayed three peaks (Figure 5.6 a), that are corresponding to C 1s, N 1s, and O 1s. The atomic ratios of C 1s, N 1s, and O 1s on the surfaces are 91%, 0.9% and 8.1% respectively. In general, carbonized fibers with more than 90% carbon content can be considered as carbon fibers, and over 99% carbon content are regarded as graphite fibers. For the deconvoluted C $_{1s}$ spectra, there are two main peaks at ~284.8 eV and ~285.9 eV . The peak at ~284.8 eV can be attributed to C–C and C=C, which is very predominant in the sample, while the peak at ~285.9 eV can be contributed from C-N groups (Chiang et al., 2021).

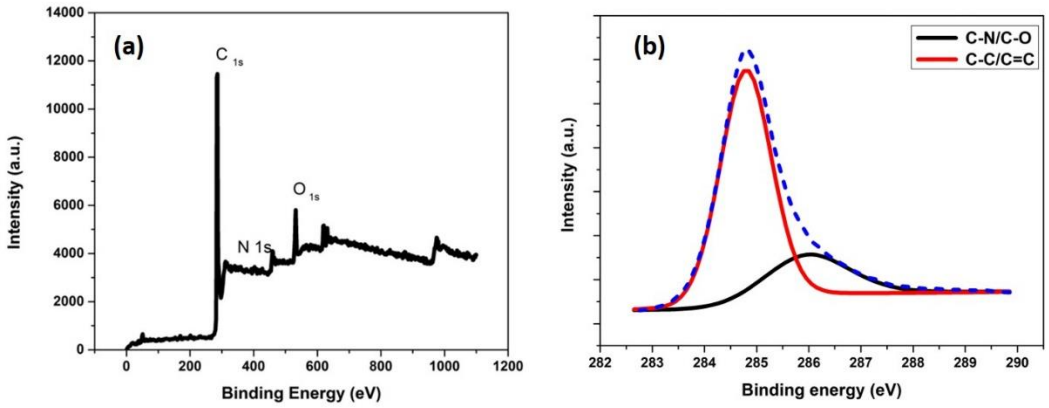

Figure 5.6: XPS Spectrum of (a) carbon nanofiber mats and (b) deconvoluted C1s spectra.

The full XPS spectrum of zirconia loaded carbon nanofiber mats are presented in Figure 5.7 (a). From the Figure, the survey spectra displayed peaks that are corresponding to C 1s, N 1s, O 1s, Zr 3p and Zr 3d . That signifies the presence of zirconia in the carbonized fibers. The deconvoluted Zr 3d spectra was taken (in Figure 5.7 b) , and two main peaks at ~182.5 eV and ~184.9 eV was observed . These both peak

are associated with doublet peaks of Zr 3d (Gondal et al., 2018). The energy difference between both the peaks is 2.4 eV. From this we can confirm that embedded zirconia was intact after carbonization and zirconia did not react with carbon forming any byproducts.

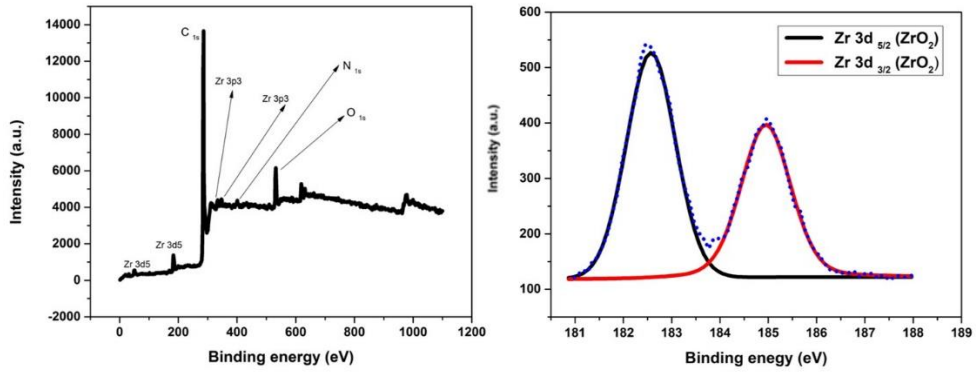

Figure 5.7: XPS Spectrum of (a) Zirconia loaded carbon nanofiber mats, (b) deconvoluted Zr 3d spectra

5.4.4. Raman Analysis

The Raman spectrum of carbonized carbon nanofiber mat and zirconia embedded carbon fiber mats are depicted in Figure 5.8. The peaks corresponding to the defect band (D peak) and the graphitic band (G band) near 1335 and 1593 cm^{-1} are observed for all the samples. There is, however, a slight variation in peak positions of the zirconia loaded and unloaded samples and is probably associated with the difference in chemical bond length. The higher value of bond length shifts the peak to lower wavenumbers and vice versa. So, if the bond length changes due to some external or internal causes, there is a shift in Raman spectra. Hence, the slight shift in the zirconia-loaded samples may be due to embedded zirconia leading to a change in bond length. The I_D/I_G ratio (the ratio of the D peak intensity to the G peak intensity) of samples A, B, C, and D are found to be 1.086, 0.987, 0.985, and 0.979, respectively. It is observed that the incorporation of zirconia has a marginal effect in decreasing I_D/I_G ratio. I_D peak and I_G peak corresponds to sp^2 bonding carbon atoms that are disordered and ordered in the sample (Y. Wang et

al., 2003). Therefore, the decrease in I_D/I_G ratio indicates an increased mole fraction of graphitic carbon in the fibers.

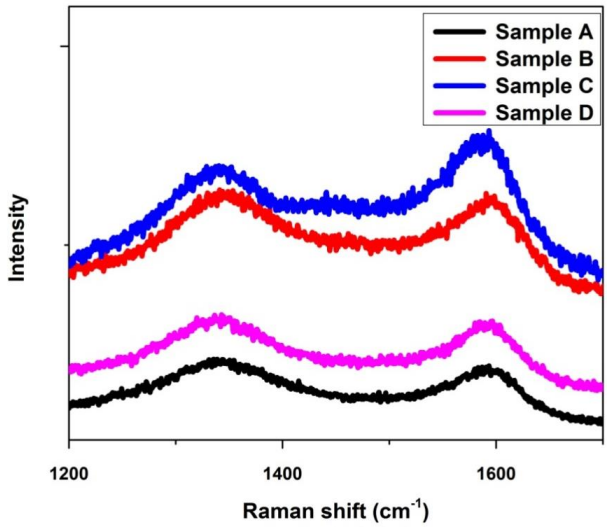

Figure 5.8: Raman spectrum of ZrO_2 loaded carbon nanofiber mats (of samples A, B, C & D).

5.4.5. AC Conductivity Measurements

The real and imaginary permittivity of all carbonized samples with and without ZrO_2 was tested, and AC conductivity of these samples were calculated using equation (5.1) and are presented in Figure 5.9. From the Figure, it can be observed that the AC conductivity of ZrO_2 embedded samples is higher than neat carbon fibers, and the nanofibers obtained from sample C have the highest conductivity among all the loadings. The real permittivity largely depends on the polarization degree of material, and imaginary permittivity reveals the energy dissipation of material. Therefore, as the zirconia content increases in the sample, the polarization degree increases, thereby improving the real permittivity. The increase in imaginary permittivity speaks about the heat dissipation characteristic of zirconia-loaded carbon fiber mats and its potential for attenuation in EMI shielding applications. The AC conductivity, therefore, increased in accordance with the imaginary permittivity of the samples. Overall, in these composites,

the permittivity has a significant effect on the EMI shielding capability of the samples, which will be explained in the following section. The permittivity in the material is the contribution of both the carbon fiber and the zirconia content. In the present study, the material sample C (PAN/ZrO_2 2:1) was found to have the optimum value (permittivity). Considering other combinations with more zirconia content, the contribution of carbon fiber is less and hence may affect the properties negatively. Therefore, sample C has better EMI property compared with other combinations and pure carbon fibers, and the optimum concentration of carbon to zirconia is found to be 2:1.

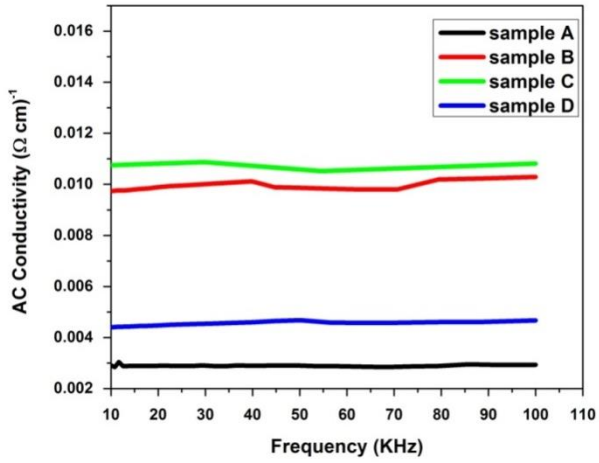

Figure 5.9: AC conductivity of ZrO_2 loaded carbon fiber mats

5.4.6. Electromagnetic Interference Shielding Studies

5.4.6.1: Effect of Zirconia Loading

The ability of a material to attenuate EM waves is calculated by the total shielding effectiveness, usually denoted in dB. Shielding effectiveness per unit thickness is another useful attribute to compare the performance of sheet samples as absorption loss increases linearly with sheet thickness (Hong et al., 2017). In Figure 5.10, the electromagnetic shielding effectiveness of carbonized mats is depicted. It can be clearly understood from the Figure that compared to the unloaded mat, all other zirconia-loaded mats have superior performance and, sample C, have the best shielding capability among

all mats throughout the frequency range. Absorption is the main mechanism for shielding because carbon fiber, along with zirconia, acts as a material with high permittivity coupled with a high dielectric constant and dielectric loss. The same has already been confirmed with the AC conductivity measurements. The average EMI SE_T values of samples A, B, C and D are -7.7dB, -9.8 dB, -15.6 dB and -10.3 dB respectively. It is exciting to see that mats with only ~0.1 mm thickness can offer such SE_T value at such a small thickness. These are very significant values if the specific SE_T values are estimated(Hong et al., 2017). From the obtained results, the effect of high permittivity in enhancing the EMI property can be seen clearly. Compared to other compositions, sample C displayed the best EMI SE_T, and hence for further study on the effect of thickness on EMI shielding capability, only sample C is tested and compared with sample A. When compared to all other samples, the Sample C has the optimal content of zirconia and carbon fiber for effectively shielding the EM waves. The combination of conductive carbon in fibrous form, high permittivity zirconia along with layered structure together contributed for effective shielding. The mechanism includes the reflection between the carbon fibers, polarization in zirconia and improved absorption by the carbon fibers.

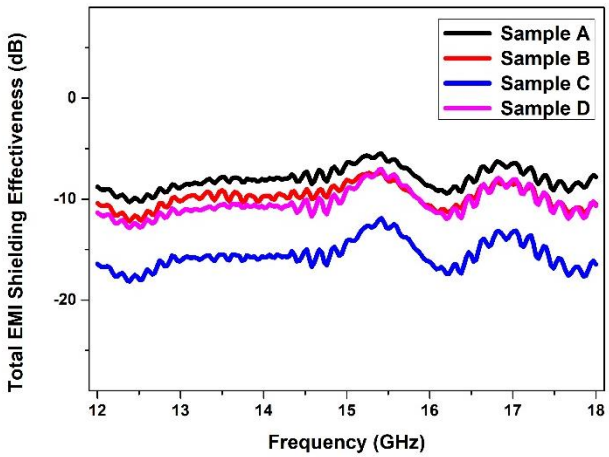

Figure 5.10: Total EMI shielding effectiveness of electrospun carbon mats

Epoxy on its own is a non-conducting and insulting material, and SE_T of epoxy is found to be less than -5 dB (towards zero) in the Ku band. So, independently epoxy alone cannot be used as an EMI Shield (Deeraj et al., 2020). However, for ZrO_2/carbon fiber/epoxy laminas, the SE_T is 16.7 to 18.8 dB. The average EMI SE_T values are tabulated in table 5.3. From the table, it can be concluded that there is an apparent increase of SE_T value after composite preparation; which signifies the combined effect of carbon fiber and epoxy in enhancing the EMI values of the resulting composite. On the contrary, higher amounts of zirconia after carbonization compared to other samples made sample D more brittle in nature. Hence the preparation of composites based on sample D using a hand layup set up was a bit difficult.

Table 5.3: Average EMI SE_T values

Sample	Carbon fiber mat	Sample	CF/epoxy composite
A	-7.71±2.5	AE	-16.7±2.3
B	-9.83±2.3	BE	-17.2±4.8
C	-15.56±2.6	CE	-18.8±2.2
D	-10.26±2.5	DE	Not Available

5.4.6.2. The Effect of Thickness

The effect of thickness of these mats on EMI shielding was studied by making samples of different thickness by stacking these mats together, and the results are presented in Figure 5.11. The EMI shielding of any material is dependent on the sample thickness and often directly proportional to thickness. It can be deduced from Figure 9 that, for sample C, the average shielding effectiveness reached -94 dB at a thickness of ~ 0.8 mm when compared with the neat carbon fiber without zirconia (sample A). There is almost a 1.5 times (150%) increase in the SE_T for this zirconia-loaded sample compared

to the unloaded zirconia sample. It can be concluded, based on the results obtained so far that, these mats have good specific shielding properties comparatively and are potential material for EMI shielding applications in the Ku band (satellite communication). In table 5.4, a comparison with the results of the present work and previous works is presented. The direct comparison of the material performance with values cannot be made as the thickness of materials are different, and in some cases, the thickness of the material is not available. Even then, in the present work, the zirconia-loaded samples are found to be comparable or superior to reported works in literature because an EMI shielding effectiveness of -94 dB for the thickness of 0.72 mm was achieved. The specific total shielding effectiveness of the sample is calculated to be ~ -130 dB/mm, which is very significant. Compared to previously reported materials like flexible graphite (129 dB/mm) (Luo, 1996) , graphene foam (84 dB/mm) (Shen et al., 2016), graphene aerogel (12 dB/mm) (Song et al., 2015), and CNF mats (63 dB/mm) (Bayat et al., 2014), the materials presented in this work are superior or comparable. In case of absorption dominant materials, the EMI shielding is directly proportional to the thickness of the sample. i.e., when the test sample is having more thickness the absorption component will be more there by improving overall shielding effectiveness. So, in our case single layered mat is not giving needed 20 dB effectiveness at that minimal thickness. So we kept stacking of these layers as a strategy to increase the thickness and thereby improving the shielding effectiveness.

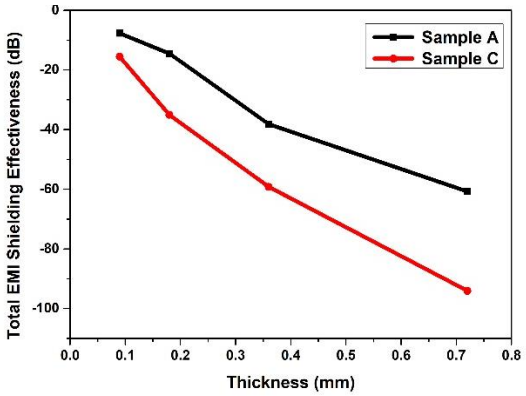

Figure 5.11: Variation of total EMI shielding effectiveness with thickness.

5.4.7. Dynamic Mechanical Analysis

The mechanical and thermal stabilities of EMI shields are also to be inspected along with their EMI shielding capability. During the practical application scenario, the shields may be subjected to different mechanical cycles and thermal profiles. Hence, exploring these properties is a requisite to understand the chance of shield damage during practical use. The storage modulus and mechanical damping factor (tan δ) of CNF/epoxy composites are presented in Figure 5.12. The Figure also clearly reveals that the storage modulus of zirconia loaded samples (sample BE, CE & DE) is higher than the neat sample (sample AE) throughout the entire temperature range. This implies that the inorganic filler (zirconia) embedded in carbon nanofibers improved the stiffness of carbon fibers, thereby increasing the overall modulus of the entire system and hence improve the reinforcement capability of carbon nanofiber mats. Among all the combinations studied, BE demonstrated the highest modulus, followed by sample CE. This implies that sample BE & CE has the optimal zirconia/carbon ratio to strengthen the epoxy matrix. However, when this optimal ratio is exceeded (sample DE), the sample properties decrease probably due to agglomeration of zirconia particles coupled with the brittle nature of sample D, thereby leading to a detrimental effect on the storage modulus. The peak of tan delta curves can determine the Tg temperature. In the case of tan delta peaks, it can be seen that the Tg values of epoxy composites and peak intensity of epoxy composites decreased with zirconia loading. From the previous results on the mechanical properties of electrospun nanofiber epoxy composites, it is well established that the Tg in filled polymers is dependent on the filler loading. The initial drop in Tg may be related to adsorption/deactivation of the curing agent by CNF mats, leading to lower crosslinking density as the fiber loading goes up (Sancaktar et al., 2009; Xu et al., 2004).

Ozden et al. (Özden-Yenigün et al., 2012) investigated the reinforcing ability of electrospun MWCNTs/P(St-co-GMA) composite nanofibers in an epoxy matrix and compared them with neat epoxy composites. They observed a significant increase in the

storage modulus and an increase in flexural modulus (more than 20%) when a single layer mat is used as reinforcement (fiber weight percent of 0.2%). In this present work, zirconia incorporated carbon fibers are used as reinforcement in an epoxy matrix and compared its dynamic mechanical properties with neat carbon fiber/epoxy composites. From the results, zirconia-loaded carbon fiber samples have enhanced storage modulus, which can be attributed to the combined effect of inherent fiber strength and effective stress transfer between the fiber and matrix. Furthermore, the zirconia embedded in the fiber further contributes to improving the inherent fiber strength at optimal loading (samples BE and CE). However, when the zirconia loading is beyond the optimal level, the fiber becomes brittle, and the strength decreased as a result (sample DE) compared to the remaining samples. In this work, a comparison between zirconia-loaded carbon fiber/epoxy composites was made with neat carbon fiber composites, and their properties were studied in detail. Compared with neat carbon fiber composites, the zirconia-loaded carbon fiber composites were found to be superior in nature. The comparison of values with neat epoxy clearly showed that the storage modulus is much better for the zirconia embedded carbon fiber epoxy composites, further supporting its capability to be an effective EMI shield at adverse conditions.

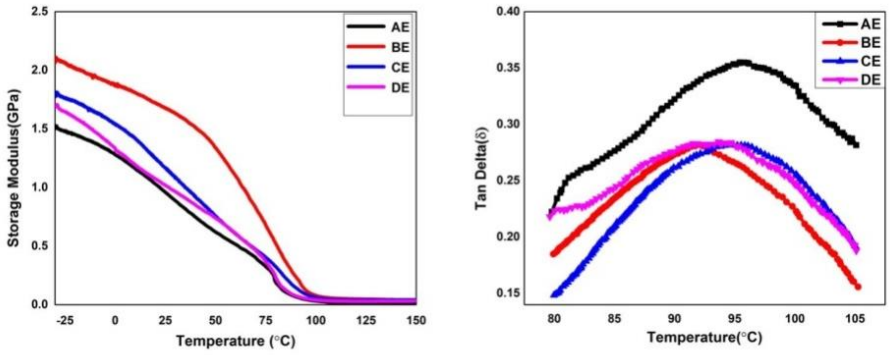

Figure 5.12: Dynamic mechanical properties of ZrO_2/CF/Epoxy composites with respect to temperature

Table 5.4: Comparison of EMI SE_T of few electrospun materials

S.No	Material (thickness)	EMI Shielding (dB)	Reference
1	Mxene/PU fabric(double layers, thickness: NA)	21	(Yuan et al., 2020)
2	PVP/Fe_3O_4 nanofibers (1 mm)	22	(Nasouri et al., 2018)
3	CNT/PAN fibers (0.15 mm)	30	(I.-H. Chen et al., 2010)
4	TiO_2/SiO_2/PPy/rGO film (0.26 mm)	30	(Huang et al., 2019)
5	MWCNT/PS fibers (thickness: NA)	32	(Qavamnia et al., 2016)
6	Zirconia@carbon fiber (8 layers stacked, 0.72 mm)	-94 dB	This work

5.5. Conclusions

Zirconia@PAN nanofiber mats were prepared at various compositions by varying zirconia content by utilizing the electrospinning technique. These mats were then further carbonized to form Zirconia@CNFs at a temperature of 1000°C in a inert high temperature oven. The potential of these ZrO_2@carbon mats in reinforcing and

inducing electromagnetic interference shielding characteristics to the epoxy matrix was then investigated in detail with respect to zirconia: carbon ratio and thickness of samples. The dynamic mechanical analysis was used to confirm the successful stiffening of the epoxy matrix by these carbon fibers. The total electromagnetic shielding effectiveness of carbon mats and carbon mat epoxy laminas was tested, and excellent specific effectiveness was noted in the Ku band. Further, the carbon mats were stacked, and excellent shielding effectiveness beyond -90 dB was noticed at 8 layers (thickness of < 0.8 mm). Thus, ZrO_2@CNFs, especially (sample C), have the potential to be used as efficient and effective EMI shielding material, and the epoxy-based structural composites prepared from these mats are suitable candidates for structural and shielding applications.

CHAPTER 6

ELECTROSPUN TiC@ TiO_2 NANOPARTICLES INCORPORATED CARBON FIBER AND THEIR EPOXY COMPOSITES FOR EMI SHIELDING APPLICATIONS

This chapter deals with the preparation and characterization of TiC@ TiO_2 nanoparticle embedded carbon fibers prepared from TiC/PAN fibers. Further these electrospun mats were used as reinforcements in epoxy polymer and composites were prepared. These composites were found to have enhanced mechanical properties along with improved EMI shielding performance

Part of this chapter has been published in Nano-structures and Nano-objects (2022), DOI: 10.1016/j.nanoso.2022.100912

6.1. Introduction

In this technology age, the pollution associated with electromagnetic interference (EMI) is increasing day by day as there is a rapid increase in various electronic and electrical devices. So, urgent attention is needed to minimize this electromagnetic pollution and safeguard electronic devices and humankind from the harsh side effects of EMI. EMI shielding is a phenomenon in which undesired electromagnetic waves are either absorbed or reflected with the help of suitable material shields. These shields offer sufficient interference shielding and improve the workability of electronic devices. Metals are the obvious choice for this purpose as they reflect electromagnetic waves. However, metals are replaced by absorption dominant materials because of their inherent weight, corrosion, and secondary EMI characteristics. Lightweight materials like foams, aerogels, and electrospun fibers are hot areas of research for EMI shielding. Carbon-based products are mainly investigated as they are wave-absorbing materials with a comprehensive range of architectures. Carbon nanotubes, graphene-based, and carbon fibers are potential candidates for modifications and development of advanced EMI shielding materials for high-end applications (Chung, 2001; Geetha et al., 2009; Kuruvilla et al., 2019).

The electrospinning technique is a versatile nanofabrication process to prepare fibers at sub-micron and nano dimensions (Jiang et al., 2018; L. Liu et al., 2020; Raman et al., 2021). By selectively optimizing the process parameters like polymer concentration, acceleration voltage, flow rate, and additional setups, fiber dimension, morphology, and shape can be prepared. Electrospun fibers offer unique characteristics like high aspect ratio, high surface area, the possibility of blending different polymers, different material combinations, deposition on other substrates, relatively cheap cost, ease of scaling up ability, and many more to other fabrication techniques. These spun fibers have applications in sensing, composite reinforcement, EMI shielding, bio-medical, filtration, catalysis, and energy storage.

One significant possibility of electrospun fibers is the ease of converting them into carbonaceous fibers by thermal treatment at high temperatures. Thus, developed carbon fibers have attracted the scientific community's attention due to their potential and enhanced applications. The conversion of electrospun fiber to carbon fiber involves two sets (1) stabilization and (2) carbonization. By carefully optimizing both, we can successfully develop carbon fibers. Few studies on the graphitization of these fibers are also reported. By incorporating metal/metal oxide/other reinforcements in these fibers, individual filler embedded carbon fibers are developed after carbonization. Thus composite fibers find many excellent usages in material science (Aboagye et al., 2015; Gopiraman et al., 2019; Im et al., 2011; Mao et al., 2013).

Titanium carbide (TiC), a transition metal carbide, is a refractory ceramic material with good Young's modulus, low mass density, electrical conductivity, thermal stability, high hardness, and chemical resistance (Guo et al., 2018; Zhou et al., 2016). TiC in the shape of nanorods, nanowires, nanoparticles finds lots of exciting applications across various fields of material science (Fallahdoost et al., 2016; Popov et al., 2018; Saba et al., 2018; Tao et al., 2011; Xia et al., 2017; Yuan, Cheng, Kong, et al., 2014; Yuan, Cheng, & Zhang, 2014). Since their first discovery in 2011, TiC based MXenes is the most studied material in value-added applications (Anasori et al., 2017; Hou et al., 2020; X. Liu et al., 2020; Nam et al., 2020). TiC incorporated composite carbon fibers prepared via electrospinning route are interesting materials of study as these composite fibers benefit from the high electric conductivity of TiC and fibrillar carbon structure, imparting high surface area.

Zhu et al. prepared TiC reinforced carbon nanofibers by directly electrospinning PAN/Ti composite precursor solution followed by pyrolysis. They reported that the mechanical property (tensile strength) tests of TiC/carbon nanofiber membranes are 4 times higher than the neat carbon nanofiber membranes (Zhu et al., 2009). Atchison et al. prepared ultrafine TiC/C nanofibers from titanium butoxide and PVP combinations

and compared it with ZrC/C and NbC/C nanofibers (Atchison et al., 2015). Cho et al. prepared TiC-C fibers from PAN and TiO_2 combinations by electrospinning and subsequent carbothermal reduction and studied the properties(Cho et al., 2015). Levitt et al. prepared $Ti_3C_2T_x$ loaded electrospun carbon fibers and studied them for supercapacitor applications (Levitt et al., 2019). Li et al. prepared 2D $Ti_3C_2T_x$ nanosheets (MXene) and single-walled carbon nanotube deposited latex devices and investigated their application as wearable antennas and EMI shields. They observed that these latex devices could sustain 800% areal strain and shielding performance of ≈52 dB by stacking ten layers. Thus, they concluded that these wireless systems could stable wireless transmission and obstruct EM absorption by the human body(Li et al., 2020). Stott et al. prepared TiC@TiO_2 core shell particles by electrochemically and thermally oxidizing TiC particles (Stott et al., 2006). Bhattacharjee et al. presented a detailed review on core-shell based nanomaterials for shielding applications (Bhattacharjee & Bose, 2021).

In this chapter, we prepared TiC nanoparticle embedded PAN fibers using the electrospinning technique. After spinning, the morphology of fibers is observed in SEM and TEM to see the dispersion of embedded TiC and fiber profiles. These fiber mats were further subjected to stabilization and carbonization to converting these spun mats to TiC embedded carbon fiber mats. This conversion lead to the formation of TiC core and TiO_2 shell type nanostructures, embedded carbon fibers. These carbon mats are observed using SEM to see the fiber stability after carbonization. The XRD, Raman spectra, and conductivity of these mats were investigated to study the properties of fibers. In addition, these mats were investigated for electromagnetic interference shielding in the Ku band. To the best of our knowledge, this is the first such effect to investigate the EMI shielding performance of core-shell TiC@ TiO_2 embedded fibers, especially in the 12-18 GHz frequency range. Further, these shielding values are compared with the already reported materials.

6.2. Experimental section

6.2.1. Preparation of TiC Embedded PAN Fibers

The calculated amount of TiC powder is taken in DMF and bath sonicated for a minimum of 1 hr. PAN solution in DMF is added to the polymer concentration of 10 w % and stirred overnight for a homogenous mixture. Later the mixture is probe sonicated and afterward filled in a plastic syringe. In an ESPIN-NANO horizontal electrospinning setup, this solution is drawn into fibers by adjusting the electrospinning parameters onto the aluminum-wrapped rotating collector. This mat is carefully removed, and further characterization is done. A similar process is followed for preparing mats of different compositions. The details of samples and processing conditions are mentioned in Table 6.1.

Table 6.1: Optimized parameters for electrospinning process

Sample Code	**Composition**	**Acceleration voltage (KV)**	**Flow rate (ml/hr)**	**Collector speed (rpm)**	**Distance (in cms)**	**Sample code after carbonization**
PAN alone	1 gm of PAN in 10 ml DMF	9	1.5	1100	13	T alone
PAN/TIC (1:1)	1 gm of PAN + 1 gm of TiC in 10 ml DMF	11	1.5	1100	13	T 1-1
PAN/TIC (2:1)	1 gm of PAN + 0.5 gm of TiC in 10 ml	10	1.5	1100	13	T 2-1

	DMF					
PAN/TIC (3:1)	1 gm of PAN + 0.33 gm of TiC in 10 ml DMF	10	1.5	1100	13	T 3-1

6.2.2. Preparation of Nanofiller Embedded Carbon Fibers

The mats obtained after electrospinning are carefully kept inside an air oven at 220 °C for 1 hr. Afterward, these mats are kept inside a high-temperature furnace at 1000 °C for 4 hrs at a heating rate of 2 °C/min for carbonization. Subsequently, the samples are cooled to room temperature, and these carbon mats are characterized further.

6.2.3. Preparation of TiC@TiO_2 Loaded Carbon Fiber/Epoxy Composites

The prepared carbon mats and TiC@TiO_2 loaded carbon fiber mats are used as reinforcement and epoxy as the matrix material, epoxy composites were made with hand-layup technique. In Figure 1, the schematic of the formation of carbon fibers and carbon fiber/epoxy composites were presented.

6.3. Characterization Techniques

The morphology of TiC incorporated electrospun mats were observed in both Scanning electron microscope and transmission electron microscope to observe the spun fibers. After carbonization, the carbon fiber mats were observed in SEM to observe the nanofiller incorporated carbon fibers. Powder X-ray diffraction (XRD) patterns were

recorded from 5˚ to 90˚ at 45 kV and 30mA. Raman spectra were recorded using a laser of 532nm. The total electromagnetic shielding effectiveness was measured using a vector network analyzer with a wave-guide adaptor in 12–18 GHz frequency range. The surface resistance of the samples is tested by Agilent SMU B2900 two-probe instrument. The value is measured by keeping the probes at distance of 1 cm. The scattering parameters were recorded and were used to estimate the total shielding effectiveness using the input and output power. The dynamic mechanical studies of the prepared carbon fiber/epoxy composites were investigated by dynamic mechanical analyzer in tension mode. Rectangular specimens $(25 \times 10 \times 0.5\, mm^3)$ were taken, and the test was performed from a temperature range of 30 ˚C to 150 ˚C, at a heating rate of 2 ˚C/min.

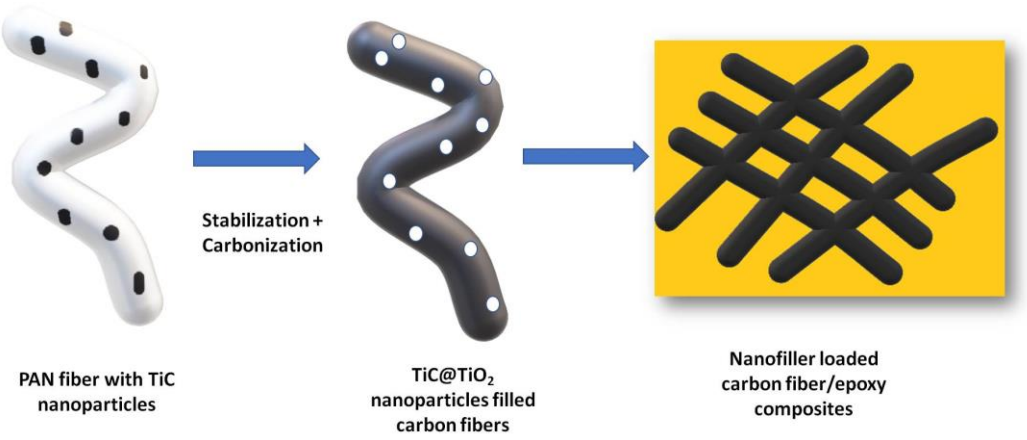

Figure 6.1: Schematic for preparation of carbon fiber and their epoxy composites

6.4. Results and Discussions

6.4.1. Morphology

After electrospinning, the morphology of the spun mats is observed in SEM & TEM, and the micrographs are presented in Figures 6.2 and 6.3, respectively. In Figure

6.2(a), the well-defined fibrillar structure of PAN fibers is visible. These fibers are uniform and bead-free, and the diameters of the fibers are measured in ImageJ software and tabulated in Table 6.2. In Figures 6.2(b) & 6.2(c), the fibers prepared from PAN/TiC solutions are presented. From the microscopic images, fine dispersion of TiC nanoparticles in PAN fibers is observed, and the mean diameters of fibers increased. The increased fiber diameter is because of the increased viscosity of polymer solution after adding TiC nanopowder. TiC has a high density, and these particles tend to segregate at the bottom, so proper sonication and mixing is essential to forming a homogeneous mixture and thereby getting good dispersion in fibers.

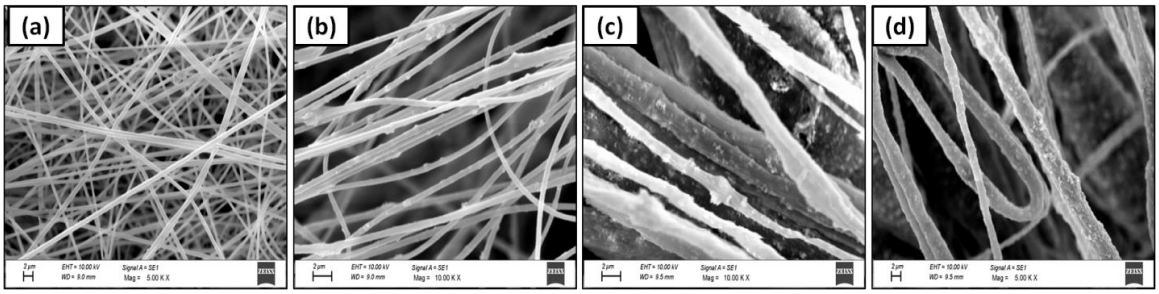

Figure 6.2: SEM micrographs of TiC loaded PAN fibers, (a) PAN alone, (b) PAN/TiC (3/1), (c) PAN/TiC (2/1) and (d) PAN/TiC (1/1).

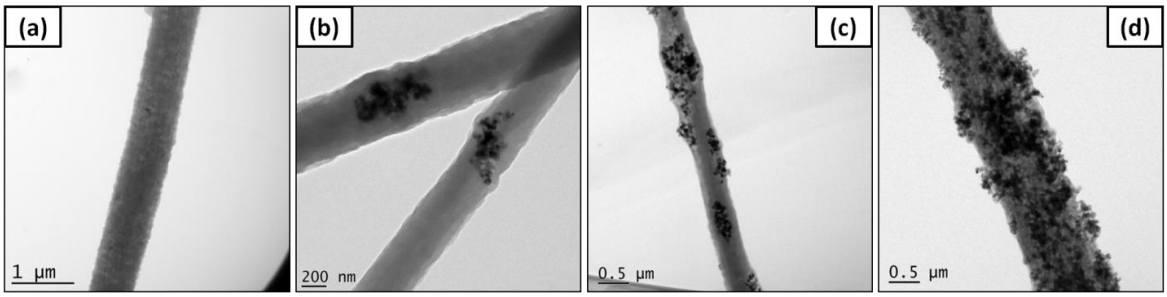

Figure 6.3: TEM micrographs of TiC loaded PAN fibers, (a) PAN alone, (b) PAN/TiC (3/1), (c) PAN/TiC (2/1) and (d) PAN/TiC (1/1).

Table 6.2: Average diameters of electrospun fibers before and after carbonization

Before carbonizing	Sample code	Average diameter (in nm)	After carbonizing	Sample code	Average diameter (in nm)
	PAN alone	637.5±49.01		T	522±65.7
	PAN/TiC (3/1)	652.1±33.24		T 3 1	540±24.24
	PAN/TiC (2/1)	1045.55±57.09		T 2 1	992.5±78.04
	PAN/TIC(1/1)	2332.4±766.91		T 1 1	1092±319.79

The TEM micrographs depicted in Figure 6.3 implies the location of embedded TiC nanopowder inside PAN fibers. We can observe smooth plain fibers of PAN in Figure 6.3(a). The TiC particles embedded inside the PAN fiber is observed in Figure 6.3(b), 6.3(c) & 6.3(d). The scanning electron micrographs of prepared carbon fibers are depicted in Figure 6.4(a), from which well-defined carbon fibers can be observed. The nanofiller incorporated carbon fibers are presented in Figure 6.4(b), 6.4(c) & 6.4(d) respectively**.** From these micrographs the fine dispersion of nanoparticles inside the carbon fibers can be observed and the fibers are stable and not fused or melted during the carbonization process.

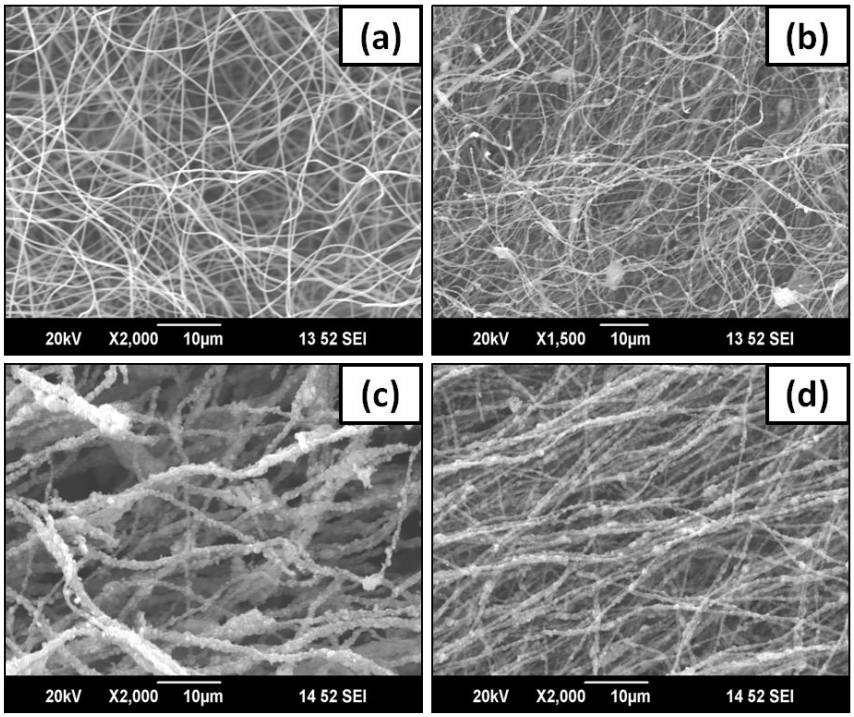

Figure 6.4: SEM micrographs of TiC loaded carbon fibers, (a) T alone, (b) T 3 1 (c) T 2 1and (c) T 11.

6.4.2. Raman Spectra

The Raman spectra of nanofiller loaded carbon fiber mats are presented in Figure 6.5. From the Figure, we can see all the mats displayed the D band and G band around 1336 and 1596 cm^{-1} respectively. from the Figures, the I_D/I_G was found to see the graphitic content of the carbon mats, this ratio was found to be 1.1, 0.91, 0.84 for T 31, T 21 and T 11 respectively. This ratio is less than, I_D/I_G of neat carbon fiber which is 1.08. So the nanofiller loaded carbon fibers displayed better graphitic carbon than neat fiber, and the graphitic structure is enhanced with filler loading. This is because as the nanofiller was included earlier to carbonization these fillers acted like a template helping to formation of graphitic carbon where more the filler loading, the more the templating effect and formation of graphitic carbon.

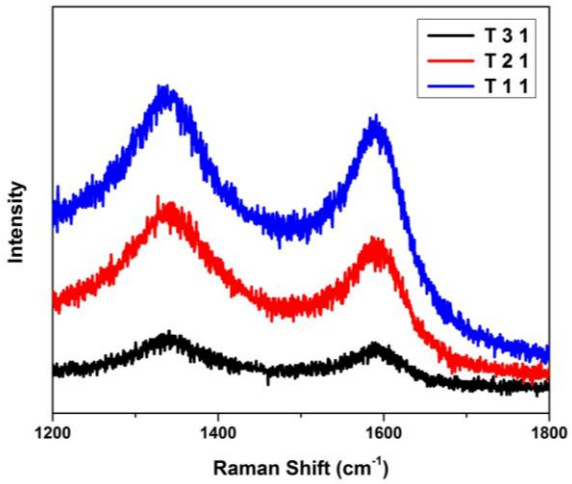

Figure 6.5: Raman spectra of TiC loaded carbon fibers

6.4.3. XRD Studies

The XRD profiles of carbon mats and nanofiller embedded carbon mats are taken and depicted in Figure 6.6(a). The XRD profile of pure TiC particles as procured is presented in Figure 6.6(b). From the XRD curves of carbon fibers mats (in Figure 6.6(a)), neat carbon fibers have a peak at ~25 degrees, that corresponds to carbon. While the nanofiller loaded mats displayed additional peaks along with TiC peaks. The additional peaks corresponds to titanium dioxide, which confirms us that that during the formation of carbon fibers, the embedded titanium carbide is getting surface oxidized to titania. Thus resulting in the *in-situ* formation of titanium carbide/ titanium oxide core-shell type of structures. For getting better understanding of this concept, XPS analysis was done and presented in next section. From the XRD curves, it is evident that titanium oxide is formed during the carbonization process

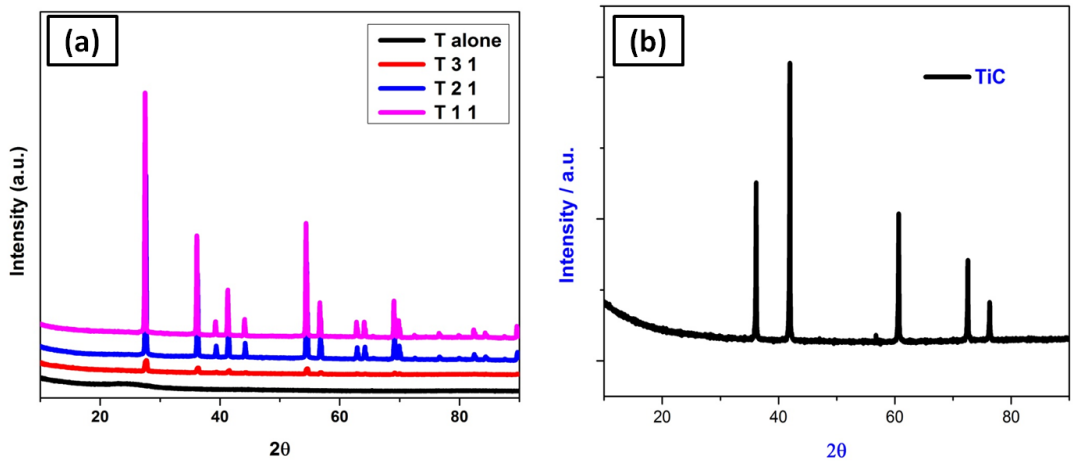

Figure 6.6: XRD curves of (a) TiC loaded carbon fibers, (b) pure TiC particles

6.4.4. XPS Studies

To understand the elemental compositions and the chemical states of the samples, the XPS analysis was done. The XPS spectrums of nanofiller loaded carbon fiber mats after carbonization and before carbonization are presented in Figure 6.7 and Figure 6.8 respectively. From the deconvoluted Ti 2p spectrum it is clear along with the Ti-C peak at ~ 461 eV, the peaks corresponding to Ti-O at ~ 459 eV and ~465 eV are presented. This confirms the formation of the titania on the surface of the titanium carbide particles. So, the entire TiC filled carbonized fibers are surface oxidized and expected have a TiO_2 surrounding the incorporated TiC particles. To further confirm this scenario, the pre-carbonized mat, i.e., the stabilized fiber mat is taken and the XPS spectra is taken. From the results (Figure 6.8), all the elements C, O, N and Ti are observed in the mats. From the deconvoluted curves of Ti 2p, we can see the peaks of Ti-C and Ti-O. The peak at ~455 eV and ~461 eV corresponds to Ti-C, where the peak at ~ 459 eV and ~465 eV corresponds to the Ti-O. so, these results shows the these surface oxidization is happening during the stabilization process and further progressing during carbonization process. As during the stabilization process, the electrospun mats

are being kept in air oven in presence of oxygen at 220 °C. During this period the oxygen in the oven, is attacking the titanium carbide and surface oxidizing it. As we know, stabilization is a compulsory process to obtain good quality carbon fibers without fusing; this step is mainly responsible for the formation of titanium oxide. Thus these results confirm the in-situ formation of titania, during the carbon fiber preparation process.

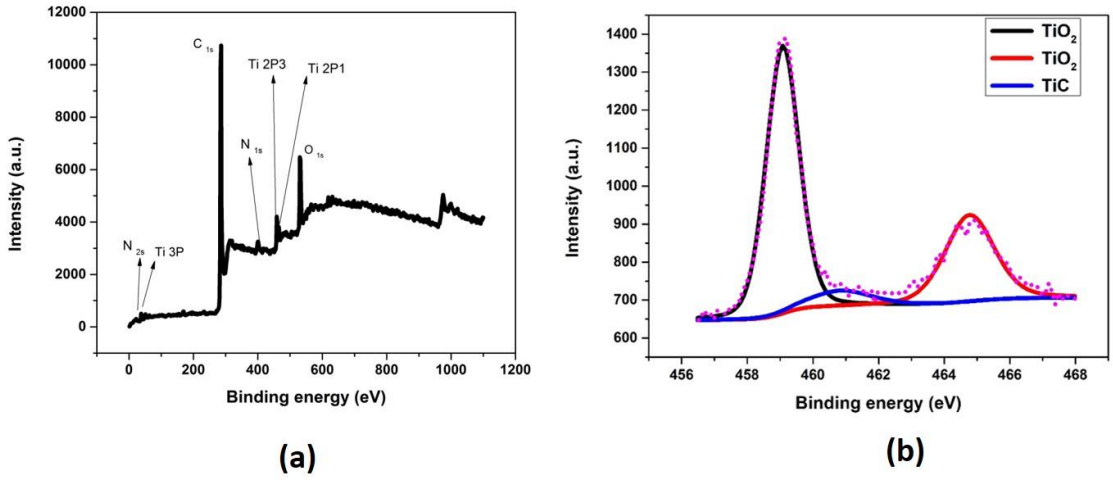

Figure 6.7: XPS curves of carbonized fibers (sample T 11)

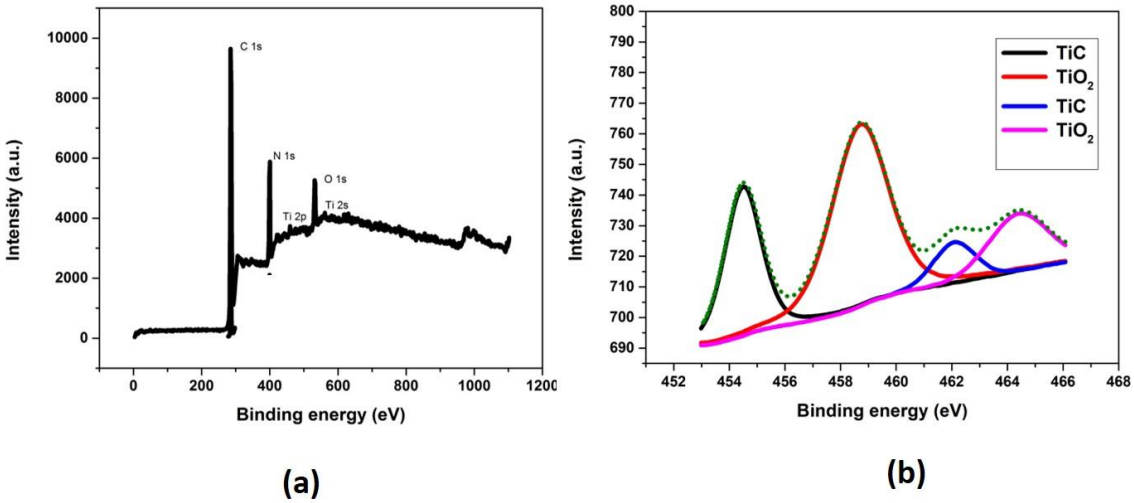

Figure 6.8: XPS curves of stabilized fibers (sample PAN/TIC (1/1))

6.4.5. Surface Resistance Studies

The surface resistance of carbon fibers and nanofiller loaded carbon fibers was tested and presented in Figure 6.9. The samples were tested using a two probe measuring instrument, at a distance of 1 cm and the conductance of the samples was measured. The reciprocal of the conductance is calculated which is the resistance of the system. From the curves, the surface resistance of the nanofiller loaded samples is observed to be more than neat carbon fibers and the resistance decreased with nanofiller loading. The increase in conductivity is because of the formation of the titanium oxide. These titanium oxide formation act as a barrier against the free flow of electrons and restrict the conductivity of the system. But, as the amount of filler loading increased, the resistance of the samples is observed to decrease. From these results, we can conclude that for all carbonized samples, the conductivity remains more or less the same.

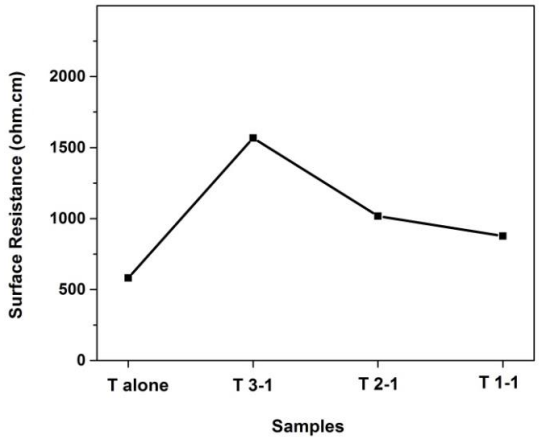

Figure 6.9: Surface resistance of TiC loaded carbon fibers

6.4.6. EMI shielding effectiveness

6.4.6.1. EMI shielding effectiveness of carbon mats

The capability of a shield to attenuate EM waves is determined by the total shielding effectiveness, generally denoted in dB. Specific shielding effectiveness, which

is specific shielding effectiveness per thickness (dB/mm) is another attribute to compare the performance of sheet samples (Hong et al., 2017). The electromagnetic shielding effectiveness of the prepared nanofiller-carbonized mats is presented in the Figure 6.10. From the Figure, we can observe that the than compared to the neat carbon mat, all other TiC@TiO_2 nanoparticle loaded mats have superior EMI shielding performance and, sample T 11, have the best shielding capability among all mats throughout the frequency range. In the case of nanofiller loaded composites, the presence of titanium carbide, high dielectric material titanium oxide along with the carbon fiber structure contributed to the improved electromagnetic performance of the samples. The in-situ formation of titanium oxide during the carbonization process significantly helped in enhancing the dielectric constant thereby gradually increasing the electromagnetic absorbing property. Titania is observed to significantly improve the microwave absorbing property and EMI property in polymer composites(Phang et al., 2008; Singh et al., 2014).

In case of specific EMI shielding effectiveness, all the carbonized samples displayed a SSE_T of above 100 dB/mm. which means a sample of thickness 1mm thickness offers a SET of 100 dB, which is very high compared to the commercial requirement of 20 dB. These values are either comparable to or superior than previous available materials in literature. Of all the combinations, T 11 showed highest shielding effectiveness, determining that this is the optimum combination of the polymer and the filler for obtaining better effectiveness. These carbon mats can be used as such for the practical application but it has some limitations like surface damage during operation, moisture absorption etc. So, these mats are used as reinforcement in epoxy matrix to eliminate these limitations and present a reliable structural composite material. In the case of EMI shielding materials with different structures, morphology porosity and functionality plays an important role in determining the shielding property. In this case, the carbon fibers are with a core-shell type of structures to improve the property. So along with the effect of carbon fiber, we have core-shell materials for improving the polarizations and reflections in the material. So, the overall shielding effectiveness is

improved. The combination of layered carbon structure, conductive carbon in fibrous form, core-shell type filler helps in improving the shielding performance.

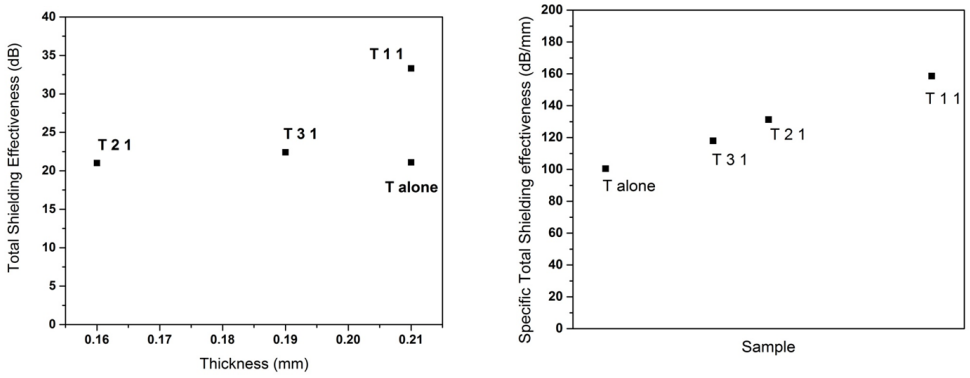

Figure 6.10: EMI SE_T of TiC loaded carbon fibers

6.4.6.2. EMI shielding effectiveness of carbon mat/epoxy composites

The shielding effectiveness of prepared epoxy samples was measured and the specific shielding effectiveness is calculated and presented in Figure 6.11. From the Figure we can see that all nanofiller loaded carbon fiber/epoxy composites are having better shielding effectiveness than neat carbon fiber/epoxy samples and the performance improved with filler loading. Epoxy polymer is an insulting thermosetting material it will not offer any noteworthy resistance to incoming EM waves, it just acts a matrix material. The shielding property is associated mostly to the carbon fiber inside the epoxy. So, these results show that the prepared carbon fiber/epoxy composites are potential EMI shielding materials and can be used as such in commercial applications.

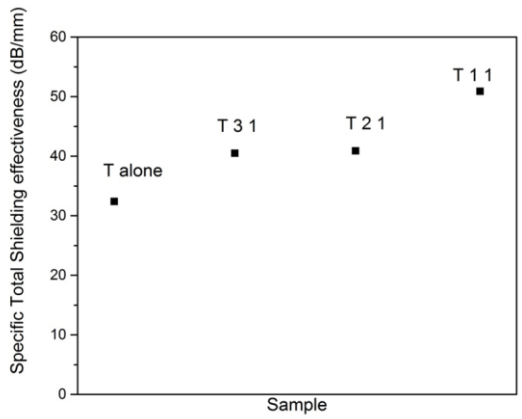

Figure 6.11: EMI SE_T of TiC loaded carbon fibers/Epoxy composites

6.4.7. Dynamic Mechanical Studies of Carbon Mat/Epoxy Composites

In Figure 6.12, the dynamic mechanical properties of nanofiller incorporated carbon fiber/epoxy composites is presented. The mechanical performance of the composites is a main factor than determines their performance during practical application. The storage modulus profiles of all the nanofiller loaded shields are presented in Figure 6.12, from which a positive impact of nanofiller on the modulus can be observed. Throughout the entire profiles, samples T 2 1 and T 1 1 displayed enhanced modulus, displaying the capability of nanofiller loaded carbon fiber/epoxy composites to have better load bearing capabilities. This is indicative of the stiffness improvement in the carbon fibers by TiC@TiO_2 nanoparticles, which further enhanced the overall modulus of the epoxy system. From the curves, we can see that T 1 1 sample is having the highest modulus, which confirms that this is the optimum combination of the nanofiller in the carbon fibers for achieving an overall mechanical property improvement.

In the case of tan delta peaks, it can be seen that the Tg values of epoxy composites and peak intensity of epoxy composites decreased with nanofiller content. From literature, we can say that the mechanical performance of electrospun nanofiber

epoxy composites, the filler loading influences the Tg of the system. The drop in the Tg may be attributed to the adsorption/deactivation of the curing agent by the electrospun carbon fiber mats. This results in the decrease of the crosslinking density with the increase in the overall fiber loading (Sancaktar et al., 2009; Xu et al., 2004). In this present work, TiC@TiO_2 nanoparticle incorporated carbon fibers are used as reinforcement in an epoxy matrix and its dynamic mechanical properties are compared with neat carbon fiber/epoxy composites. From the results, nanofiller loaded carbon fiber samples have enhanced storage modulus, which can be attributed to the combined effect of inherent fiber strength and effective stress transfer between the fiber and matrix.

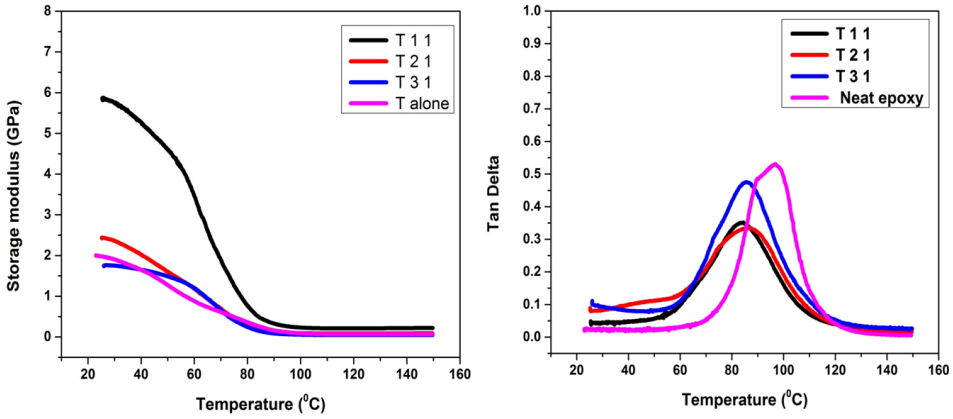

Figure 6.12: Dynamic mechanical properties of TiC@TiO_2 nanoparticles loaded carbon fibers/epoxy composites

6.5. Conclusions

TiC embedded carbon fibers were successfully prepared from the electrospinning-stabilization-carbonization procedure. The morphology of the as-spun fibers and carbonized fibers were observed in the electron microscope, and post carbonization, the fibers are noticed to retain in fibrillar structure. Furthermore, the XRD and Raman spectra of these fibers reveal the successful incorporation of these

nanoparticles and phase morphology. The XRD and XPS spectrums confirm the formation of titania during the process. The EMI shielding performance of the carbon mats with these core-shell type nanofillers is found to be significantly higher than the neat carbon fibers because of the combined effect of carbon fibers, dielectric titania and titanium carbide. Further, nanofiller loaded carbon fiber/ epoxy systems are found to have excellent mechanical performance along with good shielding properties. The sample T 11 is the optimized material combination with best shielding performance and T 11 fiber loaded epoxy composites have the best mechanical properties and shielding properties as well.

CHAPTER 7

CONCLUSIONS AND FUTURE SCOPE

7.1. Conclusions

The electrospinning process is a dependable technique for the fabrication of continuous polymeric fibers. It is feasible to prepare nonwoven fibers with different forms, shapes, orientations, and properties by adjusting and modifying the electrospinning setup. Using these electrospun fibers inside any polymer matrix is a sure assured way of developing multi-faceted composites. When incorporated in an thermosetting matrix like epoxy, these electrospun fibers offer enhancement in the mechanical, thermal, and epoxy matrices because of their super high aspect ratio, high surface area, and better interactions. We can alter the properties of the resultant epoxy composites to an enormous range by manipulating the fiber alignment, introducing surface modifications, and controlling the fiber diameter. The use of core-shell electrospun fibers or multi-level electrospun fibers has a more significant effect in modifying the epoxy composites. The use of tailored electrospun fibers to develop reinforced epoxy composites is an exciting concept. Hence by a rational choice of the type of electrospun fiber, their orientation and morphology, fiber loadings, and surface modifications, we can design advanced epoxy composites for commercial and industrial applications. This thesis investigates the preparation and characterization of electrospun fibers and their incorporation in epoxy composite systems. The influence of these fibers on the mechanical, thermal, and visco-elastic properties was studied and presented.

In chapter 1, a general description of electrospinning, electrospun fiber reinforced polymer systems, and introduction to electrospun nanofibers are presented. Chapter 2 deals with the materials and methods employed in this research. In chapter 3, the preparation of poly (styrene-co-butadiene) copolymer fibers from DMF-THF co-solvent systems is presented. For obtaining the fibers, a polymer content of 18 w% and acceleration voltage of 10 KV is optimized. By using a light microscope and transmission electron microscope, the prepared fibers were observed. These fibers were chopped into square pieces and mixed with epoxy resin to develop SBC fiber/epoxy composites. By using scanning electron microscopy, the fractured epoxy surfaces were observed, and the toughening mechanism is proposed. The static tensile strength of fiber reinforced samples displayed an improvement of 18 w% at 2.5 w% fiber loading. At the same loading, a remarkable improvement in the fracture toughness of >100% is noticed. The dynamic mechanical properties showed an increasing trend and almost doubled with fiber loading. Thermal properties were done to check the thermal stability and the studies confirmed that the SBC fibers are not influencing the stability of epoxy. The dynamic rheological properties were studied to study the role of fiber loading on viscosity and modulus.

The role of electrospun polyimide fibers in reinforcing epoxy is described in chapter 4. This chapter deals with the preparation of electrospun nanofibers of poly (amic acid) by optimizing the spinning parameters. These mats are subjected to thermal imidization, and polyimide nanofibers are obtained. The obtained mats are chopped into pieces of pre-determined size and added to epoxy to fabricate short PI fiber epoxy composites. The dynamic mechanical properties of these composites showed a good improvement in room temperature. The fracture toughness of prepared composites show improvement in low fiber loading (20 % improvement at 1 w% loaded samples) but decreased as the fiber loading increased. This can be attributed to the generation of secondary cracks that can be observed from fractured surface images. The thermal properties of the composites showed a positive shift that signifies the role of PI in

improving thermal stability. The rheological studies of these PI loaded composites displayed an increase in the storage and loss modulus when compared to neat systems.

In chapter 5, the preparation of electrospun carbon fibers with and without inclusion of zirconia is presented. By employing the electrospinning-stabilization-carbonization strategy, carbon fibers were prepared and characterized. The morphology of the prepared fibers was observed in a scanning electron microscope before and after heat treatment. These mats were found to have good shielding effectiveness, with shielding effectiveness reaching > -90 dB for 8 layers stacked samples in the Ku band. These mats were used as reinforcement, and electrospun carbon fiber/epoxy composites were prepared. These epoxy composites displayed superior dynamic mechanical properties and EMI shielding properties, confirming the positive effect of zirconia in strengthening and improving the shielding effectiveness. These ZrO_2@CNF/epoxy composites can be used for potential industrial, radar, and military applications.

Chapter 6 deals with preparation and characterization of electrospun TiC@TiO_2 core-shell carbon fiber mats. The morphology of prepared mats and carbonized mats were observed using the scanning electron microscope. The XRD, Raman spectra, XPS, and EMI shielding characteristics of these carbon fiber samples were tested and presented. The results show the surface oxidation of TiC to TiO_2 during the conversation of PAN fiber to carbon fiber. The electromagnetic interference shielding effectiveness of these TiC@TiO_2 carbon fiber mats was tested in the Ku band (12-18 GHz), and excellent shielding effectiveness of ~ -33 dB for a single layer (thickness: 0.21mm) was observed. Further, these mats were impregnated in an epoxy matrix and electrospun carbon fiber reinforced epoxy composites were prepared. The storage modulus and EMI shielding effectiveness of these resultant epoxy composites are significant. The ease of preparation, enhanced mechanical performance, and excellent shielding capability makes these TiC@TiO_2 embedded carbon fiber mats and their epoxy composites promising structural EMI shielding materials.

7.2. Future Scope

Improving the comprehensive mechanical properties of epoxy composites without tradeoff in any one property is a major challenge. Employing nanofiber mats obtained via electrospinning for this purpose is an excellent route to improve the properties. In order to prepare high strength composites, high strength fibers are needed. This can be achieved by

- Using electrospun fibers of high strength polymers in epoxy matrices
- Nanofiller reinforced electrospun fibers can be employed as reinforcement in epoxy matrices.
- Blending of polymers before electrospinning and then incorporating them in epoxy
- Interleaved composites can be developed by using electrospun carbon fibers as the interlayer

In order to prepare effective EMI shielding materials, materials with low weight and more effectiveness are needed. For that, the research can be extended to designing novel structures and novel combinations from carbon fibers. Some of the possible ideas are;

- To prepare porous carbon fibers for EMI shielding applications
- Electrospun carbon fibers with magnetic particles can be designed for EMI Shielding applications
- Electrospun carbon fibers with hybrid fillers and studying the combined effect of these additives on EMI shielding.

REFERENCES

1. Abdel-Hady, F., Alzahrany, A., & Hamed, M. (2011). Experimental validation of upward electrospinning process. *International Scholarly Research Notices, 2011*.
2. Agarwal, S., & Greiner, A. (2011). Nanofibers by electrospinning. *Polymers for Advanced Technologies, 3*(22), 293-294.
3. Ahmadloo, E., Gharehaghaji, A., Latifi, M., Mohammadi, N., & Saghafi, H. (2017). How fracture toughness of epoxy-based nanocomposite is affected by PA66 electrospun nanofiber yarn. *Engineering Fracture Mechanics, 182*, 62-73.
4. Akangah, P., Lingaiah, S., & Shivakumar, K. (2010). Effect of Nylon-66 nano-fiber interleaving on impact damage resistance of epoxy/carbon fiber composite laminates. *Composite Structures, 92*(6), 1432-1439.
5. Al-Assafi, S., de Bruijn, N., & Al-Jumaily, A. M. (2016). Processing and characterization of PMMA nanofiber reinforced epoxy composites. *World Journal of Nano Science and Engineering, 6*(2), 58-63.
6. Al-Saleh, M. H., Saadeh, W. H., & Sundararaj, U. (2013). EMI shielding effectiveness of carbon based nanostructured polymeric materials: a comparative study. *Carbon, 60*, 146-156.
7. Al-Saleh, M. H., & Sundararaj, U. (2011). Review of the mechanical properties of carbon nanofiber/polymer composites. *Composites Part A: Applied Science and Manufacturing, 42*(12), 2126-2142.
8. Anton, F. (1934). Process and apparatus for preparing artificial threads: Google Patents.
9. Arshad, S. N., Naraghi, M., & Chasiotis, I. (2011). Strong carbon nanofibers from electrospun polyacrylonitrile. *Carbon, 49*(5), 1710-1719.
10. Aussawasathien, D., Dong, J. H., & Dai, L. (2005). Electrospun polymer nanofiber sensors. *Synthetic Metals, 154*(1), 37-40. doi: https://doi.org/10.1016/j.synthmet.2005.07.018
11. Aziz, I., Duran, H., Saleem, M., Yameen, B., & Arshad, S. N. (2021). The role of interface on dynamic mechanical properties, dielectric performance, conductivity, and thermal stability of electrospun carbon nanofibers reinforced epoxy. *Polymer Composites*.
12. Bach, Q.-V., Vu, C. M., Vu, H. T., Hoang, T., Dieu, T. V., & Nguyen, D. D. (2020). Epoxidized soybean oil grafted with CTBN as a novel toughener for improving the fracture toughness and mechanical properties of epoxy resin. *Polymer journal, 52*(3), 345-357.
13. Bai, Y., Wang, D., Zhang, Z., Pan, J., Cui, Z., Yu, D.-G., & Bligh, S.-W. A. (2021). Testing of fast dissolution of ibuprofen from its electrospun hydrophilic polymer nanocomposites. *Polymer testing, 93*, 106872.
14. Barakat, N. A., Khalil, K. A., & Kim, H. Y. (2012). Toward facile synthesizing of diamond nanostructures via nanotechnological approach: Lonsdaleite carbon nanofibers by electrospinning. *Materials Research Bulletin, 47*(9), 2140-2147.

15. Bayat, M., Yang, H., Ko, F., Michelson, D., & Mei, A. (2014). Electromagnetic interference shielding effectiveness of hybrid multifunctional Fe3O4/carbon nanofiber composite. *Polymer, 55*(3), 936-943.
16. Beachley, V., & Wen, X. (2009). Fabrication of nanofiber reinforced protein structures for tissue engineering. *Materials Science and Engineering: C, 29*(8), 2448-2453.
17. Beckermann, G. W., & Pickering, K. L. (2015). Mode I and Mode II interlaminar fracture toughness of composite laminates interleaved with electrospun nanofibre veils. *Composites Part A: Applied Science and Manufacturing, 72*, 11-21.
18. Bergshoef, M. M., & Vancso, G. J. (1999). Transparent nanocomposites with ultrathin, electrospun nylon-4, 6 fiber reinforcement. *Advanced Materials, 11*(16), 1362-1365.
19. Bigg, D. (1984). The effect of compounding on the conductive properties of EMI shielding compounds. *Advances in Polymer Technology: Journal of the Polymer Processing Institute, 4*(3-4), 255-266.
20. Blackman, B., Kinloch, A., Lee, J. S., Taylor, A., Agarwal, R., Schueneman, G., & Sprenger, S. (2007). The fracture and fatigue behaviour of nano-modified epoxy polymers. *Journal of materials science, 42*(16), 7049-7051.
21. Bode-Aluko, C. A., Pereao, O., Kyaw, H. H., Al-Naamani, L., Al-Abri, M. Z., Myint, M. T. Z., . . . Dobretsov, S. (2021). Photocatalytic and antifouling properties of electrospun TiO2 polyacrylonitrile composite nanofibers under visible light. *Materials Science and Engineering: B, 264*, 114913.
22. Borges, A. L., Münchow, E. A., de Oliveira Souza, A. C., Yoshida, T., Vallittu, P. K., & Bottino, M. C. (2015). Effect of random/aligned nylon-6/MWCNT fibers on dental resin composite reinforcement. *Journal of the Mechanical Behavior of Biomedical Materials, 48*, 134-144.
23. Brøndsted, P., Lilholt, H., & Lystrup, A. (2005). Composite materials for wind power turbine blades. *Annu. Rev. Mater. Res., 35*, 505-538.
24. Bui, N.-N., Kim, B.-H., Yang, K. S., Cruz, M. E. D., & Ferraris, J. P. (2009). Activated carbon fibers from electrospinning of polyacrylonitrile/pitch blends. *Carbon, 47*(10), 2538-2539.
25. Cao, M.-S., Song, W.-L., Hou, Z.-L., Wen, B., & Yuan, J. (2010). The effects of temperature and frequency on the dielectric properties, electromagnetic interference shielding and microwave-absorption of short carbon fiber/silica composites. *Carbon, 48*(3), 788-796.
26. Chand, S. (2000). Review carbon fibers for composites. *Journal of materials science, 35*(6), 1303-1313.
27. Chandrasekaran, S., Sato, N., Tölle, F., Mülhaupt, R., Fiedler, B., & Schulte, K. (2014). Fracture toughness and failure mechanism of graphene based epoxy composites. *Composites science and technology, 97*, 90-99.
28. Chang, S., Wang, M., Zhang, F., Liu, Y., Liu, X., Yu, D.-G., & Shen, H. (2020). Sheath-separate-core nanocomposites fabricated using a trifluid electrospinning. *Materials & Design, 192*, 108782.

29. Chang, Z. J. (2011). *Development of a polyurethane nanocomposite reinforced with carbon nanotube composite nanofibers.* Paper presented at the Materials Science Forum.
30. Chaudhary, S., Surekha, P., Kumar, D., Rajagopal, C., & Roy, P. (2015). Amine-functionalized poly (styrene) microspheres as thermoplastic toughener for epoxy resin. *Polymer Composites, 36*(1), 174-183.
31. Chen, C., Cho, M., Nam, J.-D., & Lee, Y. (2013). Cellulose diacetate reinforced with electrospun cellulose fiber: A new route to prepare an all cellulose-based composite. *Composites Part A: Applied Science and Manufacturing, 53*, 10-15.
32. Chen, C., He, Y., Xiao, G., Wu, Y., He, Z., & Zhong, F. (2018). Zirconia doped in carbon fiber by electrospinning method and improve the mechanical properties and corrosion resistance of epoxy. *Progress in Organic Coatings, 125*, 420-431.
33. Chen, D., Wang, R., Tjiu, W. W., & Liu, T. (2011). High performance polyimide composite films prepared by homogeneity reinforcement of electrospun nanofibers. *Composites science and technology, 71*(13), 1556-1562.
34. Chen, G., & Liu, H. (2008). Electrospun cellulose nanofiber reinforced soybean protein isolate composite film. *Journal of applied polymer science, 110*(2), 641-646.
35. Chen, I.-H., Wang, C.-C., & Chen, C.-Y. (2010). Fabrication and structural characterization of polyacrylonitrile and carbon nanofibers containing plasma-modified carbon nanotubes by electrospinning. *The Journal of Physical Chemistry C, 114*(32), 13532-13539.
36. Chen, J., Kinloch, A., Sprenger, S., & Taylor, A. (2013). The mechanical properties and toughening mechanisms of an epoxy polymer modified with polysiloxane-based core-shell particles. *Polymer, 54*(16), 4276-4289.
37. Chen, L. S., Huang, Z. M., Dong, G. H., He, C. L., Liu, L., Hu, Y. Y., & Li, Y. (2009). Development of a transparent PMMA composite reinforced with nanofibers. *Polymer Composites, 30*(3), 239-247.
38. Chen, Q., Wu, W., Zhao, Y., Xi, M., Xu, T., & Fong, H. (2014). Nano-epoxy resins containing electrospun carbon nanofibers and the resulting hybrid multi-scale composites. *Composites Part B: Engineering, 58*, 43-53.
39. Chen, Q., Zhang, L., Rahman, A., Zhou, Z., Wu, X.-F., & Fong, H. (2011). Hybrid multi-scale epoxy composite made of conventional carbon fiber fabrics with interlaminar regions containing electrospun carbon nanofiber mats. *Composites Part A: Applied Science and Manufacturing, 42*(12), 2036-2042.
40. Chen, Q., Zhao, Y., Zhou, Z., Rahman, A., Wu, X.-F., Wu, W., . . . Fong, H. (2013). Fabrication and mechanical properties of hybrid multi-scale epoxy composites reinforced with conventional carbon fiber fabrics surface-attached with electrospun carbon nanofiber mats. *Composites Part B: Engineering, 44*(1), 1-7.
41. Chen, W., Chen, S., Morsi, Y., El-Hamshary, H., El-Newhy, M., Fan, C., & Mo, X. (2016). Superabsorbent 3D Scaffold Based on Electrospun Nanofibers for Cartilage Tissue Engineering. *ACS applied materials & interfaces, 8*(37), 24415-24425. doi: 10.1021/acsami.6b06825

42. Chen, Y., Han, D., Ouyang, W., Chen, S., Hou, H., Zhao, Y., & Fong, H. (2012). Fabrication and evaluation of polyamide 6 composites with electrospun polyimide nanofibers as skeletal framework. *Composites Part B: Engineering, 43*(5), 2382-2388.
43. Choi, S.-S., Lee, Y. S., Joo, C. W., Lee, S. G., Park, J. K., & Han, K.-S. (2004). Electrospun PVDF nanofiber web as polymer electrolyte or separator. *Electrochimica Acta, 50*(2-3), 339-343.
44. Chuayjuljit, S., Soatthiyanon, N., & Potiyaraj, P. (2006). Polymer blends of epoxy resin and epoxidized natural rubber. *Journal of applied polymer science, 102*(1), 452-459.
45. Chun, I., & Reneker, D. H, Fong, XY Fang and J. Dietzel et al., 1999. Carbon Nanofibers from Polyacrylonitrile and mesophase pitch J. *Adv. Mater, 31*, 36-41.
46. Chung, D. (2001). Electromagnetic interference shielding effectiveness of carbon materials. *Carbon, 39*(2), 279-285.
47. Chung, D. D. L. (2000). Materials for electromagnetic interference shielding. *Journal of Materials Engineering and Performance, 9*(3), 350-354. doi: 10.1361/105994900770346042
48. Colaneri, N. F., & Schacklette, L. (1992). EMI shielding measurements of conductive polymer blends. *IEEE transactions on instrumentation and measurement, 41*(2), 291-297.
49. Correa, R., Nunes, R., & Filho, W. F. (1998). Short fiber reinforced thermoplastic polyurethane elastomer composites. *Polymer Composites, 19*(2), 152-155.
50. Cseri, L., Topuz, F., Abdulhamid, M. A., Alammar, A., Budd, P. M., & Szekely, G. (2021). Electrospun adsorptive nanofibrous membranes from ion exchange polymers to snare textile dyes from wastewater. *Advanced Materials Technologies*, 2000955.
51. Cui, C., Xiang, C., Geng, L., Lai, X., Guo, R., Zhang, Y., . . . Jiang, S. (2019). Flexible and ultrathin electrospun regenerate cellulose nanofibers and d-Ti3C2Tx (MXene) composite film for electromagnetic interference shielding. *Journal of Alloys and Compounds, 788*, 1246-1255.
52. Daelemans, L., van der Heijden, S., De Baere, I., Rahier, H., Van Paepegem, W., & De Clerck, K. (2016). Damage-resistant composites using electrospun nanofibers: a multiscale analysis of the toughening mechanisms. *ACS applied materials & interfaces, 8*(18), 11806-11818.
53. Daelemans, L., Van Paepegem, W., & De Clerck, K. (2020). Effect of interleaved polymer nanofibers on the properties of glass and carbon fiber composites *Fiber-Reinforced Nanocomposites: Fundamentals and Applications* (pp. 235-260): Elsevier.
54. De Schoenmaker, B., Van der Heijden, S., De Baere, I., Van Paepegem, W., & De Clerck, K. (2013). Effect of electrospun polyamide 6 nanofibres on the mechanical properties of a glass fibre/epoxy composite. *Polymer testing, 32*(8), 1495-1501.

55. Deeraj, B. D. S., Mathew, M. S., Parameswaranpillai, J., & Joseph, K. (2020). EMI shielding materials based on thermosetting polymers *Materials for Potential EMI Shielding Applications* (pp. 101-110): Elsevier.
56. Demir, M. M., Horzum, N., Taşdemirci, A., Turan, K., & Güden, M. (2014). Mechanical interlocking between porous electrospun polystyrene fibers and an epoxy matrix. *ACS applied materials & interfaces, 6*(24), 21901-21905.
57. Deshpande, A. P., Bhaskar Rao, M., & Lakshmana Rao, C. (2000). Extraction of bamboo fibers and their use as reinforcement in polymeric composites. *Journal of applied polymer science, 76*(1), 83-92.
58. Dong, L., Wang, G., Li, X., Xiong, D., Yan, B., Chen, B., . . . Cui, Y. (2016). PVP-derived carbon nanofibers harvesting enhanced anode performance for lithium ion batteries. *RSC Advances, 6*(5), 4193-4199.
59. Duan, G., Bagheri, A. R., Jiang, S., Golenser, J., Agarwal, S., & Greiner, A. (2017). Exploration of macroporous polymeric sponges as drug carriers. *Biomacromolecules, 18*(10), 3215-3221.
60. Duan, G., Jiang, S., Jérôme, V., Wendorff, J. H., Fathi, A., Uhm, J., . . . Greiner, A. (2015). Ultralight, Soft Polymer Sponges by Self-Assembly of Short Electrospun Fibers in Colloidal Dispersions. *Advanced Functional Materials, 25*(19), 2850-2856. doi: https://doi.org/10.1002/adfm.201500001
61. Dzenis, Y., & Wen, Y. (2001). Continuous carbon nanofibers for nanofiber composites. *MRS Online Proceedings Library, 702*(1), 1-6.
62. Feng, S. Q., Shen, X. Y., Fu, Z. Y., & Ji, Y. L. (2009). Studies on the electrospun submicron fibers of SIS and its mechanical properties. *Journal of applied polymer science, 114*(3), 1580-1586.
63. Fong, H. (2004). Electrospun nylon 6 nanofiber reinforced BIS-GMA/TEGDMA dental restorative composite resins. *Polymer, 45*(7), 2427-2432.
64. Garg, K., & Bowlin, G. L. (2011). Electrospinning jets and nanofibrous structures. *Biomicrofluidics, 5*(1), 013403.
65. Geetha, S., Satheesh Kumar, K., Rao, C. R., Vijayan, M., & Trivedi, D. (2009). EMI shielding: Methods and materials—A review. *Journal of applied polymer science, 112*(4), 2073-2086.
66. Gelves, G. A., Al-Saleh, M. H., & Sundararaj, U. (2011). Highly electrically conductive and high performance EMI shielding nanowire/polymer nanocomposites by miscible mixing and precipitation. *Journal of Materials Chemistry, 21*(3), 829-836.
67. Goodarz, M., Bahrami, S., Sadighi, M., & Saber-Samandari, S. (2017). The influence of graphene reinforced electrospun nano-interlayers on quasi-static indentation behavior of fiber-reinforced epoxy composites. *Fibers and Polymers, 18*(2), 322-333.
68. Gopiraman, M., & Kim, I. S. (2019). Preparation, characterization, and applications of electrospun carbon Nanofibers and its composites *Electrospinning and Electrospraying-Techniques and Applications*: IntechOpen.

69. Guo, F., Wang, N., Wang, L., Hou, L., Ma, L., Liu, J., . . . Zhao, Y. (2015). An electrospun strong PCL/PU composite vascular graft with mechanical anisotropy and cyclic stability. *Journal of Materials Chemistry A, 3*(9), 4782-4787.
70. Guo, H., Chen, Y., Li, Y., Zhou, W., Xu, W., Pang, L., . . . Jiang, S. (2021). Electrospun fibrous materials and their applications for electromagnetic interference shielding: A review. *Composites Part A: Applied Science and Manufacturing*, 106309.
71. Guo, H., Wang, F., Luo, H., Li, Y., Lou, Z., Ji, Y., . . . Liu, K. (2021). Flexible TaC/C electrospun non–woven fabrics with multiple spatial-scale conductive frameworks for efficient electromagnetic interference shielding. *Composites Part A: Applied Science and Manufacturing, 151*, 106662.
72. Guo, M., Guo, J., Jia, D., Zhao, H., Sun, Z., Song, X., & Li, Y. (2015). Coal derived porous carbon fibers with tunable internal channels for flexible electrodes and organic matter absorption. *Journal of Materials Chemistry A, 3*(42), 21178-21184.
73. Guo, T., Zhou, Z., Guo, H., Xiao, G., Tang, X., & Peng, M. (2014). Toughening of epoxy resin with functionalized core-sheath structured PAN/SBS electrospun fibers. *Journal of applied polymer science, 131*(23).
74. Guo, X., Deng, Y., Gu, D., Che, R., & Zhao, D. (2009). Synthesis and microwave absorption of uniform hematite nanoparticles and their core-shell mesoporous silica nanocomposites. *Journal of Materials Chemistry, 19*(37), 6706-6712.
75. Guo, Y., Pan, L., Yang, X., Ruan, K., Han, Y., Kong, J., & Gu, J. (2019). Simultaneous improvement of thermal conductivities and electromagnetic interference shielding performances in polystyrene composites via constructing interconnection oriented networks based on electrospinning technology. *Composites Part A: Applied Science and Manufacturing, 124*, 105484.
76. Haghighi, H., & Cotton, I. (2019). Analysis of the Degradation Kinetics of Kapton Film in an Aerospace Environment. 2019 IEEE Electrical Insulation Conference, EIC 2019, June, 481–484. https://doi.org/10.1109/EIC43217.2019.9046608
77. Han, S. O., Son, W. K., Youk, J. H., & Park, W. H. (2008). Electrospinning of ultrafine cellulose fibers and fabrication of poly (butylene succinate) biocomposites reinforced by them. *Journal of applied polymer science, 107*(3), 1954-1959.
78. He, J.-H., Wu, Y., & Zuo, W.-W. (2005). Critical length of straight jet in electrospinning. *Polymer, 46*(26), 12637-12640.
79. He, Y., Han, D., Chen, J., Ding, Y., Jiang, S., Hu, C., . . . Hou, H. (2014). Highly strong and highly tough electrospun polyimide/polyimide composite nanofibers from binary blend of polyamic acids. *RSC Advances, 4*(104), 59936-59942.
80. Herwan, J., Al-Bahkali, E., Khalil, K. A., & Souli, M. (2016). Load bearing enhancement of pin joined composite laminates using electrospun polyacrylonitrile nanofiber mats. *Arabian Journal of Chemistry, 9*(2), 262-268.

81. Hong, S. E., Kim, D.-K., Jo, S. M., Kim, D. Y., & Chin, B. D. (2007). Graphite nanofibers prepared from catalytic graphitization of electrospun poly (vinylidene fluoride) nanofibers and their hydrogen storage capacity. *Catalysis today*, *120*(3-4), 413-419.
82. Huang, P., Zheng, S., Huang, J., Guo, Q., & Zhu, W. (1997). Miscibility and mechanical properties of epoxy resin/polysulfone blends. *Polymer*, *38*(22), 5565-5571.
83. Huang, Y., Yang, J., Cai, H., Zhai, Y., Feng, D., Deng, Y., . . . Zhao, D. (2009). A curing agent method to synthesize ordered mesoporous carbons from linear novolac phenolic resin polymers. *Journal of Materials Chemistry*, *19*(36), 6536-6541.
84. Huang, Z.-M., Zhang, Y.-Z., Kotaki, M., & Ramakrishna, S. (2003). A review on polymer nanofibers by electrospinning and their applications in nanocomposites. *Composites science and technology*, *63*(15), 2223-2253.
85. Im, J. S., Kim, J. G., Bae, T.-S., & Lee, Y.-S. (2011). Effect of heat treatment on ZrO2-embedded electrospun carbon fibers used for efficient electromagnetic interference shielding. *Journal of Physics and Chemistry of Solids*, *72*(10), 1175-1179.
86. Im, J. S., Kim, J. G., Lee, S.-H., & Lee, Y.-S. (2010a). Effective electromagnetic interference shielding by electrospun carbon fibers involving Fe2O3/BaTiO3/MWCNT additives. *Materials Chemistry and Physics*, *124*(1), 434-438.
87. Im, J. S., Kim, J. G., Lee, S.-H., & Lee, Y.-S. (2010b). Enhanced adhesion and dispersion of carbon nanotube in PANI/PEO electrospun fibers for shielding effectiveness of electromagnetic interference. *Colloids and Surfaces A: Physicochemical and Engineering Aspects*, *364*(1-3), 151-157.
88. Im, J. S., Kim, J. G., & Lee, Y.-S. (2009). Fluorination effects of carbon black additives for electrical properties and EMI shielding efficiency by improved dispersion and adhesion. *Carbon*, *47*(11), 2640-2647.
89. Inagaki, M., Yang, Y., & Kang, F. (2012). Carbon nanofibers prepared via electrospinning. *Advanced Materials*, *24*(19), 2547-2566.
90. Iyengar, P. K., Bhat, K. A., Sangeetha, D., & Moorthy, T. V. (2013). Polymethyl methacrylate nanofiber-reinforced epoxy composite for shape-memory applications. *High Performance Polymers*, *25*(8), 1000-1006.
91. Jahanbaani, A. R., Behzad, T., Borhani, S., & Darvanjooghi, M. H. K. (2016). Electrospinning of cellulose nanofibers mat for laminated epoxy composite production. *Fibers and Polymers*, *17*(9), 1438-1448.
92. Jayan, J. S., Pal, K., Saritha, A., Deeraj, B., & Joseph, K. Graphene oxide as multi-functional initiator and effective molecular reinforcement in PVP/epoxy composites. *Journal of Molecular Structure*, 129873.
93. Jayan, J. S., Pal, K., Saritha, A., Deeraj, B., & Joseph, K. (2021). Graphene oxide as multi-functional initiator and effective molecular reinforcement in PVP/epoxy composites. *Journal of Molecular Structure*, *1230*, 129873.

94. Jayan, J. S., Saritha, A., Deeraj, B., & Joseph, K. (2020a). Synthesis of self-assembled and porous nano titania-graphene oxide hybrids for toughening the epoxy. *Polymer Composites, 41*(10), 4093-4103.
95. Jayan, J. S., Saritha, A., Deeraj, B., & Joseph, K. (2020b). Triblock copolymer grafted Graphene oxide as nanofiller for toughening of epoxy resin. *Materials Chemistry and Physics, 248*, 122930.
96. Jayan, J. S., Saritha, A., Deeraj, B. D. S., & Joseph, K. (2020c). Graphene oxide as a prospective graft in polyethylene glycol for enhancing the toughness of epoxy nanocomposites. *Polymer Engineering & Science, 60*(4), 773-781.
97. Ji, H., Zhao, R., Zhang, N., Jin, C., Lu, X., & Wang, C. (2018). Lightweight and flexible electrospun polymer nanofiber/metal nanoparticle hybrid membrane for high-performance electromagnetic interference shielding. *NPG Asia Materials, 10*(8), 749-760.
98. Ji, Q. L., Zhang, M. Q., Rong, M. Z., Wetzel, B., & Friedrich, K. (2004). Tribological properties of surface modified nano-alumina/epoxy composites. *Journal of materials science, 39*(21), 6487-6493.
99. Jian, S., Zhu, J., Jiang, S., Chen, S., Fang, H., Song, Y., . . . Hou, H. (2018). Nanofibers with diameter below one nanometer from electrospinning. RSC Adv 8 (9): 4794–4802.
100. Jiang, S., Chen, Y., Duan, G., Mei, C., Greiner, A., & Agarwal, S. (2018). Electrospun nanofiber reinforced composites: A review. *Polymer Chemistry, 9*(20), 2685-2720.
101. Jiang, S., Duan, G., Hou, H., Greiner, A., & Agarwal, S. (2012). Novel layer-by-layer procedure for making nylon-6 nanofiber reinforced high strength, tough, and transparent thermoplastic polyurethane composites. *ACS applied materials & interfaces, 4*(8), 4366-4372.
102. Jiang, S., Duan, G., Schöbel, J., Agarwal, S., & Greiner, A. (2013). Short electrospun polymeric nanofibers reinforced polyimide nanocomposites. *Composites science and technology, 88*, 57-61.
103. Jiang, S., Hou, H., Greiner, A., & Agarwal, S. (2012). Tough and transparent nylon-6 electrospun nanofiber reinforced melamine–formaldehyde composites. *ACS applied materials & interfaces, 4*(5), 2597-2603.
104. Jiang, S., Uch, B., Agarwal, S., & Greiner, A. (2017). Ultralight, Thermally Insulating, Compressible Polyimide Fiber Assembled Sponges. *ACS applied materials & interfaces, 9*(37), 32308-32315. doi: 10.1021/acsami.7b11045
105. Joshi, A., & Datar, S. (2015). Carbon nanostructure composite for electromagnetic interference shielding. *Pramana, 84*(6), 1099-1116.
106. Karacan, I., & Meşeli, H. (2018). Characterization of amorphous carbon fibers produced from thermally stabilized polyamide 6 fibers. *Journal of Industrial Textiles, 47*(6), 1185-1211.
107. Katti, P., Kundan, K., Kumar, S., & Bose, S. (2017). Improved mechanical properties through engineering the interface by poly (ether ether

ketone) grafted graphene oxide in epoxy based nanocomposites. *Polymer, 122*, 184-193.
108. Kausar, A. (2014). Mechanical, thermal, and electrical properties of epoxy matrix composites reinforced with polyamide-grafted-MWCNT/poly (azo-pyridine-benzophenone-imide)/polyaniline nanofibers. *International Journal of Polymeric Materials and Polymeric Biomaterials, 63*(16), 831-839.
109. Kausar, A. (2016). Synthesis and properties of polyimide nanocomposites self-reinforced with electrospun poly (azo-naphthyl-imide)/carbon nanotube nanofibers. *Journal of Thermoplastic Composite Materials, 29*(3), 312-326.
110. Kim, B. C., & Park, S. W. (2008). Fracture toughness of the nano-particle reinforced epoxy composite. *Composite Structures, 86*(1-3), 69-77.
111. Kim, C., Jeong, Y. I., Ngoc, B. T. N., Yang, K. S., Kojima, M., Kim, Y. A., . . . Lee, J. W. (2007). Synthesis and characterization of porous carbon nanofibers with hollow cores through the thermal treatment of electrospun copolymeric nanofiber webs. *Small, 3*(1), 91-95.
112. Kim, C., & Yang, K. (2003). Electrochemical properties of carbon nanofiber web as an electrode for supercapacitor prepared by electrospinning. *Applied physics letters, 83*(6), 1216-1218.
113. Kim, J. s., & Reneker, D. H. (1999). Mechanical properties of composites using ultrafine electrospun fibers. *Polymer Composites, 20*(1), 124-131.
114. Kondawar, S. B., & Modak, P. R. (2020). Theory of EMI shielding *Materials for Potential EMI Shielding Applications* (pp. 9-25): Elsevier.
115. Konnola, R., Deeraj, B., Sampath, S., Saritha, A., & Joseph, K. (2019). Fabrication and Characterization of Toughened Nanocomposites Based on TiO2 Nanowire-Epoxy System. *Polymer Composites, 40*(7), 2629-2638.
116. Konnola, R., Joji, J., Parameswaranpillai, J., & Joseph, K. (2015). Structure and thermo-mechanical properties of CTBN-grafted-GO modified epoxy/DDS composites. *RSC Advances, 5*(76), 61775-61786.
117. Konnola, R., Nair, C. R., & Joseph, K. (2016). High strength toughened epoxy nanocomposite based on poly (ether sulfone)-grafted multi-walled carbon nanotube. *Polymers for Advanced Technologies, 27*(1), 82-89.
118. Krishnappa, R., Desai, K., & Sung, C. (2003). Morphological study of electrospun polycarbonates as a function of the solvent and processing voltage. *Journal of materials science, 38*(11), 2357-2365.
119. Kumar, M., Hietala, M., & Oksman, K. (2019). Lignin-based electrospun carbon nanofibers. *Frontiers in Materials, 6*, 62.
120. Kumari, P., Tripathi, P., Singh, S., & Kumar, D. (2020). Electromagnetic shielding using ceramic materials *Materials for Potential EMI Shielding Applications* (pp. 315-331): Elsevier.
121. Lamastra, F., Puglia, D., Monti, M., Vella, A., Peponi, L., Kenny, J., & Nanni, F. (2012). Poly (ε-caprolactone) reinforced with fibres of Poly (methyl methacrylate) loaded with multiwall carbon nanotubes or graphene nanoplatelets. *Chemical engineering journal, 195*, 140-148.

122. Lan, F., Zhang, H., Fan, J., Xu, Q., Li, H., & Min, Y. (2021). Electrospun Polymer Nanofibers with TiO2@ NiCo-LDH as Efficient Polysulfide Barriers for Wide-Temperature-Range Li–S Batteries. *ACS applied materials & interfaces*, *13*(2), 2734-2744.
123. Lee, B.-S., Son, S.-B., Park, K.-M., Yu, W.-R., Oh, K.-H., & Lee, S.-H. (2012). Anodic properties of hollow carbon nanofibers for Li-ion battery. *Journal of Power Sources, 199*, 53-60.
124. Lee, B.-S., & Yu, W.-R. (2020). Electrospun carbon nanofibers as a functional composite platform: a review of highly tunable microstructures and morphologies for versatile applications. *Functional Composites and Structures*, *2*(1), 012001.
125. Lee, E., Song, Y., & Lee, S. (2014). *Antimicrobial property and biodegradability of lignin nanofibers.* Master's Thesis, Yonsei University, Republic of Korea.
126. Lee, J.-R., Park, S.-J., Seo, M.-K., & Park, J.-M. (2004). Preparation and characterization of electrospun poly (ethylene oxide)(PEO) nanofibers-reinforced epoxy matrix composites. *MRS online proceedings library archive, 851*.
127. Lee, K., Kim, H., Bang, H., Jung, Y., & Lee, S. (2003). The change of bead morphology formed on electrospun polystyrene fibers. *Polymer, 44*(14), 4029-4034.
128. Lee, K. J., Shiratori, N., Lee, G. H., Miyawaki, J., Mochida, I., Yoon, S.-H., & Jang, J. (2010). Activated carbon nanofiber produced from electrospun polyacrylonitrile nanofiber as a highly efficient formaldehyde adsorbent. *Carbon*, *48*(15), 4248-4255.
129. Lee, S. M. (1992). *Handbook of composite reinforcements*: John Wiley & Sons.
130. Li, B., Yuan, H., & Zhang, Y. (2013). Transparent PMMA-based nanocomposite using electrospun graphene-incorporated PA-6 nanofibers as the reinforcement. *Composites science and technology*, *89*, 134-141.
131. Li, X., Tabil, L. G., & Panigrahi, S. (2007). Chemical treatments of natural fiber for use in natural fiber-reinforced composites: a review. *Journal of Polymers and the Environment*, *15*(1), 25-33.
132. Li, Z., Lin, Z., Han, M., Mu, Y., Yu, P., Zhang, Y., & Yu, J. (2021). Flexible electrospun carbon nanofibers/silicone composite films for electromagnetic interference shielding, electrothermal and photothermal applications. *Chemical engineering journal*, *420*, 129826.
133. Liao, H., Wu, Y., Wu, M., & Liu, H. (2011). Effects of fiber surface chemistry and roughness on interfacial structures of electrospun fiber reinforced epoxy composite films. *Polymer Composites*, *32*(5), 837-845.
134. Liao, X., Ye, W., Chen, L., Jiang, S., Wang, G., Zhang, L., & Hou, H. (2017). Flexible hdC-G reinforced polyimide composites with high dielectric permittivity. *Composites Part A: Applied Science and Manufacturing*, *101*, 50-58. doi: https://doi.org/10.1016/j.compositesa.2017.06.011

135. Lin, S., Cai, Q., Ji, J., Sui, G., Yu, Y., Yang, X., . . . Deng, X. (2008). Electrospun nanofiber reinforced and toughened composites through in situ nano-interface formation. *Composites science and technology, 68*(15-16), 3322-3329.
136. Liu, J., Thompson, Z. J., Sue, H.-J., Bates, F. S., Hillmyer, M. A., Dettloff, M., . . . Pham, H. (2010). Toughening of epoxies with block copolymer micelles of wormlike morphology. *Macromolecules, 43*(17), 7238-7243.
137. Liu, Y., Chen, S., Ye, S., & Feng, J. (2016). A feasible route to balance the mechanical properties of epoxy thermosets by reinforcing a PCL-PPC-PCL toughened system with reduced graphene oxide. *Composites science and technology, 125*, 108-113.
138. Liu, Y., Ji, Y., Ghosh, K., Clark, R. A., Huang, L., & Rafailovich, M. H. (2009). Effects of fiber orientation and diameter on the behavior of human dermal fibroblasts on electrospun PMMA scaffolds. *Journal of Biomedical Materials Research Part A: An Official Journal of The Society for Biomaterials, The Japanese Society for Biomaterials, and The Australian Society for Biomaterials and the Korean Society for Biomaterials, 90*(4), 1092-1106.
139. Liu, Y., Teng, H., Hou, H., & You, T. (2009). Nonenzymatic glucose sensor based on renewable electrospun Ni nanoparticle-loaded carbon nanofiber paste electrode. *Biosensors and Bioelectronics, 24*(11), 3329-3334.
140. Liu, Z., Bai, G., Huang, Y., Li, F., Ma, Y., Guo, T., . . . Chen, Y. (2007). Microwave absorption of single-walled carbon nanotubes/soluble cross-linked polyurethane composites. *The Journal of Physical Chemistry C, 111*(37), 13696-13700.
141. Liu, Z., Bai, G., Huang, Y., Ma, Y., Du, F., Li, F., . . . Chen, Y. (2007). Reflection and absorption contributions to the electromagnetic interference shielding of single-walled carbon nanotube/polyurethane composites. *Carbon, 45*(4), 821-827.
142. Liu, S., White, K. L., & Reneker, D. H. (2019). Electrospinning Polymer Nanofibers with Controlled Diameters. IEEE Transactions on Industry Applications, 55(5), 5239–5243. https://doi.org/10.1109/TIA.2019.2920811
143. Liu, S., White, K., & Reneker, D. H. (2017). Controlled electrospinning to produce polymer nanofibers with specified diameters. 2017 IEEE Industry Applications Society Annual Meeting, IAS 2017, 2017-Janua, 1–5. https://doi.org/10.1109/IAS.2017.8101694
144. Lukáš, D., A, A, A. S., Martinová, L., A, Vodseď álková, K., A, Lubasová, D., A, A, J. C., Pokorný, P., A, Mikeš, P., A, A, J. C., & A, & M. K. (2009). Physical principles of electrospinning (Electrospinning as a nano-scale technology of the twenty-first century). Textile Progress, 40(May), 01–140
145. Lu, B., Zheng, G., Dai, K., Liu, C., Chen, J., & Shen, C. (2015). Enhanced mechanical properties of polyethylene composites with low content of electrospun nylon-66 nanofibers. *Materials Letters, 140*, 131-134.

146. Lu, X., Wang, C., & Wei, Y. (2009). One-dimensional composite nanomaterials: Synthesis by electrospinning and their applications. *Small, 5*(21), 2349-2370.
147. Ma, C., Liu, H.-Y., Du, X., Mach, L., Xu, F., & Mai, Y.-W. (2015). Fracture resistance, thermal and electrical properties of epoxy composites containing aligned carbon nanotubes by low magnetic field. *Composites science and technology, 114*, 126-135.
148. Ma, S., Liu, W., Gao, N., Yan, Z., & Zhao, Y. (2011). Synthesis and properties of LED-packaging epoxy resin toughened by a novel polysiloxane from hydrolysis and condensation. *Macromolecular research, 19*(9), 972-979.
149. Ma, X., & Zhao, G. (2011). Variations in the microstructure of carbon fibers prepared from liquefied wood during carbonization. *Journal of applied polymer science, 121*(6), 3525-3530.
150. Ma, Z., Kotaki, M., Yong, T., He, W., & Ramakrishna, S. (2005). Surface engineering of electrospun polyethylene terephthalate (PET) nanofibers towards development of a new material for blood vessel engineering. *Biomaterials, 26*(15), 2527-2536.
151. Marega, C., & Marigo, A. (2015). Effect of electrospun fibers of polyhydroxybutyrate filled with different organoclays on morphology, biodegradation, and thermal stability of poly (ε-caprolattone). *Journal of applied polymer science, 132*(31).
152. Matabola, K., De Vries, A., Luyt, A., & Kumar, R. (2011). Studies on single polymer composites of poly (methyl methacrylate) reinforced with electrospun nanofibers with a focus on their dynamic mechanical properties.
153. McGrath, L. M., Parnas, R. S., King, S. H., Schroeder, J. L., Fischer, D. A., & Lenhart, J. L. (2008). Investigation of the thermal, mechanical, and fracture properties of alumina–epoxy composites. *Polymer, 49*(4), 999-1014.
154. Meena, R., Bhattachrya, S., & Chatterjee, R. (2010). Complex permittivity, permeability and wide band microwave absorbing property of La3+ substituted U-type hexaferrite. *Journal of magnetism and magnetic materials, 322*(14), 1923-1928.
155. Mimura, K., Ito, H., & Fujioka, H. (2000). Improvement of thermal and mechanical properties by control of morphologies in PES-modified epoxy resins. *Polymer, 41*(12), 4451-4459.
156. Nakhaei, O., Shahtahmassebi, N., Roknabadi, M. R., & Behdani, M. (2016). Co-electrospinning fabrication and study of structural and electromagnetic interference-shielding effectiveness of TiO 2/SiO 2 core–shell nanofibers. *Applied Physics A, 122*(5), 1-10.
157. Neisiany, R. E., Khorasani, S. N., Lee, J. K. Y., Naeimirad, M., & Ramakrishna, S. (2018). Interfacial toughening of carbon/epoxy composite by incorporating styrene acrylonitrile nanofibers. *Theoretical and Applied Fracture Mechanics, 95*, 242-247.
158. Neppalli, R., Causin, V., Benetti, E. M., Ray, S. S., Esposito, A., Wanjale, S., . . . Marigo, A. (2014). Polystyrene/TiO2 composite electrospun

fibers as fillers for poly (butylene succinate-co-adipate): Structure, morphology and properties. *European polymer journal, 50*, 78-86.

159. Neppalli, R., Marega, C., Marigo, A., Bajgai, M. P., Kim, H. Y., & Causin, V. (2010). Poly (ε-caprolactone) filled with electrospun nylon fibres: A model for a facile composite fabrication. *European polymer journal, 46*(5), 968-976.

160. Neppalli, R., Marega, C., Marigo, A., Bajgai, M. P., Kim, H. Y., Ray, S. S., & Causina, V. (2012). Electrospun nylon fibers for the improvement of mechanical properties and for the control of degradation behaviour of poly (lactide)-based composites.

161. Ohlan, A., Singh, K., Chandra, A., & Dhawan, S. (2008). Microwave absorption properties of conducting polymer composite with barium ferrite nanoparticles in 12.4–18 GHz. *Applied physics letters, 93*(5), 053114.

162. Özden-Yenigün, E., Menceloğlu, Y. Z., & Papila, M. (2012). MWCNTs/P (St-co-GMA) composite nanofibers of engineered interface chemistry for epoxy matrix nanocomposites. *ACS applied materials & interfaces, 4*(2), 777-784.

163. Ozden, E., Menceloglu, Y. Z., & Papila, M. (2010). Engineering chemistry of electrospun nanofibers and interfaces in nanocomposites for superior mechanical properties. *ACS applied materials & interfaces, 2*(7), 1788-1793.

164. Padmavathi, R., & Sangeetha, D. (2013). Synthesis and characterization of electrospun carbon nanofiber supported Pt catalyst for fuel cells. *Electrochimica Acta, 112*, 1-13.

165. Palazzetti, R., Zucchelli, A., Gualandi, C., Focarete, M., Donati, L., Minak, G., & Ramakrishna, S. (2012). Influence of electrospun Nylon 6, 6 nanofibrous mats on the interlaminar properties of Gr–epoxy composite laminates. *Composite Structures, 94*(2), 571-579.

166. Parameswaranpillai, J., Ramanan, S. P., George, J. J., Jose, S., Zachariah, A. K., Siengchin, S., . . . Pionteck, J. r. (2018). PEG-ran-PPG Modified Epoxy Thermosets: A Simple Approach To Develop Tough Shape Memory Polymers. *Industrial & Engineering Chemistry Research, 57*(10), 3583-3590.

167. Park, K.-Y., Lee, S.-E., Kim, C.-G., & Han, J.-H. (2006). Fabrication and electromagnetic characteristics of electromagnetic wave absorbing sandwich structures. *Composites science and technology, 66*(3-4), 576-584.

168. Park, S. H., Kim, C., Choi, Y. O., & Yang, K. S. (2003). Preparations of pitch-based CF/ACF webs by electrospinning. *Carbon (New York, NY), 41*(13), 2655-2657.

169. Puglia, D., Biagiotti, J., & Kenny, J. (2005). A review on natural fibre-based composites—Part II: Application of natural reinforcements in composite materials for automotive industry. *Journal of natural fibers, 1*(3), 23-65.

170. Quan, D., & Ivankovic, A. (2015). Effect of core–shell rubber (CSR) nano-particles on mechanical properties and fracture toughness of an epoxy polymer. *Polymer, 66*, 16-28.

171. Rangappa, S. M., Siengchin, S., Parameswaranpillai, J., & Thomas, S. (2022). Handbook of Epoxy/Fiber Composites. 990. doi: 10.1007/978-981-15-8141-0
172. Rayleigh, L. (1882). XX. On the equilibrium of liquid conducting masses charged with electricity. *The London, Edinburgh, and Dublin Philosophical Magazine and Journal of Science, 14*(87), 184-186.
173. Ramakrishna, S., Fujihara, K., Teo, W., Lim, T., Ma, Z., Reneker, D. H., & Chun, I. (1996). Chapter 1 - Introduction. Nanotechnology, 7(3), 1–21. http://stacks.iop.org/0957-4484/7/i=3/a=009?key=crossref.b62a3c509c723c5a2561f1e345fc1706
174. Remiro, P. M., Cortazar, M., Calahorra, E., & Calafel, M. M. (2002). The effect of crosslinking and miscibility on the thermal degradation of an uncured and an amine-cured epoxy resin blended with poly(ε-caprolactone). Polymer Degradation and Stability, 78(1), 83–93. https://doi.org/10.1016/S0141-3910(02)00122-2
175. Reneker, D. H. (1993). 1993-Electrospinning Peocess and Application for Electrospun Fibers.
176. Reneker, D. H., & Yarin, A. L. (2008). Electrospinning jets and polymer nanofibers. Polymer, 49(10), 2387–2425. https://doi.org/10.1016/j.polymer.2008.02.002
177. Reneker, D. H., Yarin, A. L., Fong, H., & Koombhongse, S. (2000). Bending instability of electrically charged liquid jets of polymer solutions in electrospinning. Journal of Applied Physics, 87(9 I), 4531–4547. https://doi.org/10.1063/1.373532
178. Reich, S., Burgard, M., Langner, M., Jiang, S., Wang, X., Agarwal, S., . . . Greiner, A. (2018). Polymer nanofibre composite nonwovens with metal-like electrical conductivity. *npj Flexible Electronics*, *2*(1), 5. doi: 10.1038/s41528-017-0018-5
179. Romo-Uribe, A., Arizmendi, L., Romero-Guzmán, M. a. E., Sepulveda-Guzmán, S., & Cruz-Silva, R. (2009). Electrospun nylon nanofibers as effective reinforcement to polyaniline membranes. *ACS applied materials & interfaces*, *1*(11), 2502-2508.
180. Ryu, Y. J., Kim, H. Y., Lee, K. H., Park, H. C., & Lee, D. R. (2003). Transport properties of electrospun nylon 6 nonwoven mats. *European polymer journal*, *39*(9), 1883-1889.
181. Safikhani, M. M., Zamanian, A., & Ghorbani, F. (2017). Synergistic effects of retinoic acid and graphene oxide on the physicochemical and in-vitro properties of electrospun polyurethane scaffolds for bone tissue engineering. *e-Polymers*, *17*(5), 363-371.
182. Safri, S. N. A., Sultan, M. T. H., Jawaid, M., & Jayakrishna, K. (2018). Impact behaviour of hybrid composites for structural applications: A review. *Composites Part B: Engineering*, *133*, 112-121.

183. Saghafi, H., Zucchelli, A., Palazzetti, R., & Minak, G. (2014). The effect of interleaved composite nanofibrous mats on delamination behavior of polymeric composite materials. *Composite Structures, 109*, 41-47.
184. Sahu, M., & Raichur, A. M. (2019). Toughening of high performance tetrafunctional epoxy with poly (allyl amine) grafted graphene oxide. *Composites Part B: Engineering, 168*, 15-24.
185. Saini, P., Choudhary, V., Singh, B., Mathur, R., & Dhawan, S. (2009). Polyaniline–MWCNT nanocomposites for microwave absorption and EMI shielding. *Materials Chemistry and Physics, 113*(2-3), 919-926.
186. Saini, P., Choudhary, V., Singh, B., Mathur, R., & Dhawan, S. (2011). Enhanced microwave absorption behavior of polyaniline-CNT/polystyrene blend in 12.4–18.0 GHz range. *Synthetic Metals, 161*(15-16), 1522-1526.
187. Saini, P., Choudhary, V., Vijayan, N., & Kotnala, R. (2012). Improved electromagnetic interference shielding response of poly (aniline)-coated fabrics containing dielectric and magnetic nanoparticles. *The Journal of Physical Chemistry C, 116*(24), 13403-13412.
188. Salimbeygi, G., Nasouri, K., Shoushtari, A. M., Malek, R., & Mazaheri, F. (2013). Fabrication of polyvinyl alcohol/multi-walled carbon nanotubes composite electrospun nanofibres and their application as microwave absorbing material. *Micro & Nano Letters, 8*(8), 455-459.
189. Sancaktar, E., & Aussawasathien, D. (2009). Nanocomposites of epoxy with electrospun carbon nanofibers: mechanical behavior. *The Journal of Adhesion, 85*(4-5), 160-179.
190. Stott, S. J., Mortimer, R. J., Dann, S. E., Oyama, M., & Marken, F. (2006). Electrochemical properties of core-shell TiC-TiO2 nanoparticle films immobilized at ITO electrode surfaces. Physical Chemistry Chemical Physics, 8(46), 5437–5443. https://doi.org/10.1039/b610391j.
191. Shacklette, L. W., Colaneri, N. F., Kulkarni, V. G., & Wessling, B. (1992). EMI shielding of intinsically conductive polymers. *Journal of Vinyl Technology, 14*(2), 118-122. doi: https://doi.org/10.1002/vnl.730140214
192. Shakil, U. A., Hassan, S. B., Yahya, M. Y., & Nauman, S. (2020). Mechanical properties of electrospun nanofiber reinforced/interleaved epoxy matrix composites—A review. *Polymer Composites*.
193. Sharma, C. S., Sharma, A., & Madou, M. (2010). Multiscale carbon structures fabricated by direct micropatterning of electrospun mats of SU-8 photoresist nanofibers. *Langmuir, 26*(4), 2218-2222.
194. Sharma, G. K., & James, N. R. (2021). Progress in Electrospun Polymer Composite Fibers for Microwave Absorption and Electromagnetic Interference Shielding. *ACS Applied Electronic Materials, 3*(11), 4657-4680.
195. Shen, Y., Chen, L., Jiang, S., Ding, Y., Xu, W., & Hou, H. (2015). Electrospun nanofiber reinforced all-organic PVDF/PI tough composites and their dielectric permittivity. *Materials Letters, 160*, 515-517. doi: https://doi.org/10.1016/j.matlet.2015.08.019

196. Shi, S.-L., & Liang, J. (2008). The effect of multi-wall carbon nanotubes on electromagnetic interference shielding of ceramic composites. *Nanotechnology, 19*(25), 255707.
197. Shin, D., An, X., Choun, M., & Lee, J. (2016). Effect of transition metal induced pore structure on oxygen reduction reaction of electrospun fibrous carbon. *Catalysis today, 260*, 82-88.
198. Shirazi, M. M. A., Bazgir, S., & Meshkani, F. (2020). Electrospun nanofibrous membranes for water treatment. *Advances in Membrane Technologies, 57*(3), 467-504.
199. Si, Y., Fu, Q., Wang, X., Zhu, J., Yu, J., Sun, G., & Ding, B. (2015). Superelastic and Superhydrophobic Nanofiber-Assembled Cellular Aerogels for Effective Separation of Oil/Water Emulsions. *ACS Nano, 9*(4), 3791-3799. doi: 10.1021/nn506633b
200. Sihn, S., Kim, R. Y., Huh, W., Lee, K.-H., & Roy, A. K. (2008). Improvement of damage resistance in laminated composites with electrospun nano-interlayers. *Composites science and technology, 68*(3-4), 673-683.
201. Simon, R. M. (1981). EMI shielding through conductive plastics. *Polymer-Plastics Technology and Engineering, 17*(1), 1-10.
202. Simons, H. L. (1966). Process and apparatus for producing patterned non-woven fabrics: Google Patents.
203. Sisti, L., Belcari, J., Mazzocchetti, L., Totaro, G., Vannini, M., Giorgini, L., . . . Celli, A. (2016). Multicomponent reinforcing system for poly (butylene succinate): composites containing poly (L-lactide) electrospun mats loaded with graphene. *Polymer testing, 50*, 283-291.
204. Sobczyk, K., & Leluk, K. (2018). *An openwork like structures of polylactide–manufacturing and properties.* Paper presented at the E3S Web of Conferences.
205. Song, K., Wu, Q., Zhang, Z., Ren, S., Lei, T., Negulescu, I. I., & Zhang, Q. (2015). Porous carbon nanofibers from electrospun biomass tar/polyacrylonitrile/silver hybrids as antimicrobial materials. *ACS applied materials & interfaces, 7*(27), 15108-15116.
206. Song, W.-L., Wang, J., Fan, L.-Z., Li, Y., Wang, C.-Y., & Cao, M.-S. (2014). Interfacial engineering of carbon nanofiber–graphene–carbon nanofiber heterojunctions in flexible lightweight electromagnetic shielding networks. *ACS applied materials & interfaces, 6*(13), 10516-10523.
207. Stachewicz, U., Modaresifar, F., Bailey, R. J., Peijs, T., & Barber, A. H. (2012). Manufacture of void-free electrospun polymer nanofiber composites with optimized mechanical properties. *ACS applied materials & interfaces, 4*(5), 2577-2582.
208. Summerscales, J., Hall, W., & Virk, A. S. (2011). A fibre diameter distribution factor (FDDF) for natural fibre composites. *Journal of materials science, 46*(17), 5876-5880.

209. Tang, B., Liu, X., Zhao, X., & Zhang, J. (2014). Highly efficient in situ toughening of epoxy thermosets with reactive hyperbranched polyurethane. *Journal of applied polymer science, 131*(16).
210. Tang, C., & Liu, H. (2008). Cellulose nanofiber reinforced poly (vinyl alcohol) composite film with high visible light transmittance. *Composites Part A: Applied Science and Manufacturing, 39*(10), 1638-1643.
211. Taylor, G. I. (1969). Electrically driven jets. *Proceedings of the Royal Society of London. A. Mathematical and Physical Sciences, 313*(1515), 453-475.
212. Thitsartarn, W., Fan, X., Sun, Y., Yeo, J. C. C., Yuan, D., & He, C. (2015). Simultaneous enhancement of strength and toughness of epoxy using POSS-Rubber core–shell nanoparticles. *Composites science and technology, 118*, 63-71.
213. Tsimpris, C. W., & Mayhan, K. G. (1972). Thermal analysis of a poly(amic acid)-polyimide system. Thermochimica Acta, 5(2), 133–145. https://doi.org/10.1016/0040-6031(72)85018-4
214. Thomas, R., Yumei, D., Yuelong, H., Le, Y., Moldenaers, P., Weimin, Y., . . . Thomas, S. (2008). Miscibility, morphology, thermal, and mechanical properties of a DGEBA based epoxy resin toughened with a liquid rubber. *Polymer, 49*(1), 278-294.
215. Thostenson, E. T., Ren, Z., & Chou, T.-W. (2001). Advances in the science and technology of carbon nanotubes and their composites: a review. *Composites science and technology, 61*(13), 1899-1912.
216. Tian, M., Gao, Y., Liu, Y., Liao, Y., Xu, R., Hedin, N. E., & Fong, H. (2007). Bis-GMA/TEGDMA dental composites reinforced with electrospun nylon 6 nanocomposite nanofibers containing highly aligned fibrillar silicate single crystals. *Polymer, 48*(9), 2720-2728.
217. Tijing, L. D., Park, C.-H., Kang, S.-J., Amarjargal, A., Kim, T.-H., Pant, H. R., . . . Kim, C. S. (2013). Improved mechanical properties of solution-cast silicone film reinforced with electrospun polyurethane nanofiber containing carbon nanotubes. *Applied Surface Science, 264*, 453-458.
218. Tong, X. C. (2016). *Advanced materials and design for electromagnetic interference shielding*: CRC press.
219. Ura, D. P., Berniak, K., & Stachewicz, U. (2021). Critical length reinforcement in core-shell electrospun fibers using composite strategies. *Composites science and technology*, 108867.
220. Uslu, E., Gavgali, M., Erdal, M. O., Yazman, Ş., & Gemi, L. (2021). Determination of mechanical properties of polymer matrix composites reinforced with electrospinning N66, PAN, PVA and PVC nanofibers: A comparative study. *Materials Today Communications, 26*, 101939.
221. Valizadeh, A., & Farkhani, S. M. (2014). Electrospinning and electrospun nanofibres. *IET nanobiotechnology, 8*(2), 83-92.
222. van der Heijden, S., Daelemans, L., De Bruycker, K., Simal, R., De Baere, I., Van Paepegem, W., . . . De Clerck, K. (2017). Novel composite

materials with tunable delamination resistance using functionalizable electrospun SBS fibers. *Composite Structures, 159*, 12-20.

223. Varma, I. K., Goel, R. N., & Varma, D. S. (1977). Stability of polyamic acids and polyimides. 64, 101–113

224. Vijay Kumar, V., Ramakrishna, S., Kong Yoong, J. L., Esmaeely Neisiany, R., Surendran, S., & Balaganesan, G. (2019). Electrospun nanofiber interleaving in fiber reinforced composites—Recent trends. *Material Design & Processing Communications, 1*(1), e24.

225. Vu, C. M., & Bach, Q.-V. (2020). Effects of DOPO-grafted epoxidized soybean oil on fracture toughness and flame retardant of epoxy resin/rice husk silica hybrid. *Macromolecular research, 28*(9), 826-834.

226. Wang, B., & Wang, Y. D. (2011). *Effect of fiber diameter on thermal conductivity of the electrospun carbon nanofiber mats.* Paper presented at the Advanced Materials Research.

227. Wang, M., Fan, X., Thitsartarn, W., & He, C. (2015). Rheological and mechanical properties of epoxy/clay nanocomposites with enhanced tensile and fracture toughnesses. *Polymer, 58*, 43-52.

228. Wang, Q., Jian, M., Wang, C., & Zhang, Y. (2017). Carbonized silk nanofiber membrane for transparent and sensitive electronic skin. *Advanced Functional Materials, 27*(9), 1605657.

229. Wang, J., Jiang, A., Li, Y., Song, D., Li, Y., & Cheng, L. (2022). Thermal Decomposition Behavior of Polyimide Containing Flame Retardant SiO2 and Mg(OH)2. Polymers, 14(14). https://doi.org/10.3390/polym14142791

230. Wei, Y., Shi, Y., Zhang, X., Jiang, Z., Zhang, Y., Zhang, L., . . . Gong, C. (2019). Electrospinning of lightweight TiN fibers with superior microwave absorption. *Journal of Materials Science: Materials in Electronics*, 1-9.

231. Wu, J., Wang, N., Zhao, Y., & Jiang, L. (2013). Electrospinning of multilevel structured functional micro-/nanofibers and their applications. *Journal of Materials Chemistry A, 1*(25), 7290-7305.

232. Wu, M., Wu, Y., Liu, Z., & Liu, H. (2012). Optically transparent poly (methyl methacrylate) composite films reinforced with electrospun polyacrylonitrile nanofibers. *Journal of composite materials, 46*(21), 2731-2738.

233. Wu, Z. P., Li, M. M., Hu, Y. Y., Li, Y. S., Wang, Z. X., Yin, Y. H., . . . Zhou, X. (2011). Electromagnetic interference shielding of carbon nanotube macrofilms. *Scripta Materialia, 64*(9), 809-812.

234. Xu, W., Ding, Y., Jiang, S., Chen, L., Liao, X., & Hou, H. (2014). Polyimide/BaTiO3/MWCNTs three-phase nanocomposites fabricated by electrospinning with enhanced dielectric properties. *Materials Letters, 135*, 158-161. doi: https://doi.org/10.1016/j.matlet.2014.07.157

235. Xu, W., Ding, Y., Jiang, S., Zhu, J., Ye, W., Shen, Y., & Hou, H. (2014). Mechanical flexible PI/MWCNTs nanocomposites with high dielectric permittivity by electrospinning. *European polymer journal, 59*, 129-135. doi: https://doi.org/10.1016/j.eurpolymj.2014.07.028

236. Xu, W., Feng, Y., Ding, Y., Jiang, S., Fang, H., & Hou, H. (2015). Short electrospun carbon nanofiber reinforced polyimide composite with high dielectric permittivity. *Materials Letters, 161*, 431-434.
237. Xu, Y., Liu, Y., Chen, S., & Ni, Y. (2020). Current Overview of Carbon Fiber: Toward Green Sustainable Raw Materials. *BioResources, 15*(3), 7234-7259.
238. Yang, K., Edie, D. D., Lim, D., Kim, Y., & Choi, Y. (2003). Preparation of carbon fiber web from electrostatic spinning of PMDA-ODA poly (amic acid) solution. *Carbon, 41*(11), 2039-2046.
239. Yang, Y., Centrone, A., Chen, L., Simeon, F., Hatton, T. A., & Rutledge, G. C. (2011). Highly porous electrospun polyvinylidene fluoride (PVDF)-based carbon fiber. *Carbon, 49*(11), 3395-3403.
240. Yao, S.-S., Ma, C.-L., Jin, F.-L., & Park, S.-J. (2020). Fracture toughness enhancement of epoxy resin reinforced with graphene nanoplatelets and carbon nanotubes. *Korean Journal of Chemical Engineering, 37*(11), 2075-2083.
241. Yin, X., Kong, L., Zhang, L., Cheng, L., Travitzky, N., & Greil, P. (2014). Electromagnetic properties of Si–C–N based ceramics and composites. *International materials reviews, 59*(6), 326-355.
242. Yun, Y. S., Im, C., Park, H. H., Hwang, I., Tak, Y., & Jin, H.-J. (2013). Hierarchically porous carbon nanofibers containing numerous heteroatoms for supercapacitors. *Journal of Power Sources, 234*, 285-291.
243. Bhattacharjee, Y., & Bose, S. (2021). Core-Shell Nanomaterials for Microwave Absorption and Electromagnetic Interference Shielding: A Review. ACS Applied Nano Materials, 4(2), 949–972. https://doi.org/10.1021/acsanm.1c00278
244. Zeleny, J. (1917). Instability of electrified liquid surfaces. *Physical review, 10*(1), 1.
245. Zeng, Y., Li, X., Jiang, S., He, S., Fang, H., & Hou, H. (2015). Free-standing mesoporous electrospun carbon nanofiber webs without activation and their electrochemical performance. *Materials Letters, 161*, 587-590. doi: https://doi.org/10.1016/j.matlet.2015.08.154
246. Zhan, J., & Lan, P. (2012). The review on electrospun gelatin fiber scaffold. *Journal of Research Updates in Polymer Science, 1*(2), 59-71.
247. Zhang, C., Yuan, X., Wu, L., Han, Y., & Sheng, J. (2005). Study on morphology of electrospun poly (vinyl alcohol) mats. *European polymer journal, 41*(3), 423-432.
248. Zhang, J., Yang, T., Lin, T., & Wang, C. H. (2012). Phase morphology of nanofibre interlayers: critical factor for toughening carbon/epoxy composites. *Composites science and technology, 72*(2), 256-262.
249. Zhang, L. (2014). *Research on preparation and property of alternating multilayer polymer electromagnetic shielding materials.* Paper presented at the Applied Mechanics and Materials.

250. Zhang, T., Huang, D., Yang, Y., Kang, F., & Gu, J. (2013). Fe3O4/carbon composite nanofiber absorber with enhanced microwave absorption performance. *Materials Science and Engineering: B, 178*(1), 1-9.
251. Zhang, X. (2014). *Fundamentals of fiber science*: DEStech Publications, Inc.
252. Zhou, J., Zhou, M., Chen, Z., Zhang, Z., Chen, C., Li, R., . . . Xie, E. (2009). SiC nanotubes arrays fabricated by sputtering using electrospun PVP nanofiber as templates. *Surface and Coatings Technology, 203*(20-21), 3219-3223.
253. Zhou, S., Zhou, G., Jiang, S., Fan, P., & Hou, H. (2017). Flexible and refractory tantalum carbide-carbon electrospun nanofibers with high modulus and electric conductivity. *Materials Letters, 200*, 97-100. doi: https://doi.org/10.1016/j.matlet.2017.04.115
254. Zucchelli, A., Focarete, M. L., Gualandi, C., & Ramakrishna, S. (2011). Electrospun nanofibers for enhancing structural performance of composite materials. *Polymers for Advanced Technologies, 22*(3), 339-349.
255. Zussman, E., Chen, X., Ding, W., Calabri, L., Dikin, D., Quintana, J., & Ruoff, R. (2005). Mechanical and structural characterization of electrospun PAN-derived carbon nanofibers. *Carbon, 43*(10), 2175-2185.
256. Zussman, E., Yarin, A. L., Bazilevsky, A. V., Avrahami, R., & Feldman, M. (2006). Electrospun polyaniline/poly (methyl methacrylate)-derived turbostratic carbon micro-/nanotubes. *Advanced Materials, 18*(3), 348-353.

LIST OF PUBLICATIONS

International journals (Based on Thesis)

1. Deeraj, B., Saritha, A., & Joseph, K. (2019). Electrospun styrene-butadiene copolymer fibers as potential reinforcement in epoxy composites: Modeling of rheological and visco elastic data. *Composites Part B: Engineering*, *160*, 384-393.

2. Deeraj, B., Harikrishnan, R., Jayan, J. S., Saritha, A., & Joseph, K. (2020). Enhanced visco-elastic and rheological behavior of epoxy composites reinforced with polyimide nanofiber. *Nano-Structures & Nano-Objects*, *21*, 100421.

3. Deeraj B, George G, Dhineshbabu N, Bose S, Joseph K. Electrospun ZrO_2@ carbon nanofiber mats and their epoxy composites as effective EMI shields in Ku band. *Materials Research Bulletin*. 2021;144:111477.

4. Deeraj B, Shebin, Sampath S, Bose S, Joseph K. Electrospun carbon fibers embedded with core-shell TiC@ TiO_2 nanostructures and their epoxy composites for potential EMI shielding application in Ku band. *Nano-Structures & Nano-Objects*, 32, 100912.

International journals (Other Co-authored articles)

1. Siva DBD, Karingamanna J, Joseph K. High performance in-situ composites developed from polypropylene/nylon 6/carbon nanotube blend systems. Journal of Siberian Federal University. Biology. 2018;11(2):157-65

2. Rasana N, Jayanarayanan K, Deeraj B, Joseph K. The thermal degradation and dynamic mechanical properties modeling of MWCNT/glass fiber multiscale filler reinforced polypropylene composites. Composites Science and Technology. 2019;169:249-59

3. Konnola R, Deeraj B, Sampath S, Saritha A, Joseph K. Fabrication and Characterization of Toughened Nanocomposites Based on TiO2 Nanowire-Epoxy System. Polymer Composites. 2019;40(7):2629-38.

4. Jayan JS, Deeraj B, Saritha A, Joseph K. Theoretical modelling of kinetics of glass transition temperature of PEG toughened epoxy. Plastics, Rubber and Composites. 2020;49(6):237-44.

5. Jayan, J. S., Saritha, A., Deeraj, B., & Joseph, K. (2020a). Synthesis of self-assembled and porous nano titania-graphene oxide hybrids for toughening the epoxy. *Polymer Composites*, *41*(10), 4093-4103.

6. Jayan, J. S., Saritha, A., Deeraj, B., & Joseph, K. (2020b). Triblock copolymer grafted Graphene oxide as nanofiller for toughening of epoxy resin. *Materials Chemistry and Physics, 248*, 122930.

7. Jayan, J. S., Saritha, A., Deeraj, B. D. S., & Joseph, K. (2020c). Graphene oxide as a prospective graft in polyethylene glycol for enhancing the toughness of epoxy nanocomposites. *Polymer Engineering & Science, 60*(4), 773-781.

8. Raman, A., Jayan, J. S., Deeraj, B., Saritha, A., & Joseph, K. (2021). Electrospun Nanofibers as Effective Superhydrophobic Surfaces: A Brief review. *Surfaces and Interfaces*, 101140.

9. Sarath Kumar P, Jayanarayanan K, Deeraj B, Joseph K, Balachandran M. Synergistic effect of carbon fabric and multiwalled carbon nanotubes on the fracture, wear and dynamic load response of epoxy-based multiscale composites. Polymer Bulletin. 2021:1-22.

10. Deeraj BDS, Joseph K, Jayan JS, Saritha A. Dynamic mechanical performance of natural fiber reinforced composites: A brief review. Applied Science and Engineering Progress. 2021;14(4):614-23.

11. Jayan, J. S., Pal, K., Saritha, A., Deeraj, B., & Joseph, K. (2021). Graphene oxide as multi-functional initiator and effective molecular reinforcement in PVP/epoxy composites. *Journal of* Molecular Structure, 1230, 129873.

12. Akhila R, Deeraj B, Appukuttan S, Kuruvilla J. A brief review on electrospun lignin nanofibres. Journal of Siberian Federal University. Biology. 2021;14(4):465-74.

13. Deeraj, B., Jayan, J. S., Raman, A., Saritha, A., & Joseph, K. (2022). Polymeric blends and nanocomposites for high performance EMI shielding and microwave absorbing applications. Composite Interfaces. (Accepted)

Book chapters

1. Deeraj B, Jayanarayanan K, Joseph K. Development of High-Performance In-Situ Polypropylene/Nylon 6 Microfibrillar Composites. Processing and Characterization of Multicomponent Polymer Systems: Apple Academic Press; 2019. p. 135-54

2. Deeraj BDS, Mathew MS, Parameswaranpillai J, Joseph K. EMI shielding materials based on thermosetting polymers. Materials for Potential EMI Shielding Applications: Elsevier; 2020. p. 101-10.

3. Deeraj B, Jayan JS, Saritha A, Joseph K. Electrospun biopolymer-based hybrid composites. Hybrid Natural Fiber Composites: Elsevier; 2021. p. 225-52.

4. Jayan JS, Deeraj B, Saritha A, Joseph K. Biopolymer-derived carbonaceous composites and their potential applications. Hybrid Natural Fiber Composites: Elsevier; 2021. p. 253-80.

5. Deeraj B, Jayan JS, Saritha A, Joseph K. Electrospun biopolymer-based hybrid composites. Hybrid Natural Fiber Composites: Elsevier; 2021. p. 225-52.

6. Fathima S, Deeraj B, Appukuttan S, Joseph K. Carbon fiber and glass fiber reinforced elastomeric composites. Fiber Reinforced Composites: Elsevier; 2021. p. 307-40.

7. Saritha A, Deeraj BD, Jayan JS, Joseph K. Rheology of Bioepoxy Polymers, Their Blends, and Composites. Bio-Based Epoxy Polymers, Blends and Composites: Synthesis, Properties, Characterization and Applications. 2021:167-95

8. Deeraj B, Jayan JS, Saritha A, Joseph K. PLA-based blends and composites. Biodegradable Polymers, Blends and Composites: Elsevier; 2022. p. 237-81.

9. Jayan JS, Sethulekshmi A, Venu G, Deeraj B, Saritha A, Joseph K. Recycling of elastomer blends and composites. Elastomer Blends and Composites: Elsevier; 2022. p. 269-304.

10. Jayan JS, Deeraj B, Saritha A, Joseph K. Theoretical modeling and simulation of elastomer blends and nanocomposites. Elastomer Blends and Composites: Elsevier; 2022. p. 243-67.

11. Deeraj B, Jayan JS, Saritha A, Joseph K. Electrospun Fiber Reinforced Epoxy Composites. Handbook of Epoxy/Fiber Composites. 2022:990

PRESENTATIONS IN CONFERENCES/SEMINARS

Oral Presentations

- Short Invited talk in *Materials Research Society of India AGM 2019*, CSIR-NIIST, Trivandrum, 2019

- Short invited talk In *Polymers@100 webinar*, Amal Jyothi College, July 2020.

- Short Invited talk in *International Online Congress on Membranes and Membrane Assisted Processes (ICMMAP 2021),* MG University, 2021

- Invited talk in *Changing Trends in Polymer Science and Technology* 2021, NIT Calicut , 2021

- Invited talk in *International Conference on Advances in Polymer Technology (APT 21)*, May 2021, CUSAT, Cochin

- Oral presentation in *National Conference on Materials Science and Technology (NCMST 2021)*, IIST, Trivandrum

Poster Presentations

- Presented a Technical Poster in *Society for Polymer Science India (SPSI) MACRO 2018*, IISER Pune, December 2018.

- Presented a Technical Poster in *International Conference on Energy and Environment (ICEE 2k19)*, T.K.M college, Kollam, December 2019.

- Presented a Technical Poster in *International Conference on Nano Science and Technology (ICONSAT 2020)*, Kolkata, March 2020.

- Presented a Technical Poster in *National Conference on Materials Science and Technology (NCMST 2021)*, Trivandrum, December 2020.